



GP-RSS

International Joint Graduate Program in Resilience and Safety Studies



SyDE

WISE Program for
Sustainability in the
Dynamic Earth

変動地球共生学卓越大学院プログラム

**The 8th International Symposium
on Water Environment Systems
---with Perspective of Global Safety
(November 13th – 14th, 2020)**

**Department of Civil and Environmental Engineering
Graduate School of Engineering
Tohoku University**



**TOHOKU
UNIVERSITY**

Sponsors



**International Joint Graduate Program in
Resilience and Safety Studies of Tohoku University**
<http://gp-rss.tohoku.ac.jp/>



**WISE Program for Sustainability in the Dynamic
Earth of Tohoku University**
<https://syde.tohoku.ac.jp/>



**Department of Civil and Environmental
Engineering, Graduate School of Engineering,
Tohoku University**
<http://www.eng.tohoku.ac.jp/>

ORGANIZERS

Dr. So KAZAMA (Professor, Tohoku University)
Dr. Yu-You LI (Professor, Tohoku University)
Dr. Daisuke KOMORI (Associate Professor, Tohoku University)
Dr. Daisuke SANO (Associate Professor, Tohoku University)
Dr. Kengo KUBOTA (Associate Professor, Tohoku University)

SECRETARIATS

Assistant Professor, Dr. Yoshiya TOUGE [yoshiya.touge.a6\[at\]tohoku.ac.jp](mailto:yoshiya.touge.a6[at]tohoku.ac.jp)
Assistant Professor, Dr. Yu QIN [yu.qin.e8\[at\]tohoku.ac.jp](mailto:yu.qin.e8[at]tohoku.ac.jp)
DC Student, Ying SONG [song.ying.q2\[at\]dc.tohoku.ac.jp](mailto:song.ying.q2[at]dc.tohoku.ac.jp)
DC Student, Chao RONG [rong.chao.p7\[at\]dc.tohoku.ac.jp](mailto:rong.chao.p7[at]dc.tohoku.ac.jp)
DC Student, Shuka KAGEMASA [shuka.kagemasa.t2\[at\]dc.tohoku.ac.jp](mailto:shuka.kagemasa.t2[at]dc.tohoku.ac.jp)

*please change the mark [at] to "@"

PARTICIPANTS

TOHOKU University

JAPAN

Jiayuan JI	P.D.
Qing CHANG	P.D.
Ying SONG	DC student
Ziang HE	DC student
Yunzhi QIAN	DC student
Shuka KAGEMASA	DC student
Kampachiro URASAKI	DC student
Hiroyuki OHNO	DC student
Vempi Satriya Adi HENDRAWAN	DC student
Chao RONG	DC student
Yifan ZHU	DC student
Danila PODOBED	DC student
Ke SHI	DC student
Tianjie WANG	MC student
Shitong ZHOU	MC student
Zibin LUO	MC student
Amalia Nafisah Rahmani IRAWAN	MC student
Hajiem YANAGISAWA	MC student
Hayata YANAGIHARA	MC student
Chenling SUN	MC student
Qin HUANG	MC student
Runda DU	MC student
Guangze GUO	MC student
Chai YIKAI	MC student

Kyoto University**JAPAN**

Tomoyuki HINO	Professor
Temur KHUJANAZAROV	PhD
Sanjar SADYROV	DC student

Princeton University**United States of America**

Z. Jason REN	Professor
--------------	-----------

Xi'an University of Architecture and Technology**China**

Rong CHEN	Professor
Jinfan ZHANG	DC student
Yaqian LIU	MC student

China Agricultural University**China**

Mengmeng JIANG	DC student
----------------	------------

Shanghai University**China**

Jinghuan LUO	PhD
--------------	-----

Kasetsart University**Thailand**

Thapthai CHAITHONG	Professor
--------------------	-----------

Pati Regency Government Indonesia**Indonesia**

Erwan Wahyu WIBOWO

Schedule (GMT+9)

13 Nov (FRI)

8:50~8:55

Opening ceremony

8:55~9:00

Group photo

9:00~9:40

Plenary lecture I

Electroactive Membranes for Resource Recovery from Wastewater,
Prof. Z. Jason REN, Princeton University

9:40~10:20

Plenary lecture II

Mediating methane fermentation and retarding membrane fouling in
AnMBRs by carbon-based materials: efficiency and mechanism
Prof. Rong CHEN, Xi'an University of Architecture and Technology

10:20~10:30

Coffee break

10:30~12:00

Poster exhibition (Room A&B)

Topic 1: Anaerobic membrane bioreactor

Performance of an AnMBR treating real sewage at low temperature,
Jiayuan JI, TOHOKU University

Efficient treatment of municipal wastewater and biogas production by a
pilot-scale submerged anaerobic membrane bioreactor,
Tianjie WANG, TOHOKU University

High solid mono-digestion and co-digestion performance of food waste
and sewage sludge by a thermophilic anaerobic membrane bioreactor,
Shitong ZHOU, TOHOKU University

Methane fermentation of rich lipid food waste by a hollow fiber
anaerobic membrane bioreactor (HF-AnMBR),
Ziang HE, TOHOKU University

Topic 2: Anammox

Startup of a pilot-scale anammox reactor for municipal wastewater
treatment and biofilm formation,
Zibin LUO, TOHOKU University

Biofilm characterization and operation performance in a single stage
partial nitrification/anammox process with a function carrier,
Yunzhi QIAN, TOHOKU University

Topic 3: Environmental microorganism

Microbial diversity of small bacteria in activated sludge,
Shuka KAGEMASA, TOHOKU University

Application of hemin for the detection of environmental
microorganisms, Kampachiro URASAKI, TOHOKU University

Effects of altering process parameters for controlling nutrient
concentration in treated water on microbial community structure and
amoA gene in activated sludge,
Hiroyuki OHNO, TOHOKU University

10:30~12:00 Poster exhibition (Room C&D)

Topic : Hydrological ecology

A cross comparison of hydrological similarity and geological similarity
for the sub-catchments within Natori river basin,
Qing CHANG, Tohoku University

Crop yield sensitivity to drought events: a global-scale analysis of major
crops,
Vempi Satriya Adi HENDRAWAN, Tohoku University

Snow cover analysis for dam inflow prediction in Thailand,
Tomoyuki HINO, Kyoto University

The Selection of Temporal Scale for Drought Analysis using Satellite-
Based Precipitation Data,
Amalia Nafisah Rahmani IRAWAN, Tohoku University

Relationship between local and spatial probabilities of precipitation in
the Yoneshiro River catchment,
Hajiem YANAGISAWA, Tohoku University

Estimation of the risk of inland flood based on distribution of extreme
precipitation in Japan,
Hayata YANAGIHARA, Tohoku University

Evaluating the effect of dryness on wildfire in Tohoku region using
KBDI and PDSI,
Chenling SUN, Tohoku University

Evaluate the effect of fuel moisture content on the heat required for
ignition in the Tohoku Region of Japan,
Qin HUANG, Tohoku University

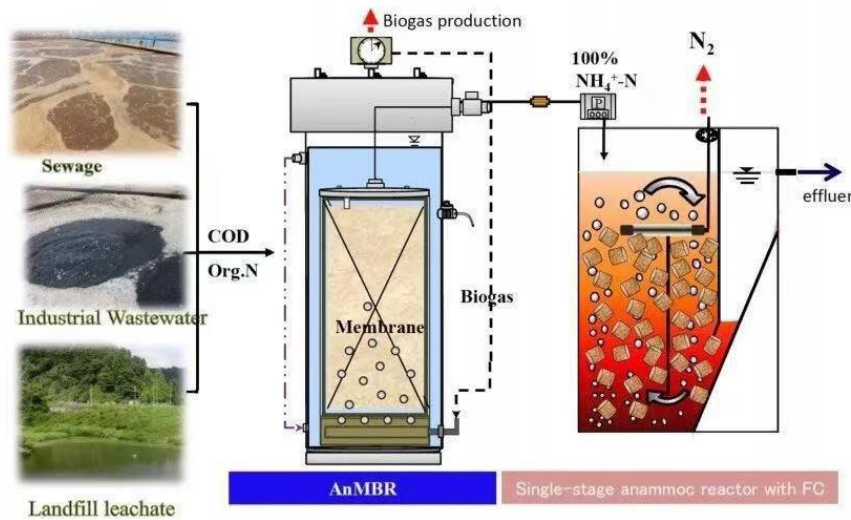
12:00~13:00	Lunch break
13:00~15:30	Oral session I
	<i>Topic 1: Advanced wastewater treatment</i>
13:00~13:15	High loading capacity of EGSB reactor with anammox-HAP sludge at extremely low temperature of 7°C, Ying SONG, TOHOKU University
13:15~13:30	Development of an energy saving type municipal wastewater treatment system by combining AnMBR and Anammox processes: pilot-scale plant study and system evaluation, Chao RONG, TOHOKU University
13:30~13:45	Treatment of municipal wastewater by anaerobic membrane bio-reactor: process performance and mass balance, Runda DU, TOHOKU University
13:45~13:50	Coffee break
	<i>Topic 2: Membrane technology</i>
13:50~14:05	Virus removal by membrane bioreactors: mechanisms and modeling efforts, Yifan ZHU, TOHOKU University
14:05~14:20	Mechanisms of MS2 bacteriophage removal in an anaerobic membrane bioreactor, Jinfan ZHANG, Xi'an University of Architecture and Technology
14:20~14:35	High rate anaerobic digestion of food wastewater in an anaerobic membrane bioreactor, Mengmeng JIANG, China Agricultural University
14:35~14:40	Coffee break
	<i>Topic 3: Bioenergy production</i>
14:40~14:55	Using an expended granular sludge bed reactor for advanced anaerobic digestion of food waste pretreated with enzyme, Jinghuan LUO, Shanghai University
14:55~15:10	Biochar sustained high-efficient anaerobic co-digestion by enhancing direct interspecies electron transfer and alleviating thermodynamic restriction, Yaqian LIU, Xi'an University of Architecture and Technology
15:10~15:25	Effect of thermal pretreatment on anaerobic digestion of sewage sludge by anaerobic membrane bioreactor, Guangze GUO, TOHOKU University

15:25~15:30	Coffee break
15:30~18:00	Oral session II
	<i>Topic: Hydrological ecology</i>
15:30~15:55	Assessment of the secondary salinization impact to the water resources in the Uzbekistan, Temur KHUJANAZAROV, Kyoto University
15:55~16:20	Simulating soil water recession coefficients using satellite-based data for antecedent precipitation index, Thapthai HAITHONG, Kasetsart University
16:20~16:40	Understanding Seasonality and Evapotranspiration of Soil Water under Tree and Grass Cover Using Natural Isotopes, Danila PODOBED, Tohoku University
16:40~16:50	Coffee break
16:50~17:10	Spatiotemporal analysis of drought indicated by scPDSI over Japan, Ke SHI, Tohoku University
17:10~17:30	The effect of wealth level and community-based environmental activities participation on environmental awareness, Erwan Wahyu WIBOWO, Pati Regency Government Indonesia
17:30~17:50	Hydrological assessment of precipitation products over high mountain regions: case study of Issyk-Kul Lake, Sanjar SADYROV, Kyoto University
17:50~18:10	Application of simple paddy field dam model for typhoon event at basin scale, Chai YIKAI, Tohoku University
18:10~18:20	Closing speech

14 Nov (Sat)

10:00~12:00	Online fieldwork <i>Topic: AnMBR&Anammox pilot-scale plant</i>
--------------------	---

Online fieldwork- AnMBR&Anammox pilot-scale plant



- New concept of organic wastewater treatment



- Pilot plant of AnMBR and One-stage Anammox in Senen sewage treatment plant

AnMBR and One-stage Anammox is a new technology to develop an energy-positive innovative sewage treatment system integrating an anaerobic membrane bioreactor (AnMBR) and anaerobic ammonium oxidation (Anammox) process. The pilot plant in Senen sewage treatment plant has a working volumes of 5 m³ for the AnMBR and 1.67 m³ for One-stage Anammox reactor and completed with a capacity of 20 m³/d after a 500-day operation.

Connection Guidance

Updated by 10th Nov, 2020

The Symposium will be held on the online meeting software of ZOOM. Please install the ZOOM in advance. The online symposium will be recorded. Please set your nickname as “[Prof/Dr/Miss/Mr]+[full name]+[Univ./Inst.]”. If you have questions, please type them in the Chatbox. The host will repeat your questions during Q&A.

For live presenters, please make sure your camera and microphone are available before joining the connection. Also keep your speaking time strictly controlled to the assigned interval, or the hosts will terminate your presentation.

The following time is presented based on the local time (GMT+9).

12th Nov, THU

18:00~	Connection Test (only for attendants in Tohoku Univ.)	Click here	Room ID: 928 6409 8120 Passcode: 
--------	---	----------------------------	---

13th Nov, FRI

8:45~18:30	Main Room	Click here	Room ID: 978 0030 6476 Passcode: 
10:30~12:00	Poster Room A	Click here	Room ID: 811 2401 9568 Passcode: 
10:30~12:00	Poster Room B	Click here	Room ID: 926 8620 5004 Passcode: 
10:30~12:00	Poster Room C	Click here	Room ID: 972 3059 8507 Passcode: 
10:30~12:00	Poster Room D	Click here	Room ID: 976 3652 2155 Passcode: 

14th Nov, SAT

10:00~12:00	Online Fieldwork	Click here	Room ID: 931 2889 8725 Passcode: 
-------------	------------------	----------------------------	---

For more technical questions, please kindly find the “General Flow” in the program or send mails to our technical staff.

Electroactive Membranes for Resource Recovery from Wastewater

○ Z. Jason Ren*, Xi Chen, Xiaobo Zhu, Joshua Jack

¹Department of Civil and Environmental Engineering, Princeton University, Princeton, USA.

*E-mail: zjren@princeton.edu

Abstract

In the past decade energy and environmental innovators have made significant advancements in recovering energy from waste materials, yet the scalability and economic benefits of such applications still face challenges, partially because of the dramatic decrease in renewable electricity price. With renewable electricity costing 2 cents per kwh to even negative in some places during some periods, how to use cheap renewable energy to maximize waste valorization can become an interesting direction. In addition, waste treatment can carry mutual benefits to renewable energy industry, as water is a common electrolyte and energy storage medium.

In this talk, I will discuss some recent progress in identifying the synergy between microbial electrochemistry and membrane processes that led to the development of new materials and systems. I will report some development on electroactive membrane electrodes that take advantage of the low-cost renewables and enable specific resource recoveries from wastewater and CO₂. While we have been focusing on energy-neutral waste treatment, maybe we can start to think broadly on carbon-negative and dollar-positive waste treatment beyond energy production.

Mediating methane fermentation and retarding membrane fouling in AnMBRs by carbon-based materials: efficiency and mechanism

○ Rong Chen^{1*}, Qian Li¹ & Gaojun Wang¹

¹ Xi'an University of Architecture and Technology, No.13 Yanta Road, Xi'an, 710055, PR China.

Abstract

This study investigated the efficiency and mechanism of carbon-based materials on promoting methane fermentation and retarding membrane fouling in anaerobic membrane reactors. The results indicate promoting syntrophic electron exchange between bacteria and archaea via direct interspecific electron transfer (DIET) is the main approach that biochar (BC) and activated carbon (AC) promoting methane fermentation. Mechanisms of BC and AC mediating DIET are different, BC acts as geobatteries while AC tends to acts as geoconductors. Membrane fouling performance indicates AC can alleviate membrane fouling in long-term operation, in which suppressing cake layer formation via impacting enrichment of microbes on membrane surface played a key role.

Keywords: carbon-based materials; biochar; activated carbon; methane fermentation; membrane fouling.

1 Introduction

Anaerobic digestion (AD) is one of the most promising for bio-waste management to attain sustainable conversion of biomass to renewable energy. However, an excessively high organic loading rate (OLR) could lead to severe volatile fatty acids (VFAs) accumulation and pH decrease of AD system, which largely hinders the methanogenesis process [1]. As an advanced AD technology, although anaerobic membrane reactor has many advantages over conventional AD technology, membrane fouling of this system still a big challenge that hinders the widespread of this technology.

To cover the VFAs accumulation and membrane fouling simultaneously, the addition of carbon-based materials is environment friendly and low-cost solution. In the hybrid system, biochar (BC) or activated carbon (AC) has the potential to act as the redox-active mediator to achieve direct interspecific electron transfer (DIET), which was beneficial for promoting CH₄ production and increased OLR via accelerating VFAs degradation. Moreover, the addition of carbon-based materials also can enhance the scouring intensity of biogas on membrane surface by resulting in more intensive hydraulic disturbance in AnMBRs, which is considered the most effective strategy for retarding membrane fouling.

In this study, the carbon-based materials (both BC and AC) were utilized to explore the efficiency and mechanism of these materials mediating methane fermentation and retarding membrane fouling in AD and AnMBRs systems.

2 Materials and methods

Biochar prepared at different pyrolysis temperatures (300, 500, 700), then the promoting efficiency of this BC on AD was tested by batch experiment to determine the optimal preparing condition. After the batch test, BC and AC were added to sequencing batch reactors and AnMBRs to investigate their promotion on AD and membrane fouling control. During long-term operation of the reactors, the mechanisms of BC and AC mediating methane fermentation and retarding membrane fouling were explored by sludge characteristics, intermediate substances content, and microbial succession in each system. Specific information about the reactors' operation and analytical methods can be found in our previous studies [2–4].

3 Results and discussion

3.1 Efficiency of BC promoting methane fermentation

The presence of BC dramatically shortened the lag time of methane production and increased the methane production rate with increased organic loading (Fig.1). The electron exchange in syntrophic oxidation of butyrate and acetate as intermediate products was significantly facilitated by BC (Fig. 2). CH₄ production and VFAs concentrations suggest biochar addition promoted syntrophic degradation of butyrate to acetate occurred under high H₂ partial pressure (Fig. 3), this is the main way that BC promotes methane fermentation [4].

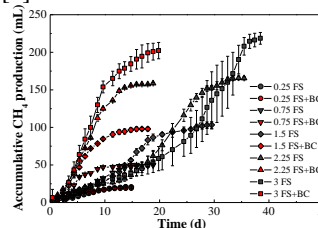


Fig. 1. Accumulative methane production at feedstock/seed sludge (F/S) ratio of 0.25, 0.75, 1.5, 2.25, and 3 in the control group (FS) and biochar-amended group (FS + BC).

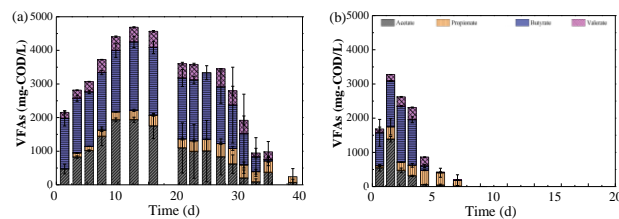


Fig. 2 Variation of VFAs at F/M of 3.0 in control (a) and BC groups (b)

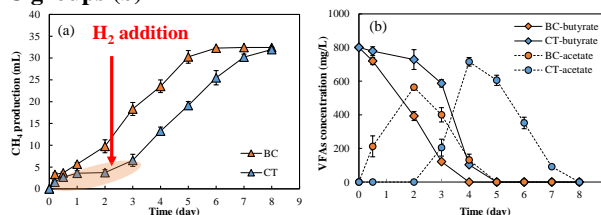


Fig.3 Effect of biochar on syntrophic oxidation under high H₂ partial pressure. (a) CH₄ production; (b) VFAs.

Performance of an AnMBR treating real sewage at low temperature

○ Jiayuan JI^{1*}, Runda DU¹, Yujie CHEN¹ & Yu-You LI^{1,2}

¹Department of Civil and Environmental Engineering, Tohoku University, Sendai 980-8579, Japan.

²Graduate School of Environmental Studies, Tohoku University, Sendai 980-8579, Japan.

*E-mail: kikaen@tohoku.ac.jp

Abstract

A 20 L hollow fiber type submerged anaerobic membrane bioreactor (AnMBR) was used to treat real sewage at 15 °C low temperature under varied hydraulic retention times (HRTs) from 6 to 24 hours. The treatment performance was evaluated by organic removal efficiency, biogas production, sludge yield, and filtration behaviors of membranes. For HRTs ranging between 16 h and 24 h, the AnMBR showed good organic removal efficiency with chemical oxygen demand (COD) and biochemical oxygen demand (BOD) removal efficiencies of about 90% and 91%, respectively. The biogas production rate was achieved 0.1 L-gas/ L-water, with approximately 81% methane content. According to the COD balance analysis, the low biogas yield and high sludge yield at HRT of 6 h and 12 h were the result of the insufficient biodegradation under the low operation temperature.

Keywords: anaerobic membrane bioreactor; real municipal wastewater; low temperature; biogas; anaerobic digestion.

1 Introduction

Recently, researches on wastewaters treatment solutions tend to achieve recovery or recycling purpose of energy and resources during the process for pollutants removal. Technologies have already been used for treating some kinds of industrial wastewaters or waste sludge and achieved the recovery or reuse of energy and resources have been reported while it is still a bit backward for applying in sewage treatment. The anaerobic membrane bio-reactor (AnMBR) integrates anaerobic digestion and membrane technology creating a new process which provided with the potential of energy recovery through the methane fermentation process in anaerobic digestion as well as the high efficiency of sludge-water separation due to the filtration by membrane. It also has been successfully applied in dealing with industrial wastewater and is considered to be a trustworthy process. If the process could be possibly applied for treating sewages as well, the wastewater treatment plants could also become net suppliers of energy, renewable resources and reclaimed water which would make a big contribution for the construction of sustainable social development. Some studies that related to the low organic strength wastewater or sewage based on man-made synthetic wastewater reported have confirmed that it is possible to be used for sewage treatment with a high efficiency of organic removal with less waste sludge produced as well as energy recovery from the produced biogas. A previous research based on synthetic sewage wastewater investigated the response of AnMBR to the temperature decreased from 25 to 10 on organic removal, membrane fouling and the microbial

community while lack of the biogas production performance. Furthermore, it is also unknown that it could be able to obtain the same effect when dealing with the real sewage wastewater.

Based on the results of successfully applied AnMBRs to the real sewage treatment in room temperature reported in previous studies, the AnMBR was used to dealing with the real sewage by operated temperatures at 15 °C (HRT 6 to 24 hours) in this study. The performance of sewages treated by AnMBR in different HRTs at low temperature condition was investigated in aspects on pollutant removal performance, gas yield, sludge yield, COD balance as well as the filtration performance.

2 Materials and methods

2.1 Consist of AnMBR and operation conditions

A 20L AnMBR with hollow fiber type membranes set inside was installed in Sen-En wastewater treatment plant (S-WWTP) located in Tagajo city, Miyagi prefecture of Japan. The influent of AnMBR was taken from the WWTP by a peristaltic pump (FP-100-1515, AS ONE, Japan). Solid-liquid separation was permeated using a micro-filtration module (MITSUBISHI CHEMICALS, Japan) by a peristaltic pump (FP-100-1515, AS ONE, Japan). Membrane module used in this research was a hollow fiber type polyvinylidene difluoride (PVDF) membrane with the pore size of 0.4 μ m.

2.2 Samples collection and analysis methods

Influent, effluent, and mixed liquor samples were regularly taken in order to analysis water quality index and the sludge traits. The analysis of COD, BOD, SS, mixed liquor suspended solid (MLSS) and mixed liquor volatile suspended solid (MLVSS) were in according with standard methods. The proportion of CH₄, CO₂, and N₂ in biogas produced was measured using a gas chromatograph (Shimadzu, GC-8A, Japan) equipped with a thermal

conductivity detector. Dissolved methane in the effluent was determined using a headspace technique which has been described by former researchers. All the methane measurements of methane gas were normalized to the standard temperature and pressure (STP: 0 degree, 1atm). The details was described in the previous research [1].

The COD balance was calculated for influent, permeate effluent, biogas produced (methane gas discharged), H₂S in the biogas produced, methane gas dissolved in the effluent and sludge growth, all was converted into COD value.

3 Results and discussion

Figure 1 shows the average COD and BOD in effluent as well as the average removal efficiency for COD, BOD and SS at different HRTs at low temperature conditions. According to the result, the effluent COD and BOD was decreased after the HRT was extended to 12 hours and the COD was finally decreased to under 40mg/L and the effluent BOD was around 10mg/L in HRT 16 and 24 hours. Therefore, the removal efficiency of COD and BOD was recovered to above 90% in HRT 16 and 24 hours. The above analysis shows that at low temperature conditions, organic removal efficiency was increased and recovered by extending HRT condition.

COD balance was calculated and shown in Figure 2. Compared with the HRT conditions of 6, 12 and 16 hours, it was found that COD amount in biogas produced was increased from the decrease of those COD amount of sludge growth and remained in effluent permeate. It was then obtained a further increase of COD amount as produced biogas due to the well biodegraded of solid organic matters as shown minus value of sludge yield in HRT 24 hours. Energy recovery potential could be generated well in HRT 16 and 24 hours as the COD amount was presented as 57.7% and 65.9%, respectively.

The TMP and flux recording data shown in Figure 3 presents the membrane performance during the long-term operation at 15°C low temperature. The CFV was declined to 116 m/h after HRT was extended to 12 hours or longer and TMP was stabled at an extremely low value in those conditions due to the smaller flux in long HRTs. This result shown that membrane filtration was performed very well in the conditions of HRT 12 hours to 24 hours even in the low temperature of 15°C.

As a result, HRT 6h at 15°C presented the weakness compared with the other conditions on organic removal, sludge yield, biogas production rate and methane content, while with strength on flux and sewage treatment capacity, with the additional data shown in Table 1. Among the HRTs implemented at 15°C low temperature, HRT 24h presented strengths on organic removal, sludge yield, biogas production rate and methane content, while the sewage wastewater treatment capacity during the HRT 24 hours was obtained only 20L per day which also resulted an underutilization operation for the AnMBR system during treatment process. Because of organic removal efficiency was not reach the standards in HRT conditions of 6 hours and 12 hours, those conditions cannot be applied in the sewage treatment in this situation.

Consequently, compared the HRTs implemented at low temperature of 15°C in this study, the suitable HRT was considered to be 16 hours in this case.

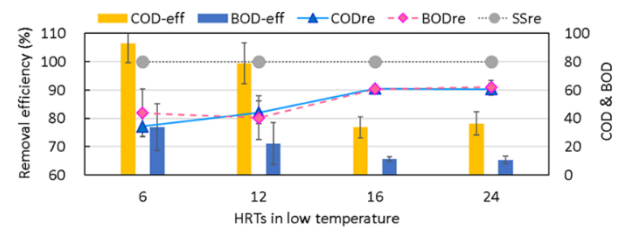


Fig. 1. Average COD, BOD, SS performance in different HRTs.

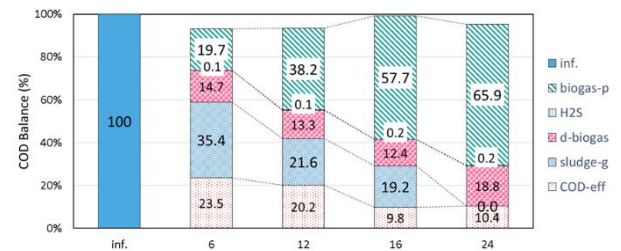


Fig. 2. COD balance in different HRTs (%).

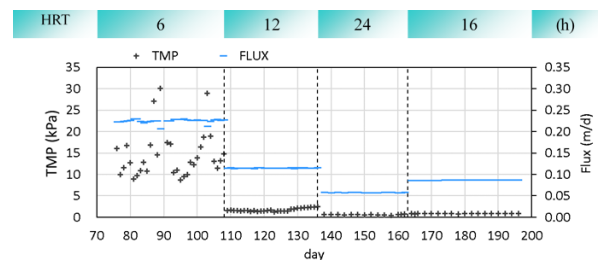


Fig. 3. TMP and flux during the long-term operation.

Table 1 Additional comparison for different HRTs.

HRT (h)	6	12	16	24
Sludge yield (g-VSS/g-COD _{rem})	0.35	0.21	0.16	-0.05
Biogas production rate (L-gas/L-water)	0.03	0.06	0.09	0.10
Methane content	66.85	74.72	80.82	80.99
Treatment capacity (L/d)	77.8	39.8	29.9	20.0

4 Conclusions

As operated at a low temperature of 15°C in different HRTs, the below conclusions can be obtained:

- (1) Applying AnMBR directly into the real sewage treatment at low temperatures, well organic pollutant removal performance with a low sludge yield could be achieved by extending the HRT condition.
- (2) A high energy recovery potential could be achieved by the generated biogas during HRT 16 and 24 hours at 15°C low temperature.

Reference

[1] J. Ji, S. Sakuma, J. Ni, Y. Chen, Y. Hu, A. Ohtsu, R. Chen, H. Cheng, Y. Qin, T. Hojo, K. Kubota, Y.Y. Li, Application of two anaerobic membrane bioreactors with different pore size membranes for municipal wastewater treatment, Sci. Total Environ. 745 (2020) 140903. <https://doi.org/10.1016/j.scitotenv.2020.140903>.

Efficient treatment of municipal wastewater and biogas production by a pilot-scale submerged anaerobic membrane bioreactor

○ Tianjie WANG^{1*}, Zhe KONG¹, Jiang WU¹, Yu QIN¹ & Yu-You LI¹

¹Laboratory of Environmental Protection Engineering, Department of Civil and Environmental Engineering, Graduate School of Engineering, Tohoku University, 6-6-06 Aza-Aoba, Aramaki, Aoba Ward, Sendai, Miyagi 980-8579, Japan.

Abstract

The operation performance of a pilot-scale submerged anaerobic membrane bioreactor (AnMBR) treating real municipal wastewater with an effective volume of 5.0 m³ was investigated at a temperature of 25°C. This demonstration plant realized a staged shortening of hydraulic retention time (HRT) from 48 h to 6 h, obtaining excellent effluent quality with the COD removal efficiency over 90% and BOD₅ removal over 95%. Biogas was recovered efficiently from municipal wastewater with a biogas production of 0.08-0.10 L L⁻¹ raw wastewater, and the methane content was 75%-80% in the biogas. A low sludge yield was also obtained in this study.

Keywords: anaerobic digestion; AnMBR; municipal wastewater; anaerobic wastewater treatment.

1 Introduction

The conventional activated sludge (CAS) process and its derivatives are the most common treatment of municipal wastewater and have been widely implemented all over the world. Despite the reliable effluent quality, the CAS process not only consumes a great quantity of energy for supplying oxygen, but also generates a large amount of excessive sludge. This research aims to develop an energy-saving and energy-creating wastewater treatment system by utilizing an anaerobic membrane bioreactor (AnMBR), combined by the anaerobic digestion treatment process and the membrane technology, which are rapidly undergoing technological development.

A demonstration plant using a pilot-scale AnMBR was conducted to investigate the anaerobic wastewater treatment performance of real municipal wastewater. As a result of long-term continuous experiments with the hydraulic retention time (HRT) shortened from 48 h to 6 h at 25°C, the COD and BOD₅ removal efficiency reached 90% and 95%, respectively. Biogas was recovered efficiently from municipal wastewater with a biogas production of 0.08-0.10 L L⁻¹ raw wastewater, and the methane content was 75%-80% in the biogas.

2 Materials and methods

The Schematic diagram of the AnMBR system is shown in Fig. 1. The influent of the AnMBR was pumped from the grit chamber effluent of a full-scale municipal treatment plant to the raw wastewater tank. The raw wastewater was treated by a drum screen to remove impurities. The effective volume of AnMBR was 5 m³, the liquid level was maintained at a height of 1910 mm, and both the raw wastewater tank and AnMBR were kept at 25°C by a constant temperature water bath system. The membrane module consisted of a total of 12 hollow fiber membrane elements, with a total membrane area of 72 m² (6 m² for each element). The hollow-fiber membrane is made of polyvinylidene fluoride (PVDF) and has a pore diameter of 0.4 μm and an outer diameter of 2.8 mm. The membrane filtration operation was 5 minutes per cycle (4 minutes for filtration, 1 minute for relaxation). Membrane maintenance method was the online back-wash applying sodium

hypochlorite (NaClO) solution and citrate solution. Biogas production was measured by a wet gas meter. The actual gas temperature (°C) and atmospheric pressure (hPa) were measured by a thermometer located outside the AnMBR. Biogas volume was standardized and calculated under the conditions of 273.15 K and 1013.25 hPa. The components of biogas including N₂, CH₄ and CO₂ were measured by gas chromatograph (GC-8A, Shimadzu, Japan).

The pH of influent, sludge, and effluent was measured in situ using a pH meter (D-71, HORIBA, Japan). AnMBR tank internal pressure (kPa), filtration flow rate (L min⁻¹), and influent and sludge temperature were detected by an automatic control system. An online transmembrane pressure (TMP) sensor displayed real-time TMP fluctuations and saved the data in the automatic control system. The Temperature, atmospheric pressure, biogas production, biogas components, and TMP were recorded daily.

Liquid samples containing influent, sludge, and effluent were collected three times a week in a 250 mL plastic sampling bottles and measured for alkalinity, COD_{Cr} (hereinafter referred to as COD), BOD₅, and ammonia-nitrogen (N-NH₄⁺). Measurements of sludge concentration represented by mixed liquor suspended solids (MLSS) and mixed volatile suspended solids (MLVSS) were measured once a week during the experimental period.

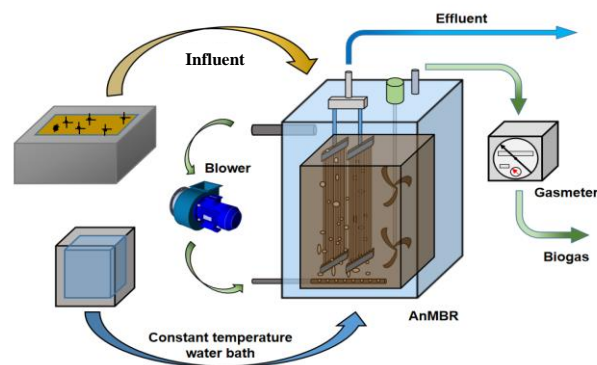


Fig. 1. Schematic of Pilot AnMBR.

3 Results and discussion

As shown in Fig. 3, the temperature of the raw wastewater and AnMBR was maintained at 25°C by the constant temperature water bath system. AnMBR was operated from the condition of HRT 48 h, and the COD removal efficiency gradually increased from 51.0% to 82.9%. This period was considered the start-up period. After nearly a month, HRT was gradually shortened to 24 h, 12 h, 8 h, and 6 h. The HRT was set to 8 h eventually because the TMP exceeded the reasonable limitation (30 kpa) under the 6 h HRT operating conditions.

AnMBR has achieved a COD removal efficiency of over 90% and a BOD₅ removal rate of over 95% during stable operation. The effluent COD concentration was basically lower than 50 mg L⁻¹, and the BOD₅ concentration was 10 mg L⁻¹. These result shows the excellent municipal wastewater treatment performance of the pilot-scale AnMBR at 25°C.

The biogas production was relatively low while the HRT was 48 h and 24 h, but it increased dramatically when the HRT was shortened to the stable operation period of 12 h, 8 h. The methane content of biogas exceeded 75%, reaching a maximum of 81%. The biogas production rate from the raw influent was about 0.11 L L⁻¹ raw water, and the gas component was about 75% - 81% for methane, 5% - 9% for carbon dioxide, and 12% - 17% for nitrogen gas.

The membrane filtration operation mode was 4 minutes for filtration and 1 minute for relaxation, and the membrane surface was continuously washed at a biogas sparging rate of 0.9 m³ min⁻¹. The membrane filtration performance during the experimental period is shown in Table 1. ΔTMP was relatively stable During the 48 h, 24 h, and 12 h HRT periods, which were less than approximately 5 kPa. While ΔTMP gradually increased and exceeded 10 kPa, it is possible to perform online membrane backwash chemical cleaning of 500 ppm NaClO to decrease ΔTMP. When the HRT was 6 h, the maximum real-time flux was 0.33 m d⁻¹, meanwhile the membrane fouling occurred during this period progressed very quickly, and the recovery effect of the membrane filtration performance by chemical cleaning was limited.

As a method of maintaining the membrane filtration performance, the MLSS concentration was maintained at 8000-10000 mg L⁻¹, otherwise biogas sparging and online chemical cleaning were performed simultaneously, but proper flux and operation mode are also crucial.

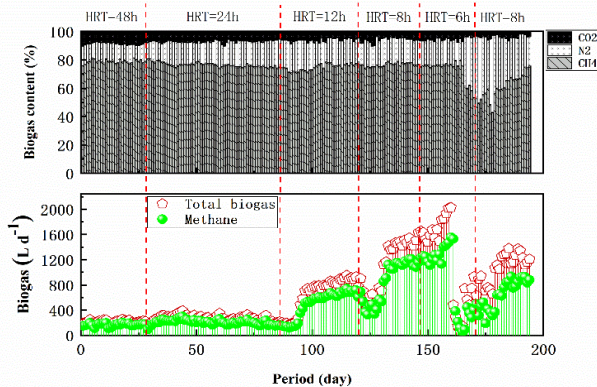


Fig. 2. Biogas production and content.

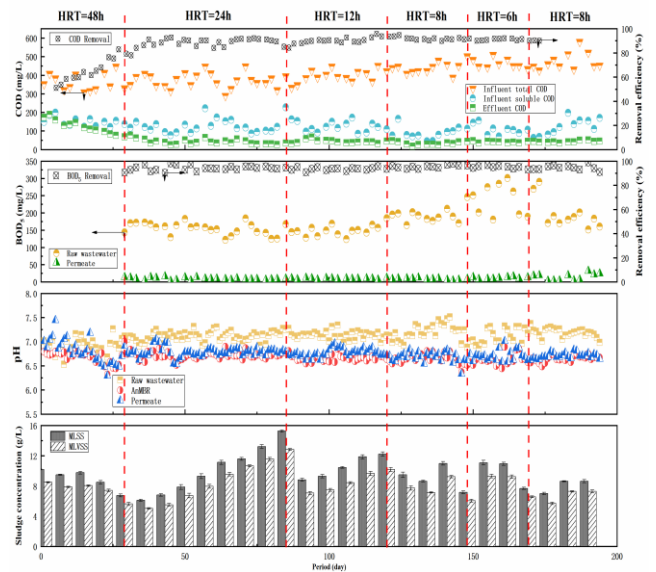


Fig. 3. Long-term performance of Pilot AnMBR.

Table 1 Membrane performance of different HRT.

Period (day)	HRT (h)	Flux (m d ⁻¹)	ΔTMP (kPa)
1-28	48	0.057	0.90-2.60
29-91	24	0.085	2.20-10.7
92-119	12	0.205	2.30-3.10
120-147	8	0.289	3.80-12.7
148-175	6	0.329	6.00-23.5
176-196	8	0.259	10.2-22.1

4 Conclusions

1) The pilot-scale AnMBR with an effective volume of 5 m³ realized effectively treating actual municipal wastewater at 25°C for the HRT of 6 h. The COD removal efficiency was over 90%, and the BOD₅ removal efficiency was over 95%. The biogas production rate from the influent was about 0.11 L L⁻¹ raw wastewater, and the gas component was about 75%-81% for methane, 5%-9% for carbon dioxide, and 12%-17% for nitrogen gas.

2) Stable membrane filtration was realized with a flux of 0.06-0.29 m d⁻¹ and a ΔTMP of 0.90-12.7 kPa under the conditions of HRT 24 h, 12 h and 8 h. However, at the maximum flux of 0.33 m d⁻¹, ΔTMP increased rapidly, and rapid membrane fouling was observed. The stable operation working flux realized in this study was about 0.30 m d⁻¹.

Reference

[1] Kong, Z., Wu, J., Rong, C., Wang, T., Li, L., Luo, Z., Ji, J., Hanaoka, T., Sakemi, S., Ito, M., Kobayashi, S., Kobayashi, M., Qin, Y., Li, Y.-Y., 2021. Large pilot-scale submerged anaerobic membrane bioreactor for the treatment of municipal wastewater and biogas production at 25 °C. *Bioresour. Technol.* 319, 124123. <https://doi.org/10.1016/j.biortech.2020.124123>

High solid mono-digestion and co-digestion performance of food waste and sewage sludge by a thermophilic anaerobic membrane bioreactor

○ Shitong ZHOU¹, Yemei LI², Hui CHENG², Guangze GUO¹, Yu-You LI^{1,2}

¹Department of Frontier Science for Advanced Environment, Graduate School of Environment Studies, Tohoku University, 6-6-06 Aoba, Aramaki-Aza, Sendai, Miyagi 980-8579, Japan.

²Department of Civil and Environmental Engineering, Graduate School of Engineering, Tohoku University, 6-6-06 Aoba, Aramaki-Aza, Sendai, Miyagi 980-8579, Japan.

*E-mail: zhou.shitong.q2@dc.tohoku.ac.jp.

Abstract

The performance of co-digestion of food waste (FW) and sewage sludge (sludge) by a thermophilic anaerobic membrane bioreactor (ThAnMBR) was firstly investigated. The long-term stable operation showed the feasibility of the utilization of ThAnMBR for mono- and co-digestion of FW and sludge at a high solid condition. Good permeate quality was obtained at all sludge ratios while the addition of sludge restricted the methane generation. For a sludge substitution with 25% TS-based substrate, the biogas yield of 0.812 L/g-VS_{fed} was at 91% and 158% that of the mono-digestion of FW and sludge respectively. Membrane performance indicated that the ThAnMBR operated stable at a high flux of 5 LMH under the high solid (~27 g/L) condition. Furthermore, membrane filtration with a 0.1 μm pore size of hollow fiber not only completely removed suspended solids but also rejected about 70% of soluble COD, 80% of soluble carbohydrates and 17% of soluble proteins.

Keywords: AnMBR; Biogas; Sewage Sludge; Food waste; Co-digestion.

1 Introduction

Since the annual waste biomass production is considerable, it is an advisable option to utilize the bioenergy to cut emissions and save resources. Anaerobic digestion (AD) plays an important role in bioenergy utilization from waste biomass in the circular society. As a multifunctional waste treatment tool, it is currently one of the most promising processes used for the treatment of various organic waste-streams, and offers significant benefits, such as greenhouse gases reduction, energy production in the form of methane-rich biogas and water purification with low energy demand.

As two of most common organic fraction of municipal wastes, sewage sludge and food waste (FD) have huge bioenergy potential. However, the AD process of each substrate both has drawbacks respectively, such as low methane yield of sewage sludge due to low C/N and possibility of volatile fatty acid accumulation and unstable operating condition of food waste because of relatively lack of nitrogen. And co-digestion is an efficient method to deal with these problems and improve biodegradation performance. A mono-digestion system involves only one substrate in the AD process, whereas a co-digestion system involves the instantaneous digestion of two or more types of feedback. The co-digestion system has been shown to have better process efficiency than the mono-digestion system with regard to process stabilization, nutrient balance, toxicity dilution, robust microbiome and ecological sustainability.

One of the biggest challenges of AD process is the poor retention of slow-growing anaerobic biomass. In contrast, anaerobic membrane bioreactor (AnMBR) can

provide many economic and environmental advantages, including smaller footprint, less sludge production, higher biomass retention, higher organic matter biodegradation efficiency and more excellent effluent quality. In the thermophilic anaerobic membrane bioreactor (ThAnMBR), membrane bioreactors are placed under thermophilic condition, typically within a temperature range of 50-60 °C, which guarantee a rapid biodegradation rate. The main purpose of this study is to investigate the feasibility of co-digestion of FW and sludge by a ThAnMBR based on long-term performance analysis.

2 Materials and methods

2.1 Substrate: FD and sludge

According to previous researches, the FW in this study was prepared based on the composition of FW in Japanese daily life. The sludge used in the experiment was consisted of primary sludge and excess sludge collected from a municipal wastewater treatment plant in Sendai, Japan. The sludge composition is based on total solid (TS) content, with 45% TS coming from primary sludge and the rest TS content coming from excess sludge, which was the same as a typical composition of sludge in Japan. As for substrate composition, FW was gradually replaced by sludge at TS ratios of 0%, 25%, 50% and 100% in different experimental phases.

2.2 Configuration of ThAnMBR and system operation

The ThAnMBR used in this study was an external AnMBR, and the schematic diagram is shown in Fig. 1. The total effective volume of ThAnMBR was 15 L, consisted of a continuously stirred tank reactor (CSTR) of 13 L and a membrane unit of 2 L. A hollow fiber membrane with pore

size of 0.1 μm and membrane area of 0.1 m^2 was inserted in to the membrane unit. The AnMBR was maintained at a thermophilic condition of 55 ± 1 $^\circ\text{C}$.

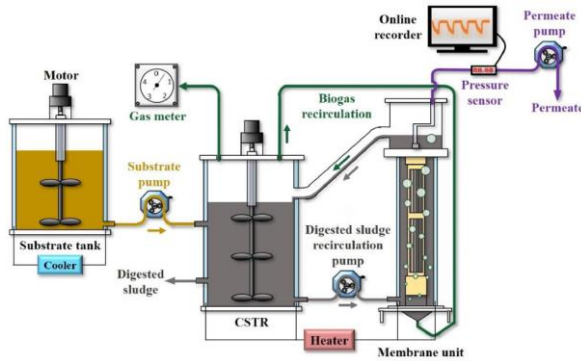


Fig. 1. The schematic diagram of the ThAnMBR

Four different kinds of substrate containing 0%, 25%, 50% and 100% of sludge were implemented in four phases respectively, during the long-term experiment. The average TS loading rate was kept at 3.20 ± 0.30 $\text{kg-TS}/\text{m}^3/\text{d}$. Membrane filtration was operated under a mode of filtration cycle included 3 min of filtration and 3 min of relaxation continuously.

3 Results and discussion

3.1 Biogas production and organic removal

The ThAnMBR system was successfully operated for over 180 days, and the ratio of 25% was considered to be the best addition ratio of sludge to the co-digestion of sludge and FW. During all the phases, the CH_4 and CO_2 content of biogas was very stable. However, the biogas production rate decreased from 2.84 to 1.31 $\text{L}/\text{L-reactor}/\text{d}$ and biogas yield decreased from 0.893 to 0.428 $\text{L}/\text{g-VS}_{\text{fed}}$ as the sludge ratio increased from 0 to 100%. The change of biogas production with different sludge ratios may be related to the organic composition of the substrates, especially the amount of carbohydrates, which have higher degradation rate. The rich carbohydrates, especially the soluble part, in FW made up for the low carbohydrates in sludge in the 25% sludge co-digestion system and further resulted in an obviously enhanced methane production compared with that of 100% sludge phase.

The quality of the permeate also can be used to assess the stability of the system. The stable concentration of TVFA at a low lever reflected steady digestion performance. The removal efficiency of the ThAnMBR system was excellent for each sludge ratio. The average removal efficiency of COD, VS, TS, carbohydrates and proteins were $97.8 \pm 0.9\%$, $97.3 \pm 1.0\%$, $93.1 \pm 1.0\%$, $99.3 \pm 0.4\%$ and $95.7 \pm 2.5\%$ respectively. The results of biogas production and organic removal efficiency are shown in Table 1.

Table 1 Effect on sludge ratio on biogas production and organic removal efficiency.

Items	Unit	Sludge ratio (%)			
		0	25	50	100
Duration	Days	~26	~69	~122	~179
Organic loading rate	$\text{kg-COD}/\text{m}^3/\text{d}$	5.44	4.91	3.84	4.31
Biogas production rate	$\text{L}/\text{L-reactor}/\text{d}$	2.84 ± 0.21	2.51 ± 0.26	1.54 ± 0.26	1.31 ± 0.08
Biogas yield	$\text{L}/\text{g-VS}_{\text{fed}}$	0.893	0.812	0.596	0.514
Removal efficiency	TS	93.1	94.4	92.9	91.9
	VS	97.9	98.4	97	96.1
	COD	98.7	98.3	97.3	96.7
	Proteins	96.3	96.6	97.7	92.1
	Carbohydrates	99.7	99.5	99.5	98.7

3.2 Membrane rejection and long-term operation

The rejection efficiency shows the ability of the membrane module to intercept substances. An obvious rejection of organic substances by the membrane under different sludge ratios is presented in Fig. 2(a). And a comparison between the concentration of S-COD, S-proteins and S-carbohydrates in digested sludge and permeate were conducted. The linear regression results showed that about 70% of S-COD in the digester was rejected by the membrane filtration and 17% and 80% for S-proteins and S-carbohydrates, respectively. (Fig.4(b), (c) and (d)).

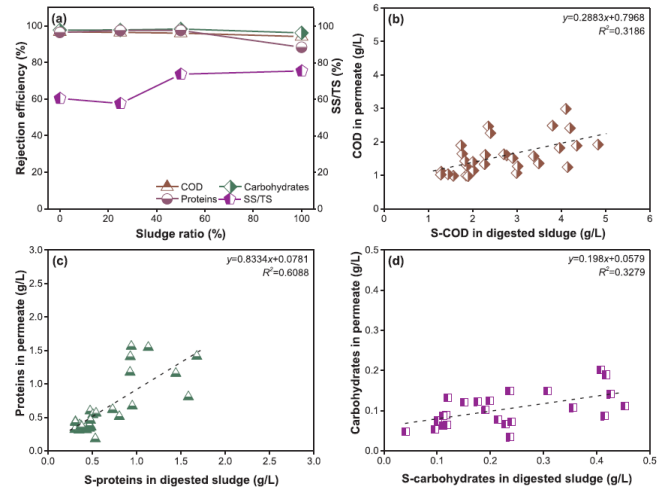


Fig. 2. (a) Rejection efficiency of COD, carbohydrates proteins by the membrane and SS/TS ratio of digested sludge at different sludge ratio; The retention of (b) S-COD, (c) S-proteins and (d)-carbohydrates by the membrane.

Membrane fouling is an unavoidable problem in the utilization of the membrane reactor. And solid in the digested sludge is an important cause of membrane fouling. In this study, the solid concentration of the ThAnMBR kept at a high level of 27.29 ± 3.34 $\text{g-TS}/\text{L}$ on average with a ratio of SS to TS over 57%. The long-term experiment results reveal that the ThAnMBR can be operated under a high flux mode (~ 5 LMH) at a high solid concentration (~ 27 g/L) and solid concentration showed a significant influence on the membrane performance. Except for the influence of solid concentration, the generation of white crystal in the permeate pipeline in 50% and 100% sludge period had a markedly deleterious effect on the membrane performance.

4 Conclusions

The mono- and co-digestion of FW and sludge were operated successfully by a ThAnMBR system at a high flux of 5 LMH under a high solid condition of 27 g/L . Biogas production changed greatly, from 0.893 to 0.514 $\text{L}/\text{g-VS}_{\text{fed}}$, with the sludge ratio increased from 0% to 100%. The membrane filtration rejected about 70% of soluble COD and had a higher rejection of soluble carbohydrates than soluble proteins.

Reference

[1] Li, Y.M. et al, High solid mono-digestion and co-digestion performance of food waste and sewage sludge by a thermophilic anaerobic membrane bioreactor, Bioresour. Technol, 310 (2020) 123433.

Methane Fermentation of Lipid-Rich Food Waste by a Hollow Fiber Type Anaerobic Membrane Bioreactor

○ Ziang HE^{1*}, Yuanyuan REN², Chen WANG² & Yu-You Li²

¹Department of Frontier Science for Advanced Environment, Graduate School of Environmental Sciences, Tohoku University, 6-6-20 Aoba, Aramaki-Aza, Aoba-Ku, Sendai, Miyagi 980-8579,

²Department of Civil and Environmental Engineering, Tohoku University, 6-6-06 Aramaki Aza Aoba, Aoba-ku, Sendai, Miyagi, 9808579, Japan

*E-mail: he.zi.ang.p8@dc.tohoku.ac.jp

Abstract

In this study, the performance of a mesophilic (37°C) HF-AnMBR (hollow fiber type anaerobic membrane bioreactor) in treating lipid rich food waste for 180 days is studied and its effectiveness is evaluated. The lipid rich food waste used in this study was made according to the pervious study. The organic loading rates (OLR) of HF-AnMBR was gradually increased from 1.63g-COD/L/d to 13.54 g-COD/L/d by increasing the lipid content from 10%, 30% and 50%. Respectively, the COD conversion efficiency was as high as 98%, 97% and 98% at OLRs of 3.27, 10.69 and 13.45 g-COD/L/d. Meanwhile, membrane fouling is the serious problem for MBR, which affects the performance of reactor, so the relationship between the reversible fouling resistance and irreversible fouling resistance was evaluated by this kind of substrate under flux of 3 L/m²/h. The long-term stable performance of AnMBR indicates that lipid rich food waste was suitable to decompose under condition of mesophilic.

Abstract: Food waste, lipid, co-digestion, AnMBR

1 Introduction

Nowadays, wastewater treatment plants have to face critical issue with strict regulation of water discharge quality. The food industry generates a plenty of milk product waste in stock breeding. According to the key facts on food loss and food waste by the Food and Agriculture Organization of the United Nations (FAO), 1/3 of food is lost or wasted during production process and human consumption globally [1]. The increasing production of food waste like milk product waste worldwide and new international regulations call for the development of new technologies to treat this biowaste. Due to high-organic content (81.9%) of food waste, many researchers have investigated the use of the anaerobic digestion in treatment of food waste, which are able to treat organic wastes efficiently, producing at the same time different value-added compounds, such as methane.

However, in anaerobic digestion system, HRT and sludge retention time (SRT) is the same parameter compare to conventional activated sludge process (CAS). Meanwhile, due to the low growing rate of archaea. The anaerobic digestion system needs a large reactor volume to maintain capability of treatment [2]. In recent years, anaerobic membrane bioreactor (AnMBR) was invented, which is able to separate HRT and SRT by retaining solids within reactor and discharging permeate through membrane filtration. This combination of MBR with anaerobic digestion brings a high biomass of archaea, which contribute to high organic loading rate (OLR). Meanwhile, applying co-digestion could be one of methods to improve the biogas yield and stability of the anaerobic digester by providing some ways i.e. adjustment of moisture content; supplying trace metal elements; maintaining an optimal pH, enhance capacity of buffer.

2 Materials and methods

2.1 Materials

The composition of the food waste used in this study is based on the earlier research, including fruit, vegetables,

meat, fish, eggs and staple foods. Which is 30%, 36%, 14% and 20%.

Table 1 Characteristics of inoculum sludge

Parameters (mg/L)	Inoculum sludge
pH	7.28-7.50
Total COD (g/L)	24.6±0.27
Total Carbohydrates	1862±99
Total Protein	13617±34
TS (g/L)	26.75
VS (g/L)	21.92
TSS (g/L)	22.62
VSS (g/L)	19.21
NH ₄ ⁺ -N	1316.38

Table 2 The composition of the food waste used

Item	Componot	Percentage in wet base
Fruit (30%)	Apple	10%
	Grapefruit (rind)	5%
	Orange (rind)	5%
	Banana (rind)	10%
Vegetables (36%)	Cabbage	12%
	Potato	12%
	Carrot	12%
Meat, fish and eggs (14%)	Meat	5%
	Fish (with born)	5%
	Egg	4%
Staple foods (20%)	Rice	10%
	Bread	5%
	Noodles	2.5%
	Chinese noodle	2.5%
Total TS		20%

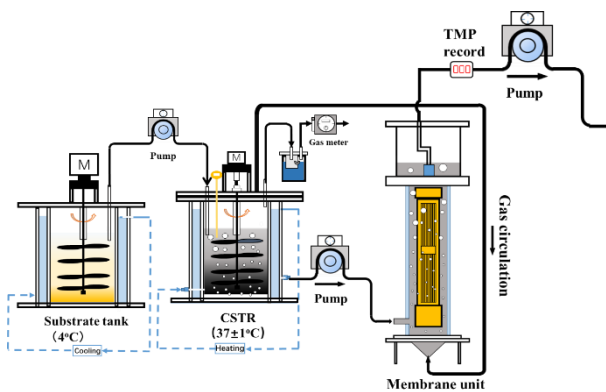


Fig. 1. diagram of HF-AnMBR used in the test

2.2 Analysis methods

Daily biogas production is measured by wet gas meter, the composition of (CH₄, CO₂ and N₂) were measured by a Shimadzu GC-8A gas chromatograph, and COD, carbohydrate, protein, ammonium nitrogen, alkalinity, TS, TSS, VS and VSS were measured according to Japan Standard Testing Method. Sludge samples were taken from the digesters and the substrate tank three times a week. The total effective volume was 15L. The membrane unit was made of polytetrafluoroethylene, with a mean pore size of 0.2 μm and an effective filtration area of 0.1 m².

3 Results and discussion

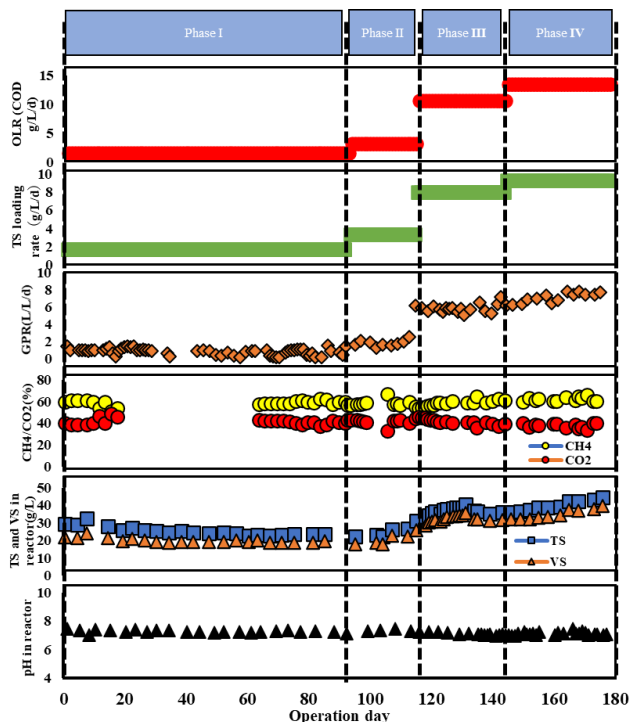


Fig. 2. Reactor performance.

The long-term operation of HF-AnMBR is shown in Fig 2. the HF-AnMBR was operated at 4 phases with different OLRs about 1.63, 3.27, 10.69, and 13.45 g-COD/L/d, when the feeding lipid-rich food waste consisted of 10%, 30%, 50% of lipid, respectively. HRT of Phase I is 30d, the rest of phase

is 15d, After a successful start-up (phase I), at lipid content of 10, 30 and 50%, the biogas production rates were 1.79 ± 0.3 , 5.79 ± 0.3 , 7.09 ± 0.57 L/L/d, respectively. The corresponding methane yields were 0.31 ± 0.1 , 0.67 ± 0.2 , 0.74 ± 0.2 , and 0.79 ± 0.2 L/g-VS, respectively. While the gradual increase of the methane yield was mainly attributed to the increasing of lipid content. pH in the reactor remained around 7.2. CH₄ and CO₂ content of biogas were stable, in the range of 58.1-61.9% and 38-41.3%, respectively. At phase IV, the OLR was 13.45g COD/L/d with 50% of lipid content, without any inhibition phenomenon like decrease of biogas production or drop of pH in reactor, this phenomenon was disagreement with the results from a previous study: it was reported that methanogens were severely inhibited when OLR was over 14.58 g COD/L/d, actually, there is no accumulate of VFA at all phase, which means a great potential ability of the HF-AnMBR to lipid-rich food waste with over 50% of lipid content. This can be attributed to the high concentration of digestion sludge in the reactor, the TS of digestion sludge was over 23.3, 23.9, 3.6, and 4.2 g/L at each phase. The high concentration of digestion sludge owing to rejection of membrane, preventing the washout of slow-growing methane-forming anaerobic microorganisms.

4 Membrane resistance distribution

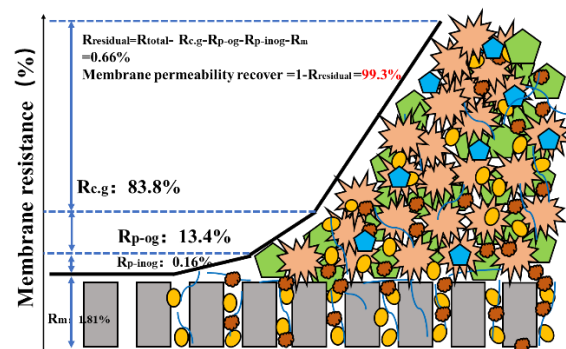


Fig. 3. Membrane fouling

The most of membrane resistance is cake layer and gel gal layer. which was contribution 83.8% to the total resistance. Next is organic matter in pore, which was contribution 13.4% to total resistance, rest of them is inorganic matter in pore and intrinsic membrane resistance, which was contribution 0.16% and 1.81% to the total resistance. With a combination of physical and chemical cleaning, helped membrane permeability recover as high as 99.3%. These results are clear evidences of the great necessity of chemical cleaning in high-strength organic wastewater treatment by AnMBR in order to recover the initial membrane permeability.

5 Conclusions

In this study, we applied the HF-AnMBR to digest the artificial lipid-rich food waste with different contents of lipid. Operating the HF-AnMBR treating lipid-rich food waste with around 10%-50% of lipid resulted in stable long-term performance. There is no inhibition phenomenon shows up during each phase due to a high concentration of biomass. The largest contribution to membrane fouling was made by cake layer and gel layer, followed by the organic fouling and inorganic fouling, accounting for 83.8%, 13.4%, and 0.16% of the total hydraulic resistance, respectively.

Startup of a pilot-scale anammox reactor for municipal wastewater treatment and biofilm formation

○ Zibin LUO^{1*}, Jiang WU^{1,2}, Yu-You LI^{1,3}

¹Department of Civil and Environmental Engineering, Tohoku University, Miyagi 980-8579, Japan

²Center for Material Cycles and Waste Management Research, National Institute for Environmental Studies, Tsukuba, 305-8506, Japan

³Graduate School of Environmental Studies, Tohoku University, Miyagi 980-8579, Japan

*E-mail: luo.zibin.q1@dc.tohoku.ac.jp.

Abstract

As conventional biological nitrogen removal process showing the shortage of high energy consumption and large floor area in wastewater treatment, anammox process, a brand new technology treating ammonium-rich wastewater efficiently, had attracted special interest recently. This study presents a successful start-up strategy of a partial nitrification-anammox (PNA) process to achieve a high nitrogen removal in the treatment of municipal wastewater. A pilot-scale anaerobic membrane bioreactor (AnMBR) was set up by coupling with an PNA reactor for testifying the feasibility for municipal wastewater treatment. After 240-days operation, the results showed that nitrogen removal efficiency of higher than 70% had been achieved at 3-hour hydraulic retention time when the ammonium concentration of the influent was about 35 mg-NH₄⁺-N/L. In the later period, biofilm formation had been observed from the scanning electron microscope.

Keywords: Partial nitrification; Anammox; Biofilm; Municipal wastewater.

1 Introduction

Anaerobic ammonium oxidation (anammox), is a cost-effective and sustainable approach for the removal of ammonium from wastewater or waste gas. In this efficient process, ammonium could be combined with nitrite to generate nitrogen gas by anammox bacteria. Compared with the conventional nitrification/denitrification process, anammox process could be carried on only in a single reactor which is compact with a small footprint, achieving low nitrogen concentration in effluent and high nitrogen removal efficiency. As a brilliant shortcut in the natural nitrogen cycle, the anammox conversion is destined to be an energy-saving process, in which 60% of operational costs or energy consumption could be saved, and CO₂ emission is reduced also.

For the reason that nitrite, the necessary substrate in anammox process, is rarely found in the common wastewater, it is vital to generate nitrite to promote anammox process to remove the ammonium. However, partial nitrification and anammox (PNA) remained the most usual way to treat ammonium-rich wastewater with wide range of applications.

According to the recent studies, PNA had been applied at full scale for treating high-strength ammonium wastewater (the concentration is over 100 mg/L) with high nitrogen removal efficiency, which is part of the state of the art now. But when it is referred to the low-strength ammonium wastewater, fewer studies had been done to prove its feasibility. However, a latest lab-scale works achieved high nitrogen removal efficiency of 75 ± 10%, using a moving bed biofilm reactor at a short HRT of 2 h when the influent ammonium concentration was 50 mg/L.^[1] By being attached to the carriers and forming the biofilm, anammox bacteria and AOB could avoid being washed out at such a short HRT and therefore, be retained in the PNA reactor.

In this study, a pilot-scale PNA reactor was started up with an anaerobic membrane bioreactor (AnMBR) which could

provide low COD/BOD concentration and low-strength ammonium wastewater. The aim of the study was to focus on (1) the treatment performance of PNA under various operation patterns or stages; (2) the biofilm formation to reveal the feasibility for practical application.

2 Materials and methods

2.1 Reactor Setup and Operation

The moving bed biofilm reactor (MBBR) possesses a working volume of 1.67 m³, equipped with a stirrer, a pH sensor and a NH₄⁺-N sensor. Hollow cylinder carriers, which made of hydrophobic polypropylene resin, were added into the reactor until the filling rate of 15%. Air would be pumped into the bottom of the reactor to supply the oxygen, which could be regulated by a rotameter attached. Artificial influent was transferred by a peristaltic pump while the effluent of AnMBR was supplied by an impeller pump. Mixed liquid from PNA reactor would flow into a 1.92 m³ radial-flow sedimentation tank and the collected sludge in the bottom was refluxed into the PNA reactor through an impeller pump. The sludge containing AOB were inoculated in the reactor and supplied with synthetic wastewater for proliferation. Anammox seed sludge were inoculated into the reactor in Day 91 and fed with synthetic wastewater as well. DO concentration and pH in the effluent were regularly measured using a DO meter (HORIBA HC-200NH, Japan) and a portal pH meter (HORIBA D-71, Japan), respectively.

The operation condition is shown in Table 1.

2.2 Sampling and analytical methods

All of the samples of influent and effluent were analyzed after being filtrated through Millipore filter units with 0.45 μm pore size. The NH₄⁺-N, NO₂⁻-N, and NO₃⁻-N concentration was measured by capillary electrophoresis (Agilent 7100, Agilent Technologies, USA).

Table 1 Operation Conditions

Stage	I	II	III	IV	V
Duration (day)	0-90	91-166	167-187	188-205	206-240
Influent type	SW		SW&MW		MW
Influent ammonia concentration (mg-NH ₄ ⁺ -N/L)	250	400-850	150	120	35
HRT (Days)	1	8.35	0.47	0.24	0.12
NLR (g-N/L/d)	0.24	0.05-0.10	0.32	0.5	0.3

SW: synthetic wastewater; MW: municipal wastewater; SW&MW: the mixture of synthetic and real municipal wastewater.

3 Results and discussion

3.1 Reactor Performance

The experiment, which had lasted for 240 days, contained 5 stages: (I) the AOB cultivation period; (II) the anammox bacteria cultivation period; (III) the SW&MW adaption period; (IV) the decreasing HRT period; (V) the stable operation period.

As is shown in Fig.1, during the stage I, in which aiming at AOB proliferation and NOB inhibition, success had been achieved due to the high FA/FNA concentration. After being inoculated and fed with synthetic wastewater, Anammox bacteria showed slowly growing activity with increasing NLR and nitrogen removal efficiency of up to 79% had been obtained in the end of stage II. Even though the ammonium concentration of influent had been dropped to 150 mg/L by using the mixture of synthetic and real municipal wastewater in the stage III, or in the case that NLR was increased to 0.5 mg-N/L/d in stage IV, AOR and ANR showed obvious increasing trend to 0.3 g-N/L/d and 0.4 g-N/L/d respectively, while NOR kept low. Finally, 80%-nitrogen removal efficiency had been achieved when low-strength ammonium wastewater with concentration of about 35 mg/L was treated in the stable operation period (stage V).

3.2 Biofilm formation

According to the Fig.2, the surface of carriers had been covered with pink and light red bacteria, which were possibly anammox bacteria. However, biofilm had been formed initially, which remained to be observed in the further study.

4 Conclusions

Efficient treatment for low-strength ammonium wastewater was achieved by using a one-stage PNA pilot plant with the nitrogen removal efficiency of 80% in the case of 3h HRT. The biofilm was under formation, which deserves for further study and observation.

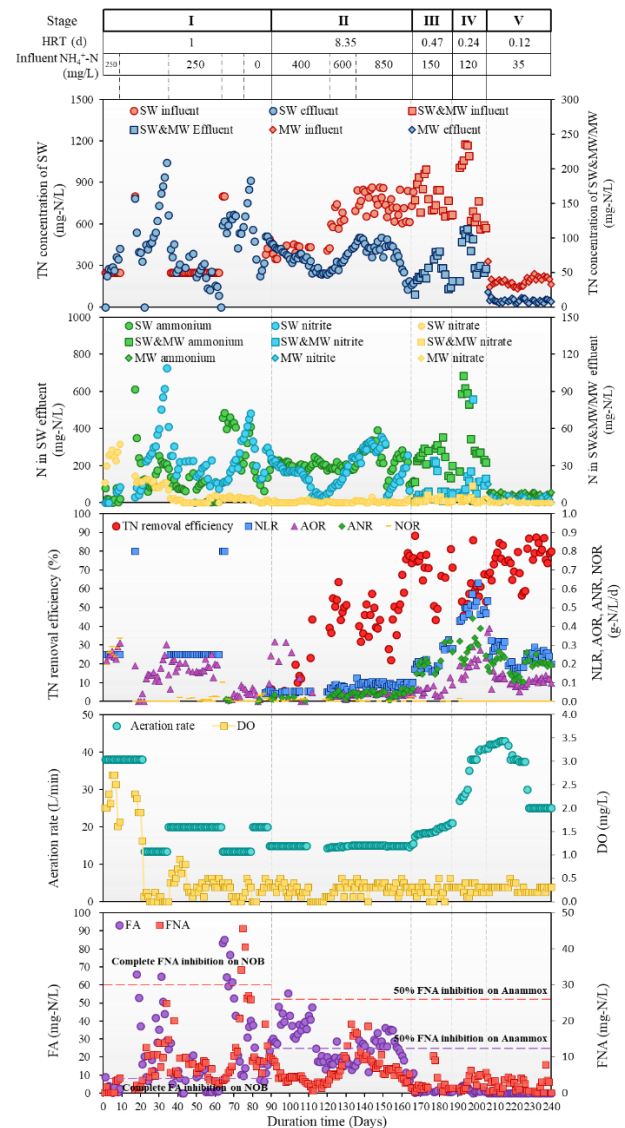


Fig. 1. Reactor Performance

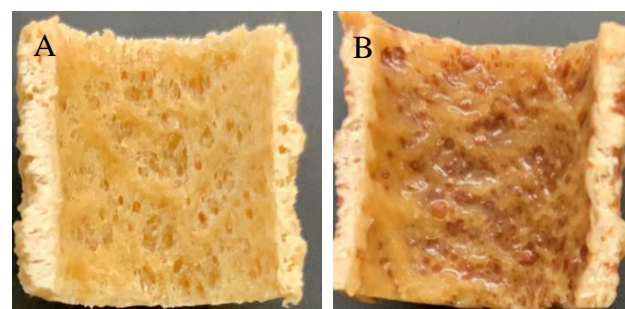


Fig. 2. Cross section of (A) new carrier; (B) carrier in stage V

Reference

[1] Rong Chen, Using Partial Nitrification and Anammox To Remove Nitrogen from Low-Strength Wastewater by Co-immobilizing Biofilm inside a Moving Bed Bioreactor, ACS Sustainable Chemistry & Engineering (2019) 1353-1361.

Biofilm characterization and operation performance in a single stage partial nitritation/anammox process with a function carrier

○Yunzhi QIAN^{1*}, Yan GUO², Junhao SHEN¹& Yu-You LI^{1,2}

¹Graduate School of Environmental Studies, Tohoku University, Miyagi 980-8579, Japan.

²Department of Civil and Environmental Engineering, Tohoku University, Miyagi 980-8579, Japan

*E-mail: qian.yunzhi.q8@dc.tohoku.ac.jp

Abstract

For single-stage partial nitritation/anammox (SPNA) process in cost-effective nitrogen treatment, the addition of functional carriers can avoid the loss of biomass and strengthen the functional bacteria activity. In this study, the biofilm characterization and operation performance were investigated at 25°C for more than one year using function carriers. In the biofilm maturation stage, a NRR of 0.78 gN/L/d was obtained with the SAA of 0.34 gN/gMLVSS/d. The accumulation of inorganic components in biofilm aging stage caused the biomass concentration in the biofilm to decrease from 4.50 gMLVSS/L to 2.50 gMLVSS/L, resulting in a decrease in the nitrogen removal rate (NRR) from 0.74 gN/L/d to 0.36 gN/L/d. Besides, the cavity created by the accumulation of nitrogen gas also reduces the effective biomass of anammox bacteria in the biofilm. After mechanical stirring, NRR can recover from 0.36 gN/L/d to 0.75 gN/L/d within 3 days. The regeneration of biofilm promotes the substrate exchange capacity of microorganism, which is the key to the restoration of SPNA nitrogen removal capacity.

Keywords: Partial nitritation; Anammox; Carrier; Biofilm

1 Introduction

Partial nitritation-anammox (PNA), as the emerging and low-cost biotechnological nitrogen removal process, is especially suitable for high-strength ammonium wastewater, such as anaerobic digestion wastewater. High concentration of NH₄⁺-N is beneficial to inhibit the activity of nitrite oxidizing bacteria (NOB) and promote the growth of anaerobic ammonium-oxidizing bacteria (AnAOB). The partial nitritation (PN) process and anammox process are carried out in a single reactor called a single-stage PNA system (SPNA), and is a space saving process. However, it's a critical bottleneck to achieve high-efficiency synergistic between ammonia oxidizing bacteria (AOB) and AnAOB in the SPNA system. NOB usually coexist in the SPNA system and compete for substrate (O₂ and NO₂⁻-N) with AOB and AnAOB^[1].

To solve the above challenges, biofilm growth systems was widely used in the SPNA process. Carrier could provide surfaces for the attachment of the slow-growing AnAOB in order to avoid the wash out of the bacteria and attain the better biomass retention ability. AnAOB can form a biofilm on the anaerobic surface of the biofilm carrier, while AOB forms a biofilm in the outer biofilm carriers in an aerobic environment. By controlling the dissolved oxygen (DO) below 0.5mg/L, the activity of NOB can be effectively inhibited. The low DO concentration is also beneficial to the formation of the double biofilm structure and the stable operation of the SPNA system.

However, most of the previous studies focused on the effect of different carrier materials on the nitrogen removal efficiency of SPNA system such as biochar, zeolites, sponges, non-woven membrane etc. Or investigate the nitrogen removal performance of the SPNA system under different conditions under short-term operation, such as different influent C/N ratios, toxic substances and different temperatures. There are few studies on the formation

characterization of biofilms and the operation performance under long-term operation.

In this study, a 5L air lift reactor (ALR) was operation for more than 300 days to study the biofilm characterization and operation performance at 25°C using function carriers. The features of the ALR SPNA process were also verified on perspectives of the nitrogen removal efficiency and the specific Anammox activity (SAA).

2 Materials and methods

2.1 Carrier

The carriers used in this study was made of Polypropylene resin (PP), which has an H×D=10mm×10mm, the specific surface area of 800m²/m³, and the specific gravity is 0.98.



Fig. 1. Photo of carriers.

2.2 Reactor setup and operation

The SPNA system was equipped with an effective volume of 5L ALR reactor, a substrate tank, an influent pump, a heater and an air pump.

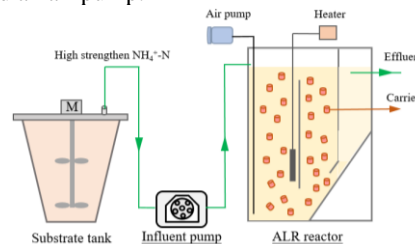


Fig. 2. Reactor configuration.

As shown in Table 1, the whole experiment was divided into 8 phases according to the nitrogen load rate (NLR).

Table 1 The experimental conditions.

Phase	Time (d)	HRT (h)	NH ₄ ⁺ -N (mg/L)	NLR (gN/L/d)
I	1-145	8	250	0.75
II	146-197	16	600	0.9
III	198-201	16	800	1.2
IV	202-230	16	600	0.9
V	231-234	27	1000	0.9
VI	235-300	16	350-600	0.53-0.9
VII	301-350	16	300	0.45
VIII	351-380	16	600	0.9

2.3 Influent and seed sludge

The reactor was fed with a synthetic influent, containing ammonium as the single nitrogen source, mineral salts, and no organic carbon. NH₄⁺-N was supplemented in the form of NH₄HCO₃. The ratio of HCO₃⁻ to NH₄⁺ of influent was fixed at 2.0 by adding approximately equal amounts of NaHCO₃ to NH₄HCO₃.

The seed sludge was obtained from a SPNA reactor. The initial mixed liquor suspended solid (MLSS) concentration of the airlift reactor was approximately 17.0 g/L.

2.4 Analysis Methods

Influent and effluent samples were measured every 2 days. The samples were filtered through 0.45μm filter prior to measurements. Ammonia, nitrite and nitrate were analyzed according to standard methods.

3 Results and discussion

From phase I to phase IV, the NLR was increased from 0.75gN/L/d to 0.9 gN/L/d, with a high nitrogen removal effectively (NRE) of 82%. After high ammonium (1000mg/L) concentration inhibition, the NLR was decreased to 0.45 gN/L/d. Then, the NLR was adjusted back to 0.9 gN/L/d after mechanical stirring within 3 days.

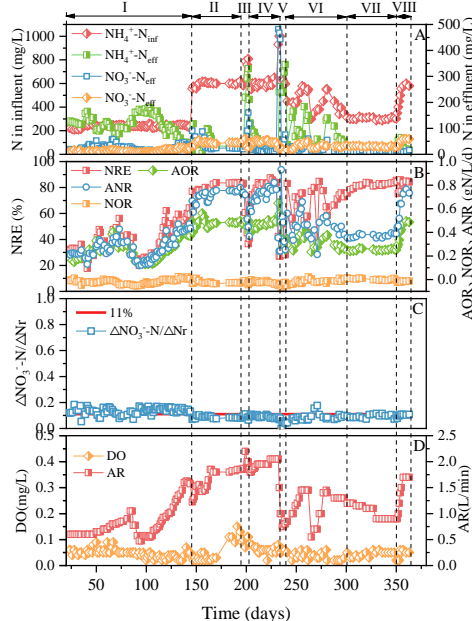


Fig. 2. The operation performance of SPNA system: N in influent and effluent (A); NRE, AOR, NOR and ANR (B); ΔNO₃-N/ΔNr (C); AR and DO (D).

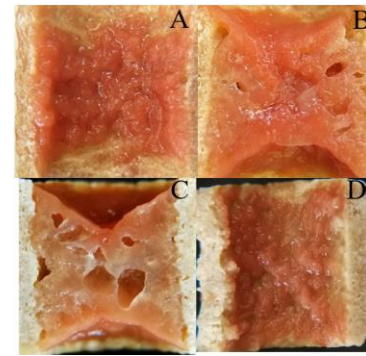


Fig. 3. Photo of biofilm: day84 (A); day214 (B); day310 (C); day360 (D).

The formation of biofilm can be divided into four stages: the biofilm formation period, the mature period, the aging period and the reactivation period. The cavity formed by nitrogen produced by anammox bacterial is one of the reasons for the poor nitrogen performance.

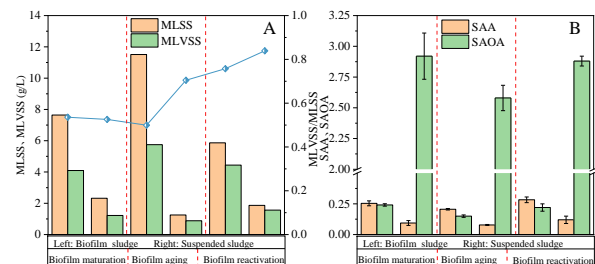


Fig. 3. Sludge concentration in different stages: MLSS, MLVSS and MLVSS/MLSS (A); SAA and SAOA (B).

The inorganic matter accumulated in the biofilm is the main factor causing the reduction of the nitrogen removal capacity of the SPNA system. MLSS concentration increased from 7.64g/L in biofilm maturation period to 11.51g/L in biofilm aging period, while the SAA decreased from 0.25 gN/gMLVSS/d to 0.21 gN/gMLVSS/d at the same time. After mechanical stirring, MLSS concentration decreased to 5.86 g/L while SAA increased to 0.28 gN/gMLVSS/d.

4 Conclusions

- 1) The SPNA process was successfully operated under NLR of 0.9 gN/L/d and NRE of 84%.
- 2) The cavities generated by nitrogen gas and the accumulation of inorganic substances are the main reasons for the decrease in NRE.
- 3) Mechanical stirring can maintain the high activity of the biofilm.

Reference

[1] Guo, Y., Chen, Y.J., Webeck, E., Li, Y.Y. 2019. Towards more efficient nitrogen removal and phosphorus recovery from digestion effluent: Latest developments in the anammox-based process from the application perspective. *Bioresour Technol*, 299(2019) 122560.

Microbial diversity of small bacteria in activated sludge

○ Shuka KAGEMASA^{1*}, Yu-You LI¹, Kengo KUBOTA¹

¹Department of Civil and Environmental Engineering, Tohoku University, Miyagi 980-8579, Japan.

*E-mail: shuka.kagemasa.t2@dc.tohoku.ac.jp

Abstract

Biological treatment is responsible for a central role in sewage treatment. Clarification of physiological characteristics and dynamics of microorganisms is of importance to understand the process. Microorganisms belonging to the uncultured lineages (candidate division) present in activated sludge are one of the factors that make it difficult to understand the sewage treatment mechanism. The previous studies showed that microorganisms belonging to the candidate division are present in a high proportion in the fractionated sample. It was assumed that microorganisms belonging to the candidate division can be detected at a high percentage by fractionating the activated sludge. In this study, we investigated microbial community of fractionated activated sludge. In the fractionated samples, the most dominant microorganism was *Saccharibacteria* regardless of the processes and season. In addition to *Saccharibacteria*, some microorganisms belonging to candidate division were detected at a high percentage in the fractionated samples. Microorganisms belonging to the candidate division detected in the fractionated activated sludge were CPR (Candidate Phyla Radiation) bacteria. It was shown that the fractionated activated sludge is characterized by the high abundance of CPR bacteria.

Keywords: *Saccharibacteria* (TM7); Ultra-small microorganisms; Candidate Phyla radiation bacteria; Filtration fractionation; Activated sludge.

1 Introduction

The minimum size of microorganisms is 0.2 to 0.3 μm , and it is generally said that this size contains a sufficient amount of biomolecules necessary for maintaining vital activity. Using the cell size characteristics of microorganisms, filter filtration is used for sterilization in the field of biology. On the other hand, it has been revealed that there were ultra-small microorganisms that pass through the filter. Ultra-small microorganisms are often defined as "cell volume less than 0.1 μm^3 ". From the report by Miyoshi et al. [1], it was shown that many of the ultra-small microorganisms that passed through the filtration filter were classified into the uncultured lineages (candidate division). Groundwater from the Tono uranium mine was filtered through a filter with a pore size of 0.2 μm , and this filtrate was further filtered through a filter with a pore size of 0.1 μm . The microorganisms captured by the 0.1 μm pore size filter belonged to candidate divisions *Parcubacteria* (OD1) and *Microgenomates* (OP11), those accounted about 44% in 16S rRNA gene clones. Another study also reported that microorganisms belonged to the candidate divisions OD1, OP11 and WEE3 were enriched in an aquifer water sample passed through the 0.2 μm pore size filter [2]. The candidate division such as OD1 and OP11 detected in the filtrate were CPR (Candidate Phyla Radiation) bacteria. CPR bacteria are a diverse group of uncultured bacterial lineages with poorly understood metabolic functions. CPR bacteria are suggested to comprise at least 15% of bacteria domain phyla. CPR bacteria are characterized by their extremely small cell size, genome size (< 1 Mbp) and their parasitism and symbiosis with other microorganisms [3]. Therefore, CPR bacteria likely are to pass through the filtration filter, and CPR bacteria can be abundantly detected by size-fractionating the sample.

Since various microorganisms are present in activated sludge in sewage treatment plant, various types of ultra-small microorganisms or CPR bacteria may be

detected at a high percentage by size-fractionating the activated sludge. We analyzed the microbial community of the fractionated activated sludge and grasped its characteristics.

2 Materials and methods

2.1 Sampling and sample pretreatment

Activated sludge was sampled from a reaction tank of the MGA sewage treatment plant (conventional activated sludge process). Activated sludge was centrifuged (7,000 \times g, 5 minutes), and the supernatant of activated sludge after centrifugation was fractionated using a filter (Stericup, 0.45 μm , 0.22 μm , 0.1 μm , Merck Millipore). In addition, since dissolved DNA (microbial DNA released extracellularly by passive and active factors) may be contained in the filtrate, a part of the filtrate was treated with DNase (Deoxyribonuclease I, NIPPON GENE).

2.2 Microbial community analysis

Microbial community analysis was performed on untreated activated sludge samples (Indicated as "Sludge"), filter samples of each pore size (Indicated as "0.45 / 0.22 / 0.1 μm Filter"), filtrate samples that passed through each filtration filter (Indicated as "0.45 / 0.22 / 0.1 μm Filtrate"), and samples in which the filtrate was DNase-treated (Indicated as "0.45 / 0.22 / 0.1 μm Filtrate_DNase"). These samples were subjected to a polymerase chain reaction using the primer set (341 Forward and 806 Reverse) targeting the V3-V4 region of the 16S rRNA gene. Then, the sequencing was performed with the Miseq System (Illumina). Sequence data analysis was performed using QIIME (database: silva).

3 Results and discussion

Figure 1 showed the result of microbial community analysis of the fractionated activated sludge. *Proteobacteria* and *Bacteroidia* accounted for 70-80% of the total bacteria of "Sludge" regardless of the treatment plant, treatment

series, and season. The microbial community of the fractionated sample (“Filter”, “Filtrate” and “Filtrate_DNase”) was different from that of “Sludge”. In the fractionated sample, the proportion of “None” became very high as the filter pore size became smaller. “None” means that it could not be identified by sequence data analysis using QIIME (database: silva). The detected “None” was reanalyzed by NCBI BLAST, but its identity could not be specified.

30-40% of the total bacteria of “0.45 µm Filtrate”, “0.45 µm Filtrate_DNase” and “0.22 µm filter” were the candidate division *Saccharimonadia* (TM7). The *Saccharimonadia* was the most dominant microorganism in the “0.45 µm Filtrate”, “0.45 µm Filtrate_DNase” and “0.22 µm filter”. The percentage of *Saccharimonadia* in “Sludge” was 3%. This tendency was confirmed regardless of the difference in treatment plant, treatment series, and season. “Filtrate_DNase” is a sample from which dissolved DNA was removed to make it with only microbial cells. Since *Saccharimonadia* was detected in “Filtrate_DNase” at the high percentage same as “Filtrate”, *Saccharimonadia* detected in the fractionated activated sludge is considered to be microbial cells. In addition, when the OTU (operation classification unit) of the detected *Saccharimonadia* were confirmed, there were OTUs showing a high percentage only in the fractionated samples. This means that *Saccharimonadia*, which has very small cell size, may be present in activated sludge. *Saccharimonadia* present in the oral cavity (TM7x) is spherical with a diameter of 0.2 to 0.3 µm, and it has been reported that it survives by parasitizing other microorganisms [4]. However, regarding *Saccharimonadia* present in activated sludge, it has not been reported that there is a very small cell size or a parasitism situation. Therefore, the *Saccharimonadia* detected in the fractionated activated sludge may be a *Saccharimonadia* with a very small cell size that has not been reported so far, and its ecological characteristics need to be verified.

Furthermore, in addition to *Saccharimonadia*, some CPR

bacteria with a higher relative abundance than “Sludge” were confirmed, especially with the “0.22 µm Filter”.

From the “0.22 µm Filter”, *Parcubacteria* was detected at 14.2% (“Sludge”:0.3%), *Gracilibacteria* (GN02) was detected at 8.94% (“Sludge”: 1.8%), and *Microgenomates* was detected at 2.8% (“Sludge”: 0.04%). By size fractionating the activated sludge, CPR bacteria were abundantly detected.

4 Conclusions

This study revealed that the fractionated activated sludge is a treasure trove of CPR bacteria. In particular, *Saccharimonadia* in activated sludge has not been reported on its small cell size or parasitism, so it is necessary to verify its ecological characteristics and isolation culture in the future study. In particular, *Saccharimonadia* in activated sludge has not been reported on its small cell size or parasitism. We plan to verify ecological characteristics and to isolate cultures of *Saccharimonadia* in future study. Other CPR bacteria will be analyzed in the same way as *Saccharimonadia*. The results obtained from this study are important knowledges for clarifying the ecological characteristics of CPR bacteria and their role in wastewater treatment.

Reference

- [1] Miyoshi, T. *et al.*, Phylogenetic characterization of 16S rRNA gene clones from deep-groundwater microorganisms that pass through 0.2-micrometer-pore-size filters, *Appl. Environ. Microbiol.*, 71 (2005), 1084–1088.
- [2] Luef, B. *et al.*, Diverse uncultivated ultra-small bacterial cells in groundwater, *Nature Communications*, 6 (2015), 6372.
- [3] Christopher T. Brown *et al.*, Unusual biology across a group comprising more than 15% of domain Bacteria, *Nature*, 523 (2015), 208–211.
- [4] Hea, X. *et al.*, Cultivation of a human-associated TM7 phylotype reveals a reduced genome and epibiotic parasitic lifestyle, *PNAS*, 112 (2015), 244-249.

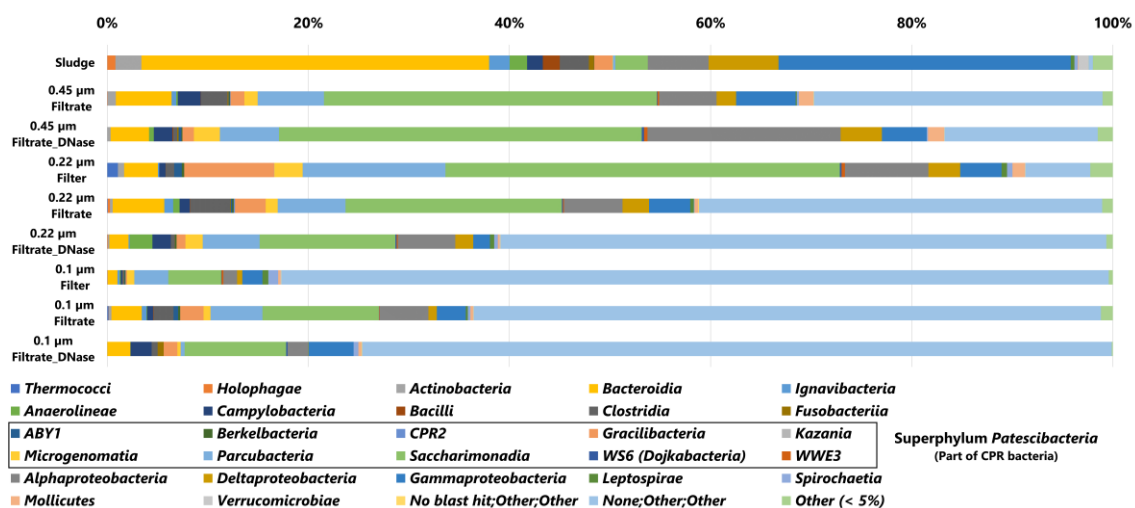


Fig. 1 Microbial community analysis result of the fractionated activated sludge

Indicated a microorganism with a relative abundance of 0.5% or more. Microorganisms with a relative abundance lower than 0.5% were grouped in “Other”. However, the microorganisms belonging to the Superphylum *Patescibacteria* were shown without omission even if the relative abundance was lower than 0.5%. Superphylum *Patescibacteria* is a collection of some of the CPR bacteria.

Application of hemin for the detection of environmental microorganisms

○ Kampachiro URASAKI^{1*}, Yu-You LI¹ & Kengo KUBOTA¹

¹Department of Civil and Environmental Engineering, Tohoku University, Miyagi 980-8579, Japan.

*E-mail: kampachiro.urasaki.p1@dc.tohoku.ac.jp

Abstract

Cell staining is widely used as it can detect microorganisms at single cell resolution. Normally, cell is stained by non-specific methods such as nucleotide staining and/or specific methods such as FISH (fluorescence *in-situ* hybridization). TSA (tyramide signal amplification) is a useful reaction because it can enhance the signal and can label cell with desired elements. TSA reaction is caused by peroxidase including hemin. In this study, we attempt to develop two novel cell staining methods by using hemin designated as the CARD-hemin-staining method and G-quadruplex-hemin-FISH. The CARD-hemin-staining method is a non-specific cell staining method that was applicable to environmental sample. G-quadruplex-hemin-FISH is a method employing hemin and G-quadruplex (guanine quadruplex) that can enhance hemin's peroxidase activity. The G-quadruplex-hemin-FISH was applied to pure cultures however any signals were not obtained so far.

Keywords: Fluorescence *in situ* hybridization; non-specific staining; hemin; DNA enzyme; TSA reaction.

1 Introduction

Cell staining is being widely used in a lot of fields as it can detect microorganisms without cultivation at single-cell resolution. Cell staining can be divided into two types, which are non-specific nucleotide staining using e.g. DAPI and specific staining such as a fluorescence *in-situ* hybridization (FISH). Nucleotide staining is just fluorescent stain thus it cannot label desired elements. FISH is an attractive tool for understanding microbial community structure because it can detect target microorganisms phylogenetically. Catalyzed reporter deposition-FISH (CARD-FISH) is a sensitive FISH that utilizes tyramide signal amplification (TSA) reaction. TSA reaction allows cell labelling with desired elements therefore CARD-FISH has been applied as a high sensitive FISH method. CARD-FISH employs horseradish peroxidase (HRP) as catalyzer, which needs cell wall permeabilization because HRP is too big to penetrate cell wall. However, there is no universal permeabilization method so that optimization for each target microorganisms is necessary [1].

Hemin (Fe (III)-proto-porphyrin IX, C₃₄H₃₂ClFeN₄O₄) has peroxidase activity as the same as HRP. Hemin's peroxidase activity can be enhanced by guanine quadruplex (G-quadruplex). G-quadruplex is one of DNA enzymes which is formed by guanine-rich sequence. Both of hemin and guanine-rich sequence have low number molecular weight compared with HRP.

In this study, a novel non-specific staining method using hemin and TSA reaction named as CARD-hemin-staining, and a novel CARD-FISH method named as G-quadruplex-hemin-FISH were developed.

2 Materials and methods

2.1 Sample preparation

The strains used in this study were *Comamonas testosteroni* and *Escherichia coli*. Both strains were cultivated in LB medium at 37°C with agitation. During exponentially growth phase, these cells were fixed in a 4% paraformaldehyde solution in phosphate buffered saline (PBS; 150 mM NaCl, 20 mM PO₄³⁻ [pH7.4]) for 12 h at 4°C, and stored in ethanol/PBS solution at -20°C. Granular sludge was fixed as soon as sampling and was stored.

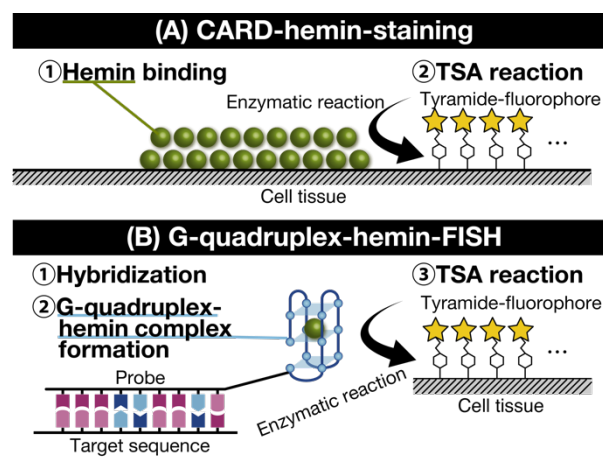


Fig.1 Scheme of (A) CARD-hemin-staining and (B) G-quadruplex-hemin-FISH

2.2 CARD-hemin-staining

CARD-hemin-staining was carried out as shown in Fig.1 (A). Hemin binds non-specifically with cell tissue and catalyzes TSA reaction. Ten μ l of 10 μ M hemin in working buffer 1 (100 mM Tris-HCl [pH 8.0], 400 mM NaCl, 40 mM KCl and 0.0016 % Triton X-100) was mounted on each well. Then glass slides were placed in humidified-chamber for 0.5 h at room temperature, subsequently immersed in PBS containing 0.05% [v/v] Triton X-100 (0.05 % PBSX) for 15 min at room temperature. For TSA reaction, 10 μ l of the working buffer 2 (10% [w/v] dextran sulfate, 0.0015 % [v/v] H₂O₂ and 0.1% [w/v] blocking reagent in PBS) containing 20 μ g/ml of fluorophore-labelled tyramide was applied to each well. Glass slides were placed into a humidified-chamber, and TSA reaction was carried out for 15 min at room temperature. Then, glass slides were immersed in 0.05% PBSX for 15 min at room temperature.

2.3 G-quadruplex-hemin-FISH

For phylogenetic cell detection, non-specific fluorescence signal must be avoided. Therefore, Triton X-100 (a non-ionic surfactant) was tested to eliminate non-specific binding of hemin with cell tissue. The working buffer 1 containing 0%, 0.01%, 0.05%, 0.1 %, 0.5% and 1 % [v/v] Triton X-100 were used for hemin binding. For

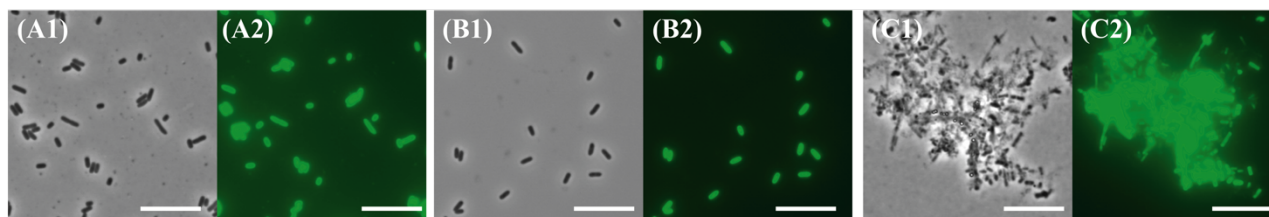


Fig.2 Detection by CARD-hemin-staining of (A) *E.coli*, (B) *C.testosteroni* and (C) granular sludge. (-1) indicates phase contrast (ET 250 ms), (-2) indicates AF488 (ET 450 ms). Scale bar 10 μm.

equilibration, the same concentration of PBSX as hemin binding was used.

The scheme of G-quadruplex-hemin-FISH is shown in **Fig.1(B)**. *In-situ* hybridization with BET42a-PS2.M (5'-GTG GGT AGG GCG GGT TGG Gtt ttt ttt ttG CCT TCC CAC TTC GTT T-3') was carried out in accordance with previous study with some modifications [2]. After *in-situ* hybridization, 10 μl of working buffer 1 was mounted on each well in order to form G-quadruplex. Glass slides were placed into a humidified-chamber for 1 h at room temperature. Then, 10 μl of 20 μM hemin in working buffer 1 with 1% [v/v] Triton X-100 was mounted on each well and incubated for 0.5 h at room temperature. The glass slide was subsequently immersed in 1% PBSX for 15 min at room temperature. TSA reaction was carried out using as beforementioned.

3 Results and discussion

3.1 CARD-hemin-staining

CARD-hemin-staining was applied to pure cultures of *E.coli* and *C.testosteroni* (**Fig.2A, 2B**). Cell-specific and clear signal was obtained from both *E.coli* and *C.testosteroni*. When the CARD-hemin-staining was applied to granular sludge (**Fig.2C**), cell-specific and clear signals were also obtained from all cells. Fluorescence signal evenly distributed within cell, and peripheral halo-shaped signals and spotty signals weren't observed. It suggests that hemin penetrated cell wall, and then evenly bound with entire of cell tissue. In short, the CARD-hemin-staining was applicable for environmental samples.

Tyramide labelled with desired element can easily be synthesized which means desired elements with tyramide can be labelled by TSA reaction. In summary, the CARD-hemin-staining method can stain specific elements such as nanogold particle.

3.2 G-quadruplex-hemin-FISH

Non-specific hemin binding gave the benefit for us. However, it hinders to develop a novel *in-situ* hybridization method. In order to eliminate non-specific fluorescence signal, Triton X-100 was tested. Non-specific signal was obtained with 0% [v/v] to 0.5% [v/v] Triton X-100 (**Fig.3A-E**), suggests that hemin non-specifically binds with cell tissue below 0.5% Triton X-100. When Triton X-100 concentration was 1%, fluorescence signal was able to be eliminated (**Fig.3F**). It indicates that Triton X-100 inhibited hemin binding so that >1% Triton X-100 can eliminate non-specific fluorescence intensity.

G-quadruplex is one of apoenzymes of hemin, and G-quadruplex-hemin complex has a significantly high peroxidase activity compared with hemin alone [3]. When G-quadruplex-hemin-FISH was applied to *C.testosteroni* in the condition that triton X-100 concentration was 1% [v/v], we did not get any signals (**Fig.4**).

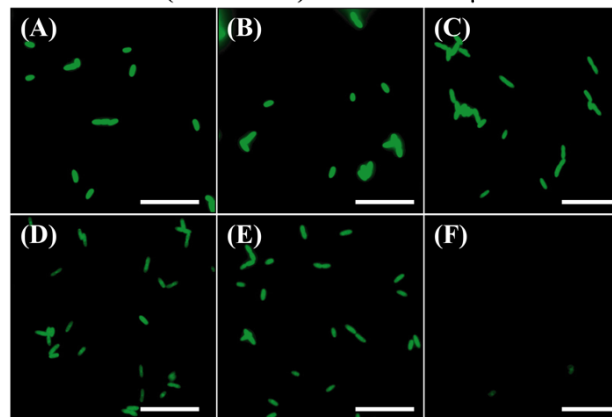


Fig.3 Detection of *E.coli* by CARD-hemin-staining in triton X-100 of (A) 0%, (B) 0.01%, (C) 0.05%, (D) 0.1%, (E) 0.5% and (F) 1.0%. Scale bar 10 μm; ET 600 ms.

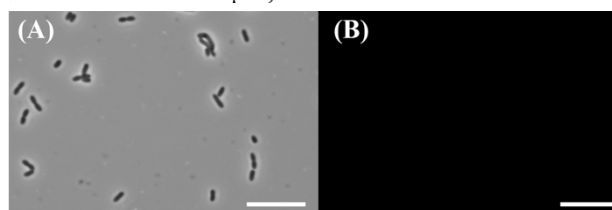


Fig.4 Detection *C.testosteroni* by G-quadruplex-hemin-FISH. (A) Phase contrast (ET 250 ms) and (B) AF488 (ET 450 ms). Scale bar 10 μm.

G-quadruplex-hemin-FISH targets ribosomal RNA (rRNA). Since ribosome is made up of large number of rRNA and protein, it seemed that the ribosome high complexity may inhibit G-quadruplex complex formation.

4 Conclusions

"CARD-hemin-staining", developed as novel non-specific staining method, was successfully applied to *E.coli*, *C.testosteroni* and granular sludge. We attempted to develop G-quadruplex-hemin FISH. However, any signals weren't obtained, thus development of G-quadruplex-hemin-FISH is in progress.

Reference

- [1] Kubota K, Imachi H, Kawakami S, Nakamura K, Harada H, Ohashi A. Evaluation of enzymatic cell treatments for application of CARD-FISH to methanogens. *J Microbiol Methods*. 72(1) (2008):54-9.
- [2] Annelie P, Jakob P and Rudolf A. Fluorescence in situ hybridization and catalyzed reporter deposition for the identification of marine bacteria. *Appl. Environ. Microbiol.* 68 (6) (2002): 3094-3101.
- [3] Paola T, Paul K. W, A. Grant M, and Dipankar S. The Peroxidase Activity of a Hemin-DNA Oligonucleotide Complex: Free Radical Damage to Specific Guanine Bases of the DNA. *J. Am. Chem. Soc.* 123 (7) (2003): 1337-1348.

Effects of Altering Process Parameters for Controlling Nutrient Concentration in Treated Water on Microbial Community Structure and *amoA* Gene in Activated Sludge

○ Hiroyuki OHNO^{1*}, Mikiko SATO¹, Yu-You LI¹ & Kengo KUBOTA¹

¹School of Engineering, Tohoku University, Miyagi 980-8579, Japan.

*E-mail: hiroyuki.ohno.t3@dc.tohoku.ac.jp.

Abstract

Currently, the main microbial community of activated sludge is the black box. In this study, we are trying to estimate the main groups of activated sludge and their functions and dynamics by applying molecular biological methods to activated sludge in wastewater treatment facilities in various parts of Japan. We are focusing on seasonal operation management implemented in areas such as the Seto Inland Sea coast. Seasonal operation management achieves and maintains water quality environmental standards for the purpose of realizing and regenerating affluent seas. However, it is a method to actively control the nutrient concentration in the treated sewage water. As a result of investigating and analyzing the effect of seasonal operation management on the microorganisms in active sludge, it was suggested that the microbial community structure changes due to seasonal operation management. In particular, it was found that the relative abundance of *Nitrospira* and *Nitrosomonas* increased. In addition, a quantitative evaluation of the *amoA* gene revealed that AOB *amoA* increased during the period of seasonal operation management.

Keywords: Activated sludge; Microbial community; Ammonium oxidization; qPCR.

1 Introduction

The activated sludge process is a wastewater treatment technology that is widely used mainly in developed countries, but it has an aspect of being operated empirically. In addition, there are not many reports on the major microbial communities present in activated sludge and their functions. Therefore, the current situation is that the dynamics and functions of microorganisms in activated sludge are regarded as a black box.

In recent years, in order to increase the concentration of nutrients in the sea area in winter, the seasonal operation management that actively release nitrogen and phosphorus has been implemented in areas such as the coast of the Seto Inland Sea. Seasonal operation management is a method of switching to an operation method that suits the purpose depending on the season. In particular, the concentration of nutrients released is important. In summer, it is released in low concentrations to preserve water quality. In winter, it is released in high concentrations for the regeneration of marine resources. However, although there are reports on changes in wastewater quality and nutrient concentration in the sea area due to seasonal operation management, there are few reports on the structure of the microbial community of activated sludge in the reaction tank.

In this study, we analyzed microbial community structure using next-generation sequencing and real-time PCR on activated sludge from two wastewater treatment plants that is undergoing seasonal operation management. In this way, we investigated the temporal changes in the microbial community structure associated with seasonal operation management and carried out a quantitative evaluation of genes related to ammonia oxidation.

2 Materials and methods

2.1 Sample Collection

From April 2018 to March 2019, activated sludge in the reaction tank was collected from two sewage treatment plants (WWTP-1 and WWTP-2) that are undergoing seasonal operation management.

2.2 Analysis of microbial community structure

DNA was extracted from the collected activated sludge sample using ISOIL for Beads Beating (NIPPON GENE), and PCR was performed using the 341F-806R primer set targeting the V3-V4 region of the 16S rRNA gene. After that, sequencing was performed by Miseq, and the structure of the microbial community in activated sludge was analyzed using QIIME.

2.3 Real-time PCR

The abundances of AOB and AOA *amoA* gene were quantified with the primer pairs using real-time quantitative PCR (qPCR) technology in LightCycler (Roche). AOB and AOA *amoA* gene abundances were quantified using primers *amoA* 1F/2R (Rotthauwe et al., 1997) and *arch-amoA* F/R (Francis et al., 2005), respectively. The amplification was conducted in 20 µL reaction mixture consisted of 10 µL SYBR TB Green Premix Ex Ta II (Takara Bio), 0.5 µL forward and reverse primers and 2.0 µL template DNA and 7.0 µL Milli-Q water. The real-time PCR protocol targeting AOB *amoA* gene involved enzyme activation and initial denaturation at 95 °C for 30 sec, followed by 45 cycles of denaturing at 95 °C for 5 s, annealing at 54 °C for 20 s and extension at 72 °C for 40 s. When targeting the AOA *amoA* gene, annealing at 54 °C for 30 sec and extension at 72 °C for 1 min. The specificity of the PCR products was checked by dissociation curve and visualized with 1.2% agarose gel electrophoresis. To obtain the standard curve, a template was prepared by the PCR products amplified using the primer set M13F and M13R from cloned DNA fragments obtained in the clone analysis, which were affiliated with AOB *amoA* gene and AOA *amoA* gene. All the PCR assays for each gene

and sample were performed at least three independent replicates. The target gene copies in the unit volume template were calculated through the standard curve.

3 Results and discussion

3.1 Analysis of microbial community structure

Figure 1 shows the temporal changes in the structure of microbial communities in activated sludge at wastewater treatment plants that are undergoing seasonal operation management. It is generally said that the *Proteobacteria* is the main constituent bacteria in activated sludge of wastewater treatment plants. In the activated sludge of the wastewater treatment plant targeted in this study, the *Proteobacteria* and *Bacteroidetes* were predominant throughout the year. In addition, as a result of β -diversity analysis, the microbial community structure in the activated sludge of the wastewater treatment plant where seasonal operation management is carried out formed a cohesive plot for each sewage treatment plant regardless of the period of seasonal operation management (data not shown). This suggests that the effect of seasonal operation management on the microbial community structure in activated sludge is small compared to the effect of the treatment process and the nature of the inflow water.

At wastewater treatment plants that carry out seasonal operation management, an increase in the relative abundance of the nitrite-oxidizing bacteria *Nitrospira* and the ammonia-oxidizing bacteria *Nitrosomonas* was confirmed over the winter (Figure. 1). At the WWTP-2, a denitrification suppression operation is carried out to suppress the supply of organic components required for the denitrification reaction by stopping the step inflow. Therefore, in the WWTP-2 in winter, it is considered that the activity of denitrifying bacteria is reduced by suppressing the supply of organic matter, and an environment is formed in which the microorganisms involved in nitrification can easily grow. It was also suggested that the structure of the microbial community in activated sludge is affected by changes in simple treatment processes such as stopping step inflow.

3.2 Quantification of *amoA* gene

The abundance of AOB *amoA* and AOA *amoA* genes in activated sludge samples from two wastewater treatment plants were quantified by Real-time PCR. Figure 2 shows the transition of the amount of AOB *amoA* in each wastewater treatment plant. From Figure. 2, it was found that the copy number of AOB *amoA* per DNA concentration increased

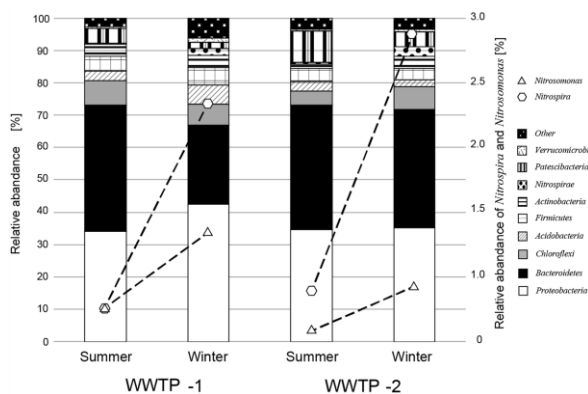


Figure. 1. Temporal changes in microbial community structure associated with seasonal operation management

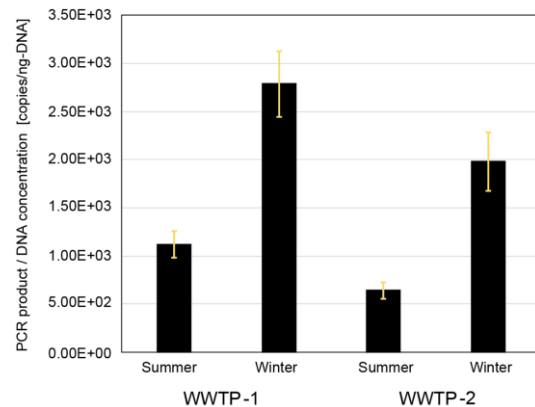


Figure. 2. Temporal change in the amount of AOB *amoA* gene in activated sludge associated with seasonal operation management

from summer to winter in WWTP-1 and WWTP-2. This confirms that the number of ammonia-oxidizing bacteria increases from summer to winter from the results of microbial structural analysis, and seasonal operation management affects the microorganisms involved in the nitrogen cycle in activated sludge. In addition, although real-time PCR was performed on AOA *amoA*, it was not possible to quantify AOA *amoA* from activated sludge of WWTP-1 and WWTP-2 throughout the year (data not shown). These facts have quantitatively revealed that the abundance of AOB changes with seasonally controlled operations. In addition, since the detailed timing and amount of change in the amount of *amoA* differ between WWTP-1 and WWTP-2, we will proceed with the analysis using the analysis results of the microbial community structure and other data such as water quality and climate.

4 Conclusions

This study clarified the structure of microbial communities in activated sludge of wastewater treatment plants, which are undergoing seasonal operation management, and the temporal changes in the amount of AOB / AOA *amoA* genes. In the future, we plan to carry out quantitative analysis of the *amoA* gene derived from Comammox, a microorganism involved in the nitrogen cycle, which has been attracting attention in recent years, and investigate whether seasonal operation management affects Comammox.

Reference

- [1] Francis CA, Roberts KJ, Beman JM, Santoro AE, Oakley BB (2005). Ubiquity and diversity of ammonia-oxidizing archaea in water columns and sediments of the ocean. *Proc Natl Acad Sci USA* 102:14683–14688.
- [2] Rotthauwe, J. H., Witzel, K. P., & Liesack, W. (1997). The ammonia monooxygenase structural gene *amoA* as a functional marker: molecular fine-scale analysis of natural ammonia-oxidizing populations. *Applied and environmental microbiology*, 63(12), 4704-4712.
- [3] Sewerage Department, Water and Disaster Management Bureau, Ministry of Land, Infrastructure, Transport and Tourism (2015). Procedure manual (draft) concerning the operation method for active management of nutrient salts contained in sewage effluent.

A cross comparison of hydrological similarity and geological similarity for the sub-catchments within Natori river basin

○ Qing CHANG^{1*}, Daisuke KOMORI¹ & So KAZAMA¹

¹Department of Civil Environmental Engineering, Tohoku University, Miyagi 980-8579, Japan.

Abstract

In the science of hydrology, similarity is an important concept which has a lot of application scenarios like flood estimation, model parametrization or regionalization. The increasing diversity and resolution of spatially distributed data on terrestrial systems greatly enhance the potential of hydrological modeling. Optimal and reasonable use of these data sources requires that we better understand which system characteristics exert primary controls on hydrological dynamics. In this study we develop and test an approach to explore how the geo-characteristic can affect the hydro-characteristic by comparing the geo and hydro similarities. Spatially distributed topographic information was used as input data and a calibrated hydrological model was used to calculate hydrological performance. Different indices were used and compared and the sub-catchments were classified into different similarities groups. The results showed that the geo-similarity can be reflected by hydro-similarity in certain degree while there is still room for improvement of accuracy.

Keywords: topographic similarity; hydrological similarity; watersheds classification; similarity matrix.

1 Introduction

The key role that surface topography plays in hydrology has long been recognized (e.g., Horton, 1945). Topography provides information about the interplay between uplift, weathering and erosion, and hence about the past morphological development of a landscape. Further, it provides a strong constraint for future hydrological and geomorphic changes and, importantly for hydrology, is the key driver and control associated with runoff generation and several other hydrological processes. This insight about the past, present and future roles played by topography is surely one reason why almost all key landscape entities in hydrology, such as watershed boundaries, hillslopes and channel networks, are derived from properties of the land-surface topography. In support of this, digital elevation models (DEMs) are available at fairly high resolutions across the globe, helping to fuel the growing popularity of spatially explicit hydrologic models.

It is therefore no surprise that hydrology does not suffer from a lack of models or indices linking geomorphic properties of a landscape with its hydrological functioning. The most popular approach is arguably the topographic wetness index (TWI). As a function of the local slope with the upslope contributing area per contour length, the TWI was originally developed to classify areas of similar functioning within a catchment and has been applied and tested in numerous studies.

However, other indices have also been proposed for linking land-surface topography with its runoff response. Hjerdt et al. (2004) developed the “downslope topographic wetness index” (also called the $\tan\beta$ index) that reflects the local hydraulic gradient in the case that flow is exclusively driven by gravity and under the assumptions of a fixed drop in elevation. They claimed that this index represents groundwater level gradients in a manner that is superior to the classical TWI approach and showed it to be less sensitive to the quality of the DEM. An approach that has recently gained considerable

attention is the “height above the nearest drainage” index (HAND). This approach assumes that water follows the steepest descent along the surface topography, and, based on these drainage paths, the corresponding elevation of each raster cell above the nearest corresponding river cell is estimated. HAND has been successfully applied and tested in numerous studies in a wide range of different landscapes.

The above-mentioned studies highlight the large potential of the topographic index and its relevance for hydrological research. From a theoretical point of view, topographic index like DEM reflects the gravitational potential energy of a given unit weight of water with the reference level set to the elevation of the nearest corresponding river. In this study, in order to represent this information in more detailed way, we will use 2 major histogram indexes: the histogram of slopes and the histogram of the distances to rivers, as the major topographic indexes. A distributed hydrological model was used to calculate the outflow and 3 hydrological indexes were used to measure the similarity. The similarity matrix of both geo-features and hydro features will be made to analyze how geo-feature can affect hydrological performance.

2 Materials and methods

2.1 study site description

The study area is Natori River basin which is located in central Miyagi prefecture, in the Tohoku region of Japan. The river's basin is 939 km² and has two primary reservoirs. The river's length is 55 km, and its tributaries are the Hirose, Masuda and Goishi Rivers. The river's flow is the greatest during the snow melt season from March to April, the rainy season from June to July and during the typhoon season from September to October. The entire basin was divided into totally 83 sub-catchments. Those sub-catchments form the basic unit of similarity analysis in this study. Fig.1 had showed the river basin and its sub-catchments.

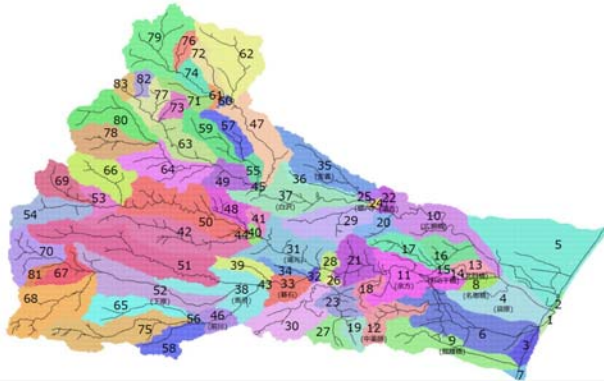


Fig. 1. The study area and the divided 83 sub-catchments.

2.2 analysis methods

Topographic data used in this study is DEM data set and river maps of the study area with 40m resolution. These data were processed and generated 2 kinds of histogram data that can describe the features of each sub-catchments: the histogram of grid slopes and histogram of grid distances to rivers. These 2 histograms will be used to compare the geo-similarity between sub-catchments and the dimension of these 2 histograms are 255. The hydrographs of each sub-catchments were calculated using a distributed model. The rainfall events used in this study include 2 largest rainfall in the past 50 years of Sendai area: the 2019-10-11 rainfall (402mm) and the 1986-08-03 rainfall (401mm).

The geo-similarity between sub-catchments were compared using the Jensen–Shannon divergence (JSD) method. This method can estimate how similar catchments are with respect to their features distributions. JSD is based on the well-known Kullback–Leibler divergence (KLD; sometimes referred as relative entropy), defined as:

$$D_{KL}(X||Y) = \sum_{x \in X} (x_i) \log_2 \frac{p(x_i)}{p(y_i)}$$

where $p(x_i)$ and $p(y_i)$ are the probabilities that X and Y are respectively in the states x_i and y_i . In brief, KLD quantifies the information loss when the probability density function of Y is used in place of X. From this, the JSD is developed by comparing each distribution to the “midpoint” distribution M, defined as

$$M = \frac{1}{N} \sum_{i=1}^n (X_i + Y_i)$$

Accordingly, the JSD represents the average divergence of N probability distribution from their midpoint distribution, A high JSD value indicates a high divergence between the distributions, with a maximum of 1. It is defined as

$$JSD = \frac{1}{N} \sum_{i=1}^N D_{KL}(X_i||M)$$

The hydrological similarity between sub-catchments were compared using the r^2 index which is very widely used in hydrology field:

$$r^2 = \left(\frac{\sum_{i=1}^n (Q_{1,i} - \bar{Q}_1)(Q_{2,i} - \bar{Q}_2)}{\sqrt{\sum_{i=1}^n (Q_{1,i} - \bar{Q}_1)^2 \sum_{i=1}^n (Q_{2,i} - \bar{Q}_2)^2}} \right)^2$$

3 Results and discussion

Figure 2(a) displays the similarity matrix of the histogram of distance to river for the 83 sub-catchments examined in this study. The fact that these distributions are relatively similar is also indicated by the JSD and the values of which are all rather small, indicating low divergence between the distributions.



Fig. 2. JSD values for the 83 research catchments between the histogram of distance to rivers. Green: <0.1, yellow: 0.1~0.2, red:>0.2.

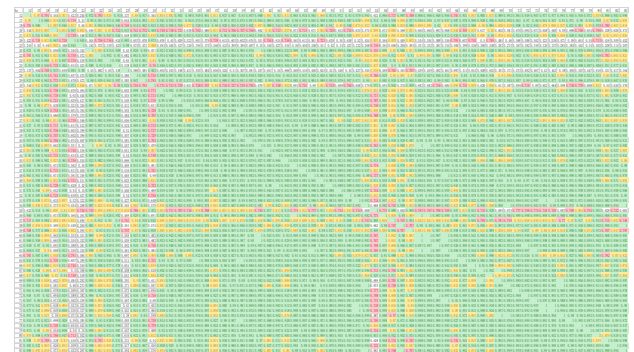


Fig. 3. R² values for the 83 research catchments between the hydrographs.

4 Conclusions

From the evaluation results, it is possible to estimate a similar water discharge prediction using the similarity of topography features. Although the accuracy is not so high, Results showing that the hydrological similarity is reflected using the geo-similarity. Even though the possibility of obtaining the relationships have been proved, it is expected that accuracy should be improved by future studies.

Reference

- [1]Hjerdt, K. N., McDonnell, J. J., Seibert, J., and Rodhe, A.: A new topographic index to quantify downslope controls on local drainage, *Water Resour. Res.*, 40, 1–6,
- [2] Horton, R.: *Erosional Development of Streams and their Drainage Basins “Hydro-Physical Approach to Quantitative Morphology”*, *Bull. Geol. Soc. Am.*, 56, 275–370, 1945

Crop yield sensitivity to drought events: a global-scale analysis of major crops

○ Vempi Satriya Adi HENDRAWAN^{1,*}, Daisuke KOMORI¹

¹ Graduate School of Environmental Studies, Tohoku University, Sendai Miyagi 980-8579, Japan

*E-mail: vempi@dc.tohoku.ac.jp

Abstract

Drought has contributed to some of the world's most severe famines. Therefore, the understanding of drought and its potential impact are key points towards mitigation, especially in the field of agriculture. There are some gaps remaining regarding drought impact analysis on crop yield such as lack of understanding in a fine resolution (e.g. grid) as previous works were mostly done in aggregated scale (country or regional) and factors influencing vulnerability are mostly based on multi-index in local scale. The analysis of historical crop yield sensitivity and drought events in grid scale is important for understanding crop-drought vulnerability variation within countries. This study investigates the response of yield of global major crops (wheat, maize, rice and soybeans) to drought events during 1983-2014 in 0.5-degree grid resolution. We used standardized precipitation evapotranspiration index (SPEI) and crop yield data to build a risk model. Results show that respectively 11%, 4%, 10%, and 11% of the total cropland for maize, rice, soybean, show yield loss (with Pearson correlation of > 0.5). The strong correlation between drought and yield anomaly and high drought vulnerability shown by high slope of linear regression are prominent in North America (US), South America (Argentina), some countries in Eastern and Southern Europe and Southern Africa (e.g. Zambia). This study highlights a linear response of yield loss risk to the drought events that can be found significantly in some parts of the world where crops are cultivated. These results are important for the further understanding of crop-drought vulnerability and signifies that mitigation efforts should be more targeted in the most vulnerable areas.

Keywords: Agriculture, Drought, SPEI, Vulnerability, Risk

1 Introduction

As reported by IPCC (2014), global warming will result in climate extreme inducing more frequent and severe natural disasters. Drought has contributed to some of the world's most severe famines (e.g. a severe drought in India affecting 300 million people in 2002 and death of 20,000 Somalis due to drought in 2010). Agriculture is the most affected sector by drought in developing countries, absorbing about 80% of all direct impacts (FAO, 2018). Developing countries are particularly vulnerable to drought because of their geography and strong dependence on subsistence agriculture (McKAY, 1988) as well as due to physical, socio-economic, knowledge and skills differences (Miyan et al., 2015). Due to its multiple effects on food security and livelihood threatening global sustainability, the diagnosis of drought vulnerability is important for future mitigation. The understanding of drought, its impact and the vulnerability are key points towards rising incidence of weather extremes with its negative impacts on agriculture.

Related previous studies have been conducted both in global and local scale. For local studies, there were mostly analysis of vulnerability based on AHP weighting scheme, GIS and remote sensing (Haque et al., 2019; Jain et al., 2015; Wu et al., 2011; Murthy et al., 2014). While in global scale there were mostly studies about physical and social vulnerability based on drought index, crop growth and hydrological model (Kamali et al., 2018). However, some gaps are still remaining as follows:

1. Previous studies were solely focusing on drought impact based on crop yield modeling,

2. Crop-drought impact analyses were mostly in done aggregated scale (country or regional),
3. Factors influencing vulnerability are defined mostly in local scale based on indexing.

The analysis of historical crop yield sensitivity and drought events in grid scale is limited. Therefore, this study investigates the response of yield of global major crops (wheat, maize, rice and soybeans) to drought events during 1983-2014 in 0.5-degree grid resolution. Furthermore, the objectives of this study are:

1. To understand crop yield sensitivity by means of crop yield response and its relationship with drought events, using statistical approach that employs historical yield dataset and global drought dataset instead of crop yield modeling,
2. To determine the crop-drought vulnerability using the disaster risk framework (see IPCC (2012) for further details).

2 Materials and methods

2.1 Materials

Datasets used in this study are shown in Table 1. All of the data are set in 0.5-degree spatial resolution and subset along period of 1983-2014 (32 years).

Table 1 Dataset used in this study

Name	Data	Use	References
SPEI base	Monthly aggregation Standardized Precipitation	Drought hazard model	(Vicente-Serrano et al., 2010)

	Evapotranspiration (SPEI)		
Crop calendar	Planting and harvesting date (Day of Year)	Exposure model	(Sacks et al., 2010)
The global dataset of historical yield (GDHY)	Crop yield (t/ha)	Risk model	(Iizumi et al., 2020)

2.2 Methods

As can be seen in Figure 1, first, the risk component for major crops is assessed by using crop yield anomaly (θ) obtained from crop yield dataset (Eq. 1).

$$\theta_t = \frac{Y_t - \bar{Y}_t}{\bar{Y}_t} \times 100\% \quad (1)$$

$$\bar{Y}_t = \frac{1}{5} \sum_{i=-2}^2 Y_{t+i} \quad (2)$$

where Y_t is crop yield (tons per hectare, t /ha) and \bar{Y}_t is 5-year centered moving average (t /ha).

The hazard component is assessed by using SPEI. Drought magnitude at year t (H_t) is computed as Eq.3.

$$H_t = - \sum_{j=0}^k S_{C-j, t} \quad (3)$$

where $S_{j,t}$ = k-month aggregated SPEI (drought) in month j and year t and C is harvest-related month in 2000 (Sacks et al., 2010; Kim et al., 2019). It should be noted that only SPEI < 0 indicating drought events are used in this analysis.

While, the exposure is represented by the explicit spatial and temporal coincidence between the hazard and risk component using a statistical correlation. The simple correlation between risk and hazard is analyzed using Pearson correlation. Then, a model of Risk Disaster using the formula shown in Figure 1 where V, R, H, E is vulnerability, Risk, Hazard, and Exposure, is used to assess the vulnerability component.

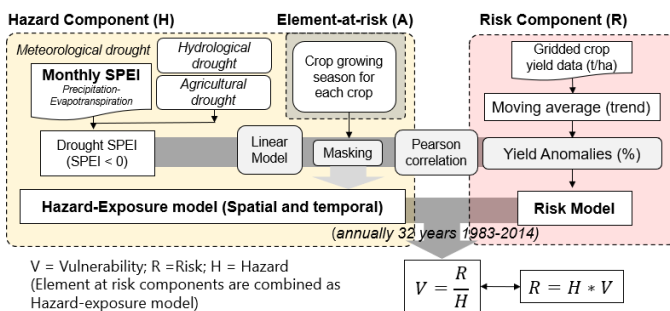


Figure 1 Study framework

3 Results and discussion

Both positive and negative correlation between drought and yield loss were shown and varied among pixels in global scale. The negative relationship, where drought affects yield loss indicates the high vulnerability areas (Figure 2).

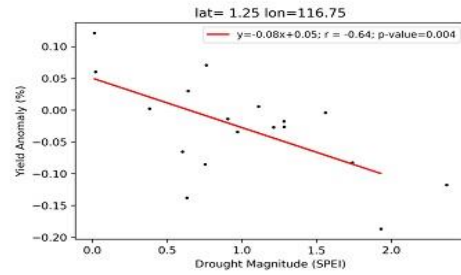


Figure 2 Regression analysis between drought event and crop yield loss (source: analysis)

Maize and wheat suffer the most drought impact (Figure 3). Results show that respectively 11%, 4%, 10%, and 11% of the total cropland for maize, rice, soybean, show yield loss (with Pearson correlation of > 0.5) during 1983-2014. The strong correlation and high drought vulnerability are prominent in North America (US), South America (Argentina), some countries in Eastern and Southern Europe and Southern Africa (e.g. Zambia).

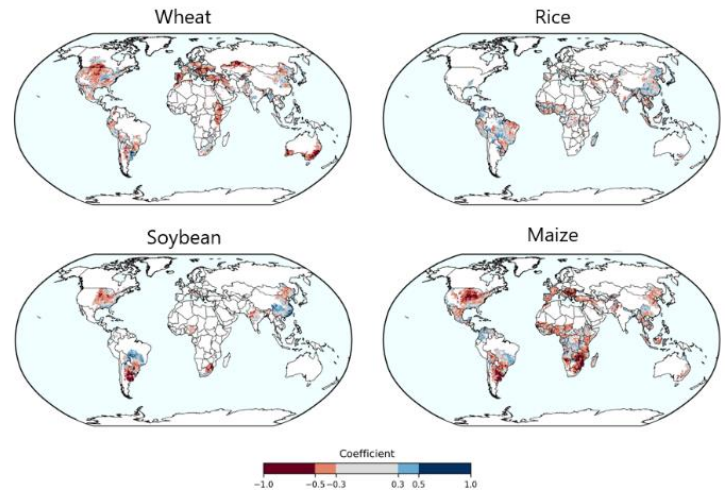


Figure 3 Correlation analysis between drought event and crop yield loss (source: analysis)

Conclusion

This study is mainly aimed to investigate the response of yield of global major crop to droughts events, and to determine the crop-drought vulnerability using disaster risk framework. This study highlights a linear response of yield loss risk to the drought events. It can be found significantly in some part of the world where crops are cultivated. This results are important for the further understanding of crop-drought vulnerability and signifies that mitigation efforts should be more targeted in the most vulnerable areas.

Selected references

- [1] IPCC, 2014: Climate Change 2014: Synthesis Report. Contribution of Working Groups I, II and III to the Fifth Assessment Report of the Intergovernmental Panel on Climate Change.
- [2] UNISDR, 2015: The Human Cost of Weather-Related Disasters 1995-2015
- [3] IPCC, 2012: Managing the Risks of Extreme Events and Disasters to Advance Climate Change Adaptation.
- [4] FAO, 2018: 2017-The impact of disasters and crises on agriculture and food security.
- [5] CRED & UNISDR, 2018: Economic Losses, Poverty & DISASTERS 1998-2017.

Snow cover analysis for dam inflow prediction in Thailand

○ Tomoyuki Hino^{1*}, Kenji Kenji¹, Shigenobu Tanaka²

¹Graduate School of Engineering, Kyoto University, Kyoto,615-8510, Japan.

²Disaster Prevention Research Institute, Kyoto University, Kyoto,611-0011 Japan.
 hino.tomoyuki.77e@st.kyoto-u.ac.jp

Abstract

The purpose of this study is to develop the optimum operation method for large-scale dams in Thailand. The 2011 flood in Thailand severely damaged the Chao Phraya River basin in Thailand. After the disaster, the government is considering new management methods. In this study, we analyzed the relationship between the snow cover distribution of the Eurasian continent and the Asian monsoon in order to predict the inflow of dams. Using the inflow data of Bhumibol dam and Sirikit dam, and the snow water equivalent calculated by the land surface model SiBUC, we analyzed the relationship between snow cover on the Eurasian continent and dam inflow in Thailand during the period from 1980 to 2016. The results suggest that anomaly in snow cover on the Tibetan Plateau in February has negative correlation with dam inflows in May and September.

Keywords: *Bhumibol dam; Sirikit dam; reservoir operation; Chao Phraya River*

1 Introduction

In 2011, a large-scale flood occurred in the Chao Phraya basin in Thailand. The largest flood damage in history in Thailand has had a great impact not only on Thailand but also on the world economy. After the disaster, the Thai government has been working on hydraulic control measures in the Chao Phraya River basin, and efficient operation of large-scale dam reservoirs is being considered. In this study, so far, global precipitation and SST have been analyzed to predict dam inflow in Thailand. In this time, we analyzed whether the snow cover on the Tibetan Plateau affects the inflow of dams in Thailand. According to Yasunari.T (1989)[1], it is pointed out that snow cover on the Tibetan Plateau may affect the summer Indian monsoon. Considering this theory, it is possible that if the snowfall on the Tibetan Plateau in winter is higher than normal, the monsoon will weaken and the precipitation in Thailand will decrease. Using this relationship, we can predict the inflow of dams in Thailand in the summer from the snowfall on the Tibetan Plateau in the previous winter. In this study, in order to clarify the above-mentioned relationship, the relationship between the inflow of two large-scale dams in Thailand and the snow water equivalent in the Tibetan Plateau was analyzed from 1980 to 2016.

2 Materials and methods

2.1 Study area

The targets of this study are the Bhumibol dam and the Sirikit dam located in northern Thailand. The Bhumibol dam has a total reservoir capacity of 13.4 billion m³ and the Sirikit dam has a total reservoir capacity of 9.5 billion m³, and its main purpose is to supply water to irrigation sites. These dams store water from July to



Fig. 1 Study Area and Dams

December and discharge it as irrigation water from January to June.(Fig.2)

Table 1 Specifications of two dams

Name	Bhumibol dam	Sirikit dam
Catchment area(km ²)	26,386	13,130
Annual Inflow(10 ⁶ m ³)	5,256	5,600
Maximum Strage(10 ⁶ m ³)	13,462	9,508

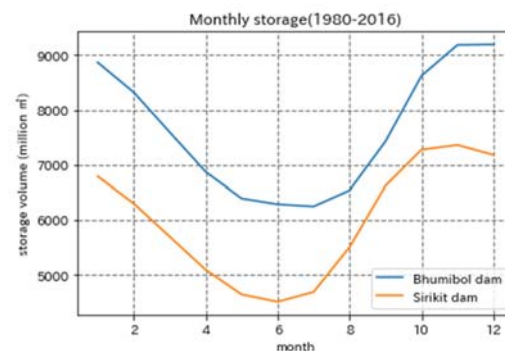


Fig. 2 Monthly storage of two dams

2.2 Model and Climate Forcing

Describe the experimental settings of the land surface model SiBUC used to calculate the Snow Water Equivalent (SWE). SiBUC uses precipitation, downward shortwave radiation, downward longwave radiation, temperature, wind velocity, atmospheric pressure, and specific humidity as meteorological forcing data, and calculates the vertical heat, water, and radiation balance. These meteorological forcing data are created from JRA55 with 60km resolution. The analysis period was from 1980 to 2016 (37 years) according to the obtained dam inflow data. The advantage of using reanalyzed data like JRA55 is its high update frequency. Thus, before a rainy season, we can use model simulation data to predict dam inflow during the following rainy season in advance.

2.3 Methods and Results

The relationships of snow water equivalent (SWE), Monsoon wind velocity and dam inflow in Thailand were analyzed by correlation analysis.

The used SWE data are annual maximum value of SWE (usually in February) on Tibetan Plateau. The used wind velocity data are average monthly wind velocity of the Bay of Bengal on each month. The used dam inflow data are the average monthly dam inflow on each month.

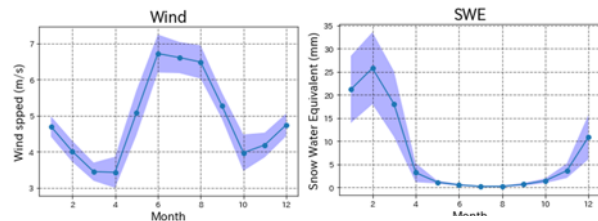


Fig. 3 Monthly Wind velocity in Bengal Bay (band is standard deviation $\pm\sigma$)

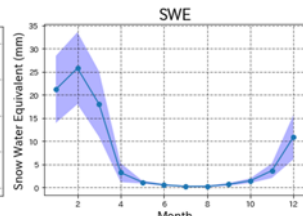


Fig. 4 Monthly SWE in Tibetan Plateau (band is standard deviation $\pm\sigma$)

The correlation coefficient was calculated from the maximum SWE value on each grid and the monthly average wind velocity in the Bay of Bengal on each month of the rainy season. It is suggested that there is a relatively strong negative correlation between SWE on Tibetan Plateau and monsoon wind velocity in May and September. (Fig.5, Fig.6)

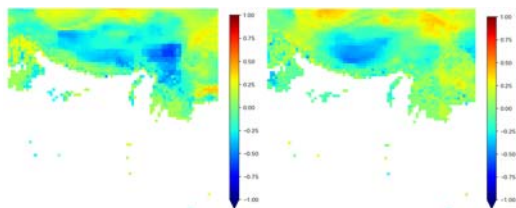


Fig. 5 Correlation Coefficient Map between SWE and Wind velocity (May)

Fig. 6 Correlation Coefficient Map between SWE and Wind velocity (September)

The correlation coefficient is calculated from average monthly dam inflow on each month and monthly average wind velocity in the Bay of Bengal on each month of the rainy season. It is suggested that there is a negative correlation between dam inflow in Thailand and monsoon wind velocity in May of the rainy season.

Regarding Bhumibol dam, relatively strong positive correlation is analyzed in September as well. (Fig.7)

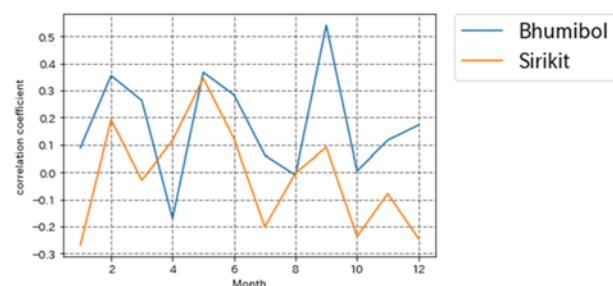


Fig.7 Correlation Coefficient between Monthly Wind velocity and Monthly each dam inflow on each month

The correlation coefficient was calculated from average monthly dam inflow on each month and maximum value of

SWE in Tibetan Plateau. it is suggested that there is a relatively strong negative correlation between SWE on Tibetan Plateau and Bhumibol dam inflow in September. Regarding Bhumibol dam, it is suggested that, over rainy season(from May to October), there is a negative correlation between dam inflow in Thailand on Tibetan Plateau and monsoon wind velocity. On the other hand, regarding Sirikit dam, it is suggested that there is a weak negative correlation between dam inflow in Thailand on Tibetan Plateau and monsoon wind velocity from June to October.

In 2011, there was a weak negative anomaly of SWE in the Tibetan Plateau area. On the other hand, in 2006, when the annual inflow of Bhumibol dam was the second largest in 37 years, there was a negative deviation of SWE over a wide area of the Tibetan Plateau. (Fig.9)

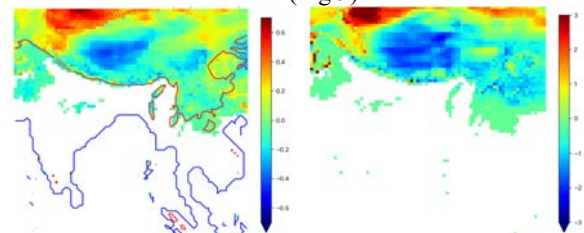


Fig. 8 Correlation Coefficient Map between SWE and Bhumibol dam inflow (September)

Fig. 9 Anomaly of SWE (maximum for a year) in Tibetan Plateau in 2006

3 Discussion

Inflows due to typhoon precipitation are considered to have little relation to the effects of monsoons. Therefore, it is considered that the inflow due to the typhoon is a factor that lowers the correlation coefficient. A relatively strong correlation appears at the beginning and end of the rainy season, but since there is a weak correlation from June to August, it is a challenge to investigate the relationship between snow cover and monsoon strength from June to August

4 Conclusions

The purpose of this study is to efficiently operate a large-scale dam in Thailand, and in order to predict the inflow in advance, we analyzed whether the snowfall on the Tibetan Plateau affects the inflow of the dam. As a result, it is suggested that the snow cover on the Tibetan Plateau affects the strength of the Southeast Asian monsoon.

Regarding Bhumibol dam, there is a negative correlation between dam inflow during the rainy season and SWE on the Tibetan Plateau. it is founded that the SWE condition in early spring is an important factor in predicting dam inflow during rainy season.

Reference

- [1]安成 哲三, 1989 :ユーラシア大陸の積雪と ENSO - 雪氷・大気・海洋結合系の提唱-. 地学雑誌, 98-5, 613-622.
- [2]Saw.O.2009, Inflow Prediction for long-term reservoir operation through lag correlation analysis of global meteorological information. Doctoral Dissertation, Graduate School of Engineering, Kyoto University
- [3]Tanaka.K.2004. Development of the New Land Surface Scheme SiBUC Commonly Applicable to Basin Water Management and Numerical Weather Prediction Model. Doctoral Dissertation, Graduate School of Engineering, Kyoto University: Kyoto;289

The selection of temporal scale for drought analysis using satellite-based precipitation data

○Amalia Nafisah Rahmani IRAWAN¹, Daisuke KOMORI² & Vempi Satriya Adi HENDRAWAN¹

¹Graduate School of Environmental Studies, Tohoku University, Miyagi 980-8577, Japan.

²Department of Civil and Environmental Engineering, Tohoku University, Miyagi 980-8577, Japan.

*E-mail: amalia.nafisah.rahmani.irawan.q3@dc.tohoku.ac.jp.

Abstract

The availability of precipitation data is an important aspect for several purposes, one of them is drought analysis. However, the limitations in the availability of measured precipitation data (MPD) makes satellite-based precipitation data become one of the alternative sources that can be utilized. This study aims to examine the agreement between local measured (MPD) and satellite-based precipitation data (GSMaP) in West Java, Indonesia and determine an appropriate temporal scale to be used for drought analysis. Interpolation of MPD is also conducted using Inverse Distance Weighted (IDW) method to obtain the spatial precipitation distribution. From the correlation analysis results of point dataset and area dataset, it can be concluded that the appropriate temporal-scale that can be used for drought analysis is a 90-days period. In addition, the area dataset analysis has larger mean error and root mean square error values compared to the point dataset.

Keywords: Precipitation Data; Satellite-based Data; IDW; Drought Analysis; Temporal Scale.

1 Introduction

Many studies have been carried out in various fields that utilize precipitation data for various purposes. Research on drought will also rely heavily on the precipitation data, especially when drought can be understood as a condition when an area experiences a water deficit from its normal condition. However, nowadays there are many limitations in the availability of precipitation data, either it does not have enough data spatiotemporally or data not available publicly. The common precipitation data that can be used are measured precipitation data that have an advantage of high accuracy but only available on the point scale area. To assess drought, the spatial precipitation data is also needed. In the area without rainfall-gauge, satellite-based precipitation data can be used because it has a higher spatial resolution but also has many uncertainties that can cause low accuracy when predicting the precipitation value. So, the utilization of satellite-based precipitation data for drought assessment, must be preceded by assessing the agreement of precipitation data between local measurements and the satellite-based dataset.

Previous studies have shown the use of satellite-based weather data for different purposes, including drought analysis by comparing it first with the local data. For example, Mourtzinis et al., (2017) studied about the applicability of satellite-based precipitation data for agricultural application across the US Corn Belt. In this research, the objectives are i) to examine the agreement between local measured precipitation data (MPD) and satellite-based precipitation data (GSMaP) for point data analysis and interpolated-MPD and GSMaP for area data analysis, ii) determine the appropriate temporal scale that can be used for drought analysis, and iii) assessing the spatial distribution of the rainfall distribution.

West Java is one of the provinces in Indonesia with the rainy season from October - March and the dry season from April - September and dominated by agricultural land which is very vulnerable to climate related hazards, such as drought and flood. The results of this study will be helpful to get a better understanding of utilizing the satellite-based

precipitation data especially in the area with a limited measured precipitation data for drought analysis.

2 Materials and methods

2.1 Precipitation Data

The daily measured precipitation data (MPD) are obtained from Meteorology, Climatology, and Geophysical Agency in Indonesia from January 1981 - March 2013 with missing data for some period in some stations. There are a total of 52 stations across 16 regencies in West Java with average coverage reaching 680.38 km² per station.

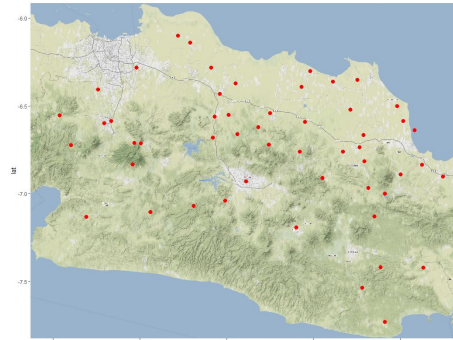


Fig. 1. The Location of 52 Rain Gauge Stations in West Java (represented by red dots)

Meanwhile, the satellite-based precipitation data collected from Japan Aerospace Exploration Agency (JAXA) which provide the near real-time rainfall data on their product called Global Satellite Mapping of Precipitation (GSMaP). The daily precipitation data are available from March 2000 - present date and were retrieved across West Java with 0.1° x 0.1° resolution.

2.2 Analysis Methods

The total precipitation for different timescale (daily, weekly, biweekly, 30-days, 60-days, 90-days, 120-days, 150-days, 180-days, 210-days, 240-days, 270-days, 300-days, 330-days, and 360-days) were calculated for the period between April 2000 - March 2013 both for MPD and GSMaP dataset.

The bias and agreement was assessed by calculating the mean error (ME) and root mean square error (RMSE). Then,

to examine the agreement between MPD and GSMaP data, linear regression was performed and the coefficient of determination or R-square (R^2) was calculated to decide the appropriate timescale for drought. Those analysis applied both for point data analysis (52 locations of local rainfall gauge stations (MPD) and the grid from GSMaP that coincided with those stations) and area data analysis. For the area data analysis, the interpolation of MPD dataset was conducted using Inverse Distance Weighted (IDW) method with $0.1^\circ \times 0.1^\circ$ resolution (the same with GSMaP resolution).

3 Results and discussion

3.1 Point Data Analysis

Figure 2 summarizes the agreement between MPD and GSMaP where horizontal axis indicates the various timescale and vertical axis indicates the value of R^2 . It can be seen that the agreement performed a parabolic pattern for the daily until 360-days scale with the turning point during the 150-days period and an anomaly during the 180-days period where the sudden decrease of R^2 values happened. This pattern and anomaly was predicted to be caused by the characteristic of the rainy and the dry season of the country which happened every 6 months. Also, the result will depend on the characteristics of the season for each region.

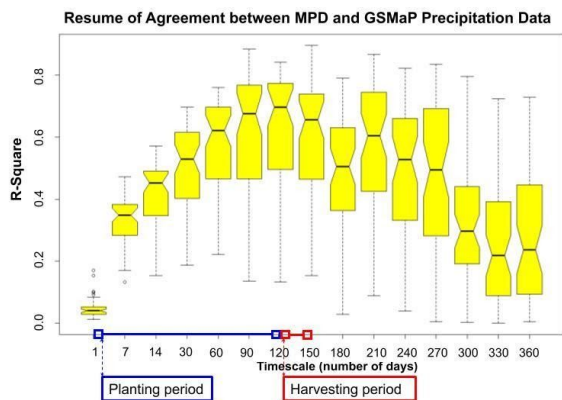


Fig. 2. Resume of agreement between MPD and GSMaP data for various timescale

Based on this result, it can be concluded that the acceptable timescale that can be considered to be used for drought assessment is a 90-days (3-months) period when the value of R^2 reaches the peak. For additional information, the blue line on the horizontal axis indicates the planting period of paddy occurred within 120 days and the red line indicated the harvesting period which usually occurred in the 30 days after the planting period ended. This result shows a good agreement of the two datasets occurred during the paddy's planting and harvesting period, so the timescale can be used for monitoring agricultural drought that might affect the paddy during crop season.

3.2 Area Data Analysis

Basically, the analysis to examine the area dataset is the same with point data analysis, the major difference lies in the interpolation method of MPD. The resume of R-square which examines the agreement between interpolated-MPD and GSMaP data can be seen in Figure 3. Generally, the pattern is the same with point dataset analysis (Figure 2), but unlike the point dataset result, during 150-days period or during harvesting period, the agreement shows more stable R-square value and starts decreasing during 180-days

period.

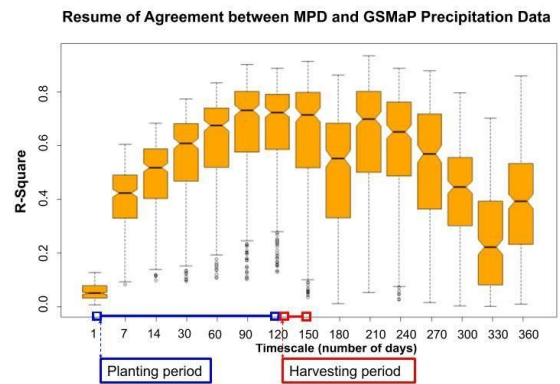


Fig. 3. Resume of agreement between interpolated-MPD and GSMaP data for various timescale

To see the difference in spatial distribution of precipitation between interpolated-MPD and GSMaP dataset, Figure 4 shows the map of West Java with information about 90-days R-square values on each grid from various timescale. The greenish color indicated higher R-square values which mean better agreement between two dataset, meanwhile the reddish color indicated lower R-square values or lower agreement between the dataset. The good agreement is an important aspect to be considered, because in this context, it can be interpreted that there is a strong relationship between the GSMaP dataset and the interpolated-MPD dataset or the difference between two precipitation dataset was much lower.

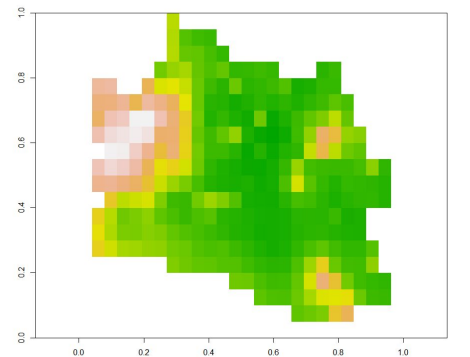


Fig. 4. Map of distribution R-square value for 90-days timescale

Conclusions

For the location with limited measured precipitation data, the satellite-based data can be utilized by assessing the agreement between the two datasets first. In West Java, it is suggested that the drought analysis can be conducted by using GSMaP precipitation data with 3-months period timescale, both for point dataset or area dataset. Further research needs to be done to validate the result before GSMaP dataset can be used for drought analysis, especially for agricultural applications.

Reference

- [1] Mourtzinis, S. et al, From grid to field: Assessing quality of gridded weather data for agricultural applications, *European Journal of Agronomy*, 82 (2017), 163-172.
- [2] World Meteorological Organization, 2012: Standardized Precipitation Index User Guide (M. Svoboda, M. Hayes and D. Wood). (WMO-No. 1090), Geneva.

Relationship between local and spatial probabilities of precipitation in the Yoneshiro River catchment

○Hajime YANAGISAWA¹, So KAZAMA¹, Ryo INOUE²

¹Graduate School of Engineering, Tohoku University, Sendai 980-8579, Japan

²Graduate School of Information Sciences, Tohoku University, Sendai 980-8579, Japan

*E-mail : hajime.yanagisawa.q7@dc.tohoku.ac.jp

Abstract

Probability of precipitation were calculated using Radar-AMeDAS rainfall and compared with the theoretical and analytical values of spatial probabilities in the Yoneshiro River catchment. Since the spatial probability of extreme precipitation is smaller in the analysis than in the theory, we focused on the independence and dependence of extreme precipitation occurrence. This study revealed that extreme precipitation event with a 100-year return period occurs once every 2.6 years in the Yoneshiro River catchment, and extreme precipitation actually occurs over an area that is theoretically thought to have little or no occurrence, and that there is a limit to the area of extreme precipitation occurrence.

Keywords: return period; extreme precipitation; radar-AMeDAS rainfall.

1. Introduction

Climate change associated with global warming will change the rainfall pattern in Japan, and short duration rainfall is likely to increase across the country in the future¹). Extreme precipitation event is sometimes represented as "once in 50 years" in terms of its return period at a location. Such extreme precipitation often causes widespread damage²). Therefore, it is important to know the probability of extreme precipitation over a large area in order to reduce the damage of future disasters. The purpose of this study is to evaluate the relationship between the point-occurrence probability and the spatial-occurrence probability in extreme precipitation.

2. Methods and Data

2.1 Study area

The target area is the Yoneshiro River catchment located in the north part of Akita Prefecture. It is the fifth largest river in the Tohoku region with a total length of 136 km and a drainage area of 4100 km².

2.2 Data sources

Radar-AMeDAS rainfall data were used to determine the probability of extreme precipitation events. The period covered is 29 years, from 1988 to 2016. The target area is divided into 18 meshes from east to west and 15 meshes from north to south, for a total of 270 meshes. 1 mesh is about 5 km square. The data size is unified to a coarse data size by averaging fine resolution data.

2.3 Spatial probability of precipitation

The annual maximum hourly precipitation was extracted from the Radar-AMeDAS rainfall data. The probability density functions of extreme precipitation were generated using the annual maximum hourly precipitation for each mesh, the GEV distribution and the PWM method, and the spatial distribution of extreme precipitation was generated. By comparing extreme precipitation and annual maximum hourly precipitation in each mesh, the number of years extreme precipitation event has been occurring in 29 years is calculated.

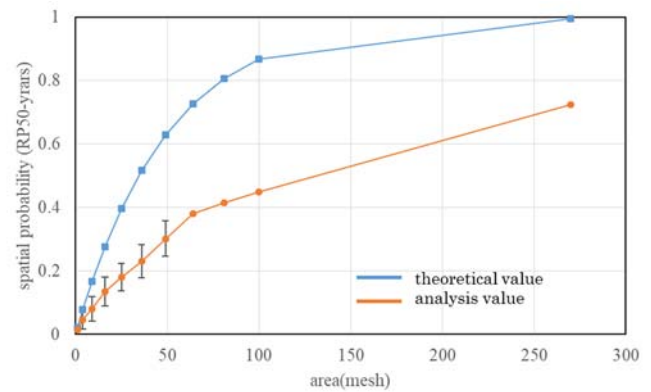


Fig. 1. Spatial-occurrence probability

The area for calculating the probability of spatial occurrence is called a compartment. Compartment should be square and not overlap in the target area. The spatial-occurrence probability is defined as "the probability of extreme precipitation greater than or equal to extreme precipitation in one or more meshes in a compartment". Figure 1 shows the spatial-occurrence probability of extreme precipitation in the 50-year return period for each compartment area. Extreme precipitation with a return period of 50 years occurs once every 1.38 years in the Yoneshiro River catchment.

2.4 Independence and Dependence of Precipitation

Next, in order to compare the spatial-occurrence probability obtained from the analysis with the theoretical probability, we calculate the theoretical value of the spatial-occurrence probability using the equation (1). The theoretical value of the spatial-occurrence probability is shown in Figure 1.

$$P = \frac{1}{n^k} \{ (n-1)^{k-1} \cdot {}_k C_1 + (n-1)^{k-2} \cdot {}_k C_2 + \dots + (n-1)^{k-k} \cdot {}_k C_k \}$$

P : space probability of precipitation ⋯(1)

k : term number (area : mesh)

n : return period (year)

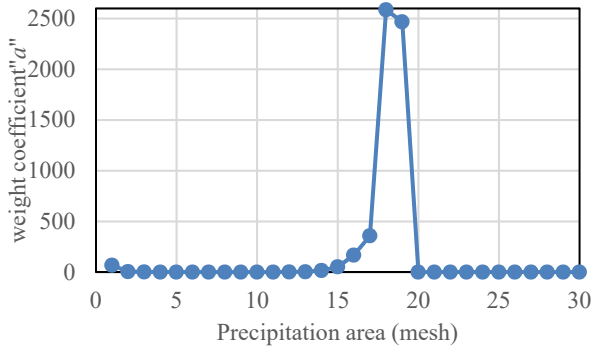


Fig. 2. Change in weight coefficient

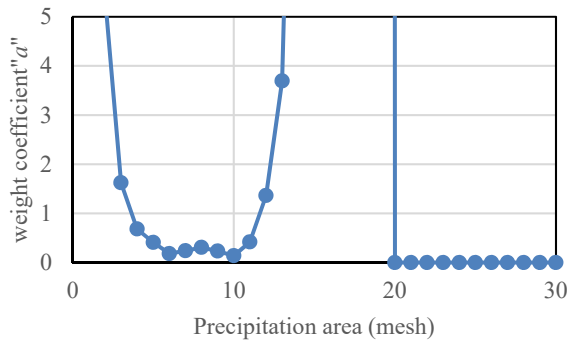


Fig. 3. Change in weight coefficient (enlarged version)

Figure 1 shows that the analytical value of the spatial-occurrence probability is lower than the theoretical value of the spatial-occurrence probability regardless of the return period. The reason for the difference between the theoretical and analytical values of the spatial-occurrence probability is related to whether or not extreme precipitation occurs independently between each mesh. We introduce a weight coefficient “a” as an indicator of independence. The weight coefficient is the ratio of the analytical value to the theoretical value of the occurrence probability for each precipitation area. The theoretical value of the spatial-occurrence probability including the weight coefficient can be calculated by Equation (2).

$$P = \frac{1}{n^k} \{ a_1 \cdot (n-1)^{k-1} \cdot {}_k C_1 + a_2 \cdot (n-1)^{k-2} \cdot {}_k C_2 + \dots + a_k \cdot (n-1)^{k-k} \cdot {}_k C_k \} \quad \dots(2)$$

$a_i (i = 1, k)$: weight coefficient

3. Results

As an example, the relationship between the weight coefficient and the precipitation area is shown in Figure 3 and 4 for a 10-year return period and 64-mesh compartment area. A weight coefficient of less than 1 indicates that the extreme precipitation occurs with high level of independence. From Figure. 3 and 4, it can be seen that up to about 11 meshes of precipitation area, the extreme precipitation occurs relatively independently at each mesh, which is in accordance with the theoretical spatial-occurrence probability. On the other hand, when the precipitation area is between 12 and 18 meshes, the value of the weight coefficient increases. This means that the extreme precipitation occurs over a wider area than is

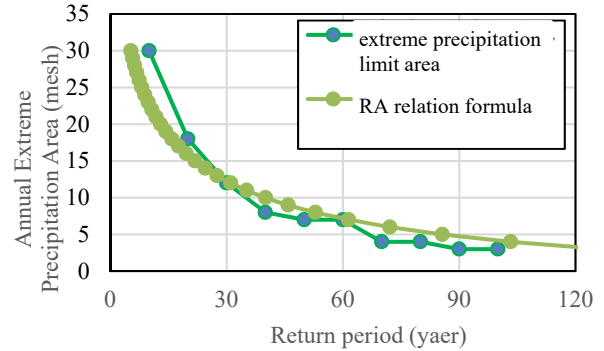


Fig. 4. RA-ralation formura and extreme precipitation limit area

theoretically possible. No precipitation was observed above 19 meshes. The results of the analysis for multiple compartment area and return period show that the area of independent extreme precipitation is a constant percentage of the compartment area, while the area of dependent extreme precipitation is constant regardless of the compartment area. For extreme precipitation with a return period longer than 60 years, independent extreme precipitation occurs over a constant area regardless of the compartment area, and dependent extreme precipitation rarely occurs.

Since there is a limit to the annual extreme precipitation area regardless of the compartment area, the extreme precipitation limit area was determined for each return relationship. These results are compared with the RA relationship (the relationship between return period and extreme precipitation area) reported by Sugawara et al.³⁾ and are shown in Figure 4. As a result, it is suggested that extreme precipitation with a return period of more than 30 years occurs once a year in the Yoneshiro River catchment, and that extreme precipitation with a return period of less than 30 years may occur more than once a year.

4. Conclusions

The following are the conclusions obtained.

- 1) The spatial-occurrence probability of extreme precipitation is smaller in the analytical value than in the theoretical value. This trend is not changed by the return period.
- 2) Comparison with the RA relation suggests that extreme precipitation with a return period of less than 30 years may occur more than once a year in the Yoneshiro River catchment.

5. Acknowledgements

We wish to thank Tohoku Regional Development Association and Mitsui Consultants Co., Ltd for their generous financial assistance. This research was supported by the Social Implementation Program on Climate Change Adaptation Technology (SI-CAT) of MEXT, Japan

6. Reference

- [1]. Global warming prediction information, Vol.8, 2013
- [2]. K. Ikeyama, T.Yoshida, Y. Minakawa, T.Kubota, Analysis of long-term changes in heavy rainfall in terms of rainfall and temporal concentration, Japan Society of Hydrology and Water Resources, p.128-, 2019
- [3]. Y. Sugawara, S. Kazama, Y. Touge : Analysis of spatial distribution characteristic of heavy rainfall using Rader-AMeDAS composite precipitation, journal of JSCE Vol.74, No.4, I_343-I348, 2018

Estimation of the risk of inland flood based on distribution of extreme precipitation in Japan

○ Hayata YANAGIHARA^{1*}, Tao YAMAMOTO¹ & So KAZAMA¹

¹Department of Civil Engineering, Graduate School of Engineering, Tohoku University, Miyagi 980-8579, Japan.

*E-mail: yanagihara.hayata.r1@dc.tohoku.ac.jp

Abstract

This study estimated the damage cost caused by inland flood in Japan based on the distribution of extreme precipitation and identified insufficient areas of flood protection for high risk. The inundation depths and the damage costs were calculated using the two-dimensional unsteady flow model and the Manual for Economic Evaluation of Flood Control Investment (Draft) published by the Ministry of Land, Infrastructure, Transport, and Tourism. In flood simulation, we set up two inundation scenarios (natural drainage scenario and poor drainage scenario) with or without drainage by gravity to rivers. The natural drainage scenario corresponds to inland floods caused by the elevation, while the poor drainage scenario corresponds to inland floods caused by drainage to rivers. As a result, the expected damage cost was estimated to be 618 billion JPY/year in the natural drainage scenario. The damage cost was the largest in Kanagawa prefecture, followed by Aichi prefecture, Osaka prefecture, Okayama prefecture, and Hokkaido prefecture. On the other hand, the expected damage cost was estimated to be 9,422.4 billion JPY/year in the poor drainage scenario. The damage cost was the largest in Tokyo Metropolis, followed by Osaka prefecture, Aichi prefecture, Hokkaido prefecture, and Saitama prefecture.

Keywords: urban flood disaster; flood simulation; economic loss; drainage by gravity to rivers.

1 Introduction

In urban areas, there are concerns that inland flood damage will increase due to climate change. It is necessary to quantitatively evaluate the spatial risk of inland flood to consider the direction and priority of adaptation measures. As a previous study on evaluation of the risk of inland flood, Karamouz *et al.* (2017)^[1] analyzed inland flood considering storm surge in Lower Manhattan, New York City. Kawagoe *et al.* (2011)^[2] estimated the inland flood risk in Fukushima prefecture. However, these studies analyzed inland flood in a limited area. In this study, we estimated the damage cost caused by inland flood in Japan based on extreme precipitation data of Kawagoe *et al.* (2008)^[3] and identified insufficient areas of flood protection for high risk.

2 Datasets

2.1 Distribution of extreme precipitation data

We used the distribution of extreme precipitation data with a 1km spatial resolution created by Kawagoe *et al.* (2008)^[3] in order to estimate the risk of inland flood considering regional climatic characteristics. The distributions of extreme precipitation data for return periods of 5, 10, 30, 50, 100, and 200 years were used.

2.2 Elevation data and land-use data

The elevation data of the fifth-order mesh used in flood simulation was obtained from the Digital National Land Information download services^[4]. The land-use data of the fifth-order mesh created by Tanaka *et al.* (2019)^[5] was used in this study. The land-use data was used for calculating inundation depths and the damage costs.

2.3 River identification data

The river identification data used in flood simulation is a combination of the following: (1) meshes classified as rivers in the land-use data, (2) meshes in the river mesh data of the

Table 1 Inundation scenario

Scenario name	Content
Natural drainage scenario	1) Precipitation with a return period of 5 years is drained away. 2) Precipitation is always drained to rivers by gravity.
Poor drainage scenario	1) Precipitation with a return period of 5 years is drained away. 2) All precipitation stays on inland.

fifth-order mesh where the section type is designated as either a Class A direct-controlled sections, Class A designated sections, or Class B river sections. The river mesh data of the fifth-order mesh was created by rasterizing the river line data of the Digital National Land Information download services^[4].

3 Method

3.1 Inundation scenario and flood simulation

In this study, we set up two inundation scenarios with or without drainage by gravity to rivers as shown in Table 1. The natural drainage scenario corresponds to inland floods caused by the elevation, while the poor drainage scenario corresponds to inland floods caused by drainage to rivers. In flood simulation, the two-dimensional unsteady flow model in the Cartesian coordinate system (Tezuka *et al.* 2014^[6]) was applied without separating the river and the floodplain. The grid size of flood simulation is the fifth-order mesh (approximately 250m×250m). The parameters used in flood simulation were based on Tanaka *et al.* (2019)^[5]. In the natural drainage scenario, the water depth of rivers was set to 0 to express drainage by gravity to rivers. On the other hand, the inflow to rivers was set to 0 in the poor drainage scenario to express poor drainage to rivers.

The current sewage system is planned to be able to drain precipitation with a return period of 5 years in many areas. Considering the increase in inland flood damage due to climate change, it is necessary to raise the level of inland flood protection. It is also necessary to consider the direction and priority of inland flood protection to reduce inland flood damage with a limited budget. Therefore, in inundation scenarios shown in Table 1, we assume that it is possible for precipitation with a return period of 5 years to drain properly. Based on the results of the analysis, we discuss the direction and priority of inland flood protection for each inundation scenario.

3.2 Estimation of the damage cost

The damage costs were calculated using the Manual for Economic Evaluation of Flood Control Investment (Draft)^[7] published by the Ministry of Land, Infrastructure, Transport, and Tourism. This study targeted only direct damage to general assets and agricultural products. The damage cost was calculated by multiplying asset values by damage rates defined by inundation depth. The expected damage cost was calculated by aggregating the annual average damage cost by the scale of precipitation which was obtained by multiplying the damage cost by occurrence probabilities of precipitation events.

4 Results and discussion

Fig.1 shows the expected damage cost by prefecture. The expected damage cost was estimated to be 618 billion JPY/year in the natural drainage scenario. The damage cost was the largest in Kanagawa prefecture, followed by Aichi prefecture, Osaka prefecture, Okayama prefecture, and Hokkaido prefecture. On the other hand, the expected damage cost was estimated to be 9,422.4 billion JPY/year in the poor drainage scenario. The damage cost was the largest in Tokyo Metropolis, followed by Osaka prefecture, Aichi prefecture, Hokkaido prefecture, and Saitama prefecture. In areas where the damage cost is high in the natural drainage scenario, precipitation tends to stay because the drainage by gravity to rivers is poor due to the terrain. In such areas, the development of pump stations is necessary to reduce the inland flood risk. In areas where the damage cost is high in the poor drainage scenario, it is necessary to improve the operability of sluicing outlets and to promote cooperation between rivers and sewers. This study is expected to provide useful information to consider the direction and priority of inland flood protection.

5 Conclusions

This study estimated the damage cost caused by inland flood in Japan based on the distribution of extreme precipitation data. The damage cost was the largest in Kanagawa prefecture, followed by Aichi prefecture, Osaka prefecture, Okayama prefecture, and Hokkaido prefecture in the natural drainage scenario which corresponds to inland floods caused by the elevation. On the other hand, in the poor drainage scenario which corresponds to inland floods caused by drainage to rivers, the damage cost was the largest in Tokyo Metropolis, followed by Osaka prefecture, Aichi prefecture, Hokkaido prefecture, and Saitama prefecture.

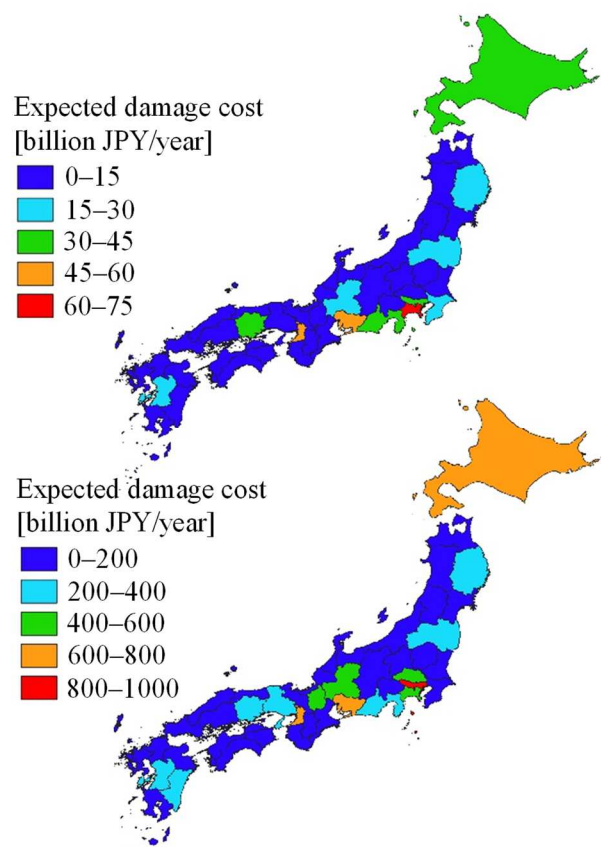


Fig. 1. The expected damage cost by prefecture (From the top to bottom: natural drainage scenario, poor drainage scenario)

Reference

- [1] Karamouz, M. *et al.*, Integration of inland and coastal storms for flood hazard assessment using a distributed hydrologic model, *Environmental Earth Sciences*, Vol.76, No.395 (2017).
- [2] Kawagoe, S. *et al.*, Projection of inland flood risk due to hourly heavy rainfall in administrative district, *Journal of Japan Society of Civil Engineers, Ser.G (Environment)*, Vol.67, No.5 (2011), pp.I_47-I_54 (in Japanese).
- [3] Kawagoe, S. *et al.*, A probability model of sediment hazard based on numerical geographic information and extreme precipitation data, *Journal of Japan Society for Natural Disaster Science*, Vol.27, No.1 (2008), pp.69-83 (in Japanese).
- [4] Ministry of Land, Infrastructure, Transport and Tourism, Digital National Land Information download services, <https://nlftp.mlit.go.jp/ksj/>.
- [5] Tanaka, Y. *et al.*, Assessment of the risk of flood and storm surge with flood control facilities, *Journal of Japan Society of Civil Engineers, Ser.B1 (Hydraulic Engineering)*, Vol.75, No.2 (2019), pp.I_109-I_114 (in Japanese).
- [6] Tezuka, S. *et al.*, Estimation of the effects of climate change on flood-triggered economic losses in Japan, *International Journal of Disaster Risk Reduction*, Vol.9 (2014), pp.58-67.
- [7] Ministry of Land, Infrastructure, Transport and Tourism, Manual for Economic Evaluation of Flood Control Investment (Draft), River Bureau (2005).

Evaluating the effect of dryness on wildfire in Tohoku region using KBDI and PDSI

○ Chenling Sun^{1*}, Yoshiya Touge¹, So Kazama¹

¹Department of Civil and Environmental Engineering, Tohoku University, Miyagi 980-8579, Japan.

*E-mail: sun.chenling.s5@dc.tohoku.ac.jp.

Abstract

There is a significant link between dryness and wildfire because dryness on a time scale of climate and weather can significantly affect the moisture content of available fuel. Many dryness indices have been developed to effectively evaluate dryness and thus be used to assess wildfire risk. Tohoku region of Japan is prone to wildfires, especially from March to May. In this study, we utilized KBDI and PDSI to evaluate the effect of dryness on wildfire in Tohoku region of Japan by comparing with wildfire statistics. Results show that KBDI is not suitable dryness index for wildfire research in the Tohoku region of Japan. On the other hand, compared the result of PDSI and wildfire statistics, it indicated that dryness will increase the probability of wildfire and severe dryness is likely to cause widespread burning. However, these two dryness indexes cannot take into account the impact of snowmelt on dryness. We need to select another index that takes into account the effects of snowmelt to analyze the impact of dryness on wildfires in the future.

Keywords: KBDI; PDSI; Wildfire; Dryness.

1 Introduction

In the coming decades, climate change will bring higher temperatures and changes in rainfall patterns. These climate changes will increase the likelihood of dryness in many parts of the world, thus creating favorable conditions for wildfires. There is a significant link between dryness and wildfire because dryness on a time scale of climate and weather can significantly affect the moisture content of available fuel. Many dryness indices have been developed to effectively evaluate dryness and thus be used to assess wildfire risk. The Keetch/Byram dryness index (KBDI) is typical index for assessing dryness and widely used in wildfire monitoring that has been applied in a variety of areas, including the United States, south eastern Australia and Malaysia. Furthermore, statistical analysis shows that KBDI is the most appropriate empirical dryness index in the Mediterranean region. Palmer (1965) developed the Palmer Dryness Severity Index (PDSI) using temperature data and physical water balance models that take into account precipitation, soil moisture, runoff, and potential evapotranspiration. The dryness index involves clear physical mechanisms, so it can be used to monitor the long-term evolution of dryness and capture the basic impact of global warming on dryness through changes in potential evapotranspiration.

Each dryness index has its own advantages and disadvantages. Neither of these two dryness indexes can consider the impact of snowmelt on dryness, so there is a limit to the evaluation effect of dryness in areas with long snowfalls. In Japan, Tohoku region is prone to wildfire. Kamaishi and Kurihara wildfires occurred successively on May 8, 2017. For Kamaishi wildfire, it was a big-scale fire and its burned area was 413ha, which was greater than the total of burned area for the whole of Japan in 2016. The purpose of this study is to use KBDI and PDSI to evaluate dryness in Tohoku of Japan, and compare the results with wildfire statistics, so as to evaluate the impact of dryness on wildfire in Tohoku region of Japan.

2 Materials and methods

2.1 Keetch/Byram dryness index

KBDI is a number representing the net effect of evapotranspiration and precipitation in producing cumulative moisture deficiency in deep duff and upper soil layers [1]. This index requires only few meteorological data, maximum daily temperature, total daily precipitation and the mean annual precipitation. The KBDI is calculated from the following equation in metric system:

$$KBDI^t = KBDI^{t-1} + DF^t - RF^t \quad (1)$$

Where DF^t is dry factor in one day, DF^t is rainfall factor.

$$RF^t = \frac{(203 - KBDI^{t-1})(0.968e^{(0.875 \times T_m + 1.552)} - 8.3) \times 10^{-3}}{1 + 10.88e^{(-0.001736 \times R_0)}} \quad (2)$$

RF^t is depended on daily precipitation. T_m represents daily maximum temperature, R_0 is the mean annual rainfall. When the daily precipitation is more than 5mm (0.2in), the daily precipitation will decrease KBDI. The value of KBDI ranges from 0 to 203mm, the larger the KBD value indicates the drier condition.

2.2 Palmer Dryness Severity Index

The calculation of PDSI requires precipitation and potential evapotranspiration, as well as the available water capacity (AWC) of the soil. Firstly, the difference between the actual precipitation (P) and climatically appropriate for existing conditions precipitation (\hat{P}) can be calculated based on the water balance. It is an indicator of water deficiency or surplus.

$$d = P - \hat{P} \quad (3)$$

The same water deficiency (d) value may reflect different humidity conditions given specific region and specific month. To correct for this aspect, the climatic characteristic K is used to weight the water deficiency.

Then, d and climatic characteristic K were used for climate correction to obtain water deficit index Z, which indicates the deviation of actual wetness/dryness conditions from the long term annual average water availability in a given region during a given month. Considering the influence of early water shortage on dryness conditions, the dryness duration and Z value of each dryness event were calculated to analyze the influence of early water shortage on dryness intensity (Equation 4). The PDSI is a standardized measure, ranging from about -10 (dry) to +10 (wet).

$$PDSI_i = 0.897PDSI_{i-1} + \frac{1}{3}Z_i$$

(4)

Daily precipitation data covering a period of 1995–2012 were obtained from the Asian Precipitation Highly-Resolved Observational Data Integration Towards Evaluation (APHRODITE) of Water Resources project and were analyzed in this study. We used wind speed, air temperature and radiation data obtained from dynamical regional downscaling of the JRA-55 reanalysis data set (DSJRA-55).

3 Results and discussion

Not only did more than 100 hectares of wildfire occur in Tohoku between 1995 and 2012, but there were also many wildfires burning less than one hectare. In order to make better use of the dryness index to analyze the impact of dryness on wildfire, we divided the discussion into three categories according to the burned area: less than 1 hectare, 1-10 hectare and more than 10 hectares. In this study, we selected the average KBDI value and the average PDSI value in the city where wildfire occurred and compared them with and wildfire statistics (Fig 1 and Fig 2).

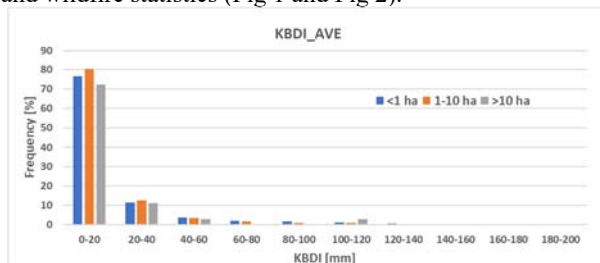


Fig. 1. Frequency of 10 intervals of KBDI in 3 categories.

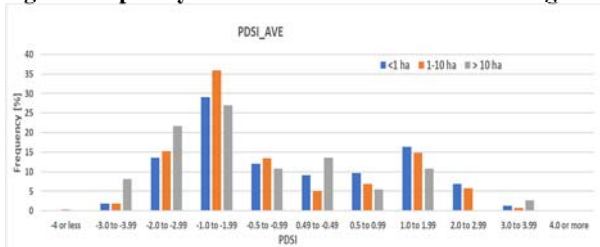


Fig. 2. Frequency of 11 intervals of PDSI in 3 categories.

The frequency in these figures was defined by following equation:

Frequency =

$$\frac{\text{Number of wildfire occurrence in the interval of KBDI or PDSI}}{\text{Number of wildfire occurrence}}$$

The KBDI value indicated that leaf litter begins to dry when the value is more than 50. However, most KBDI values are concentrated in the 0-40 mm and when KBDI is greater than 40 mm, the total frequency is less than 15%. KBDI results are similar for the three categories. Compared with wildfire statistics, it cannot be shown that the correlation between KBDI and wildfire occurrence and burned area in Tohoku region of Japan. Although KBDI is widely used, it has been indicated that there is still a need to improve the structure or application of the KBDI model, especially for climate, soil, and hydrology in areas that differ from Florida, such as tropical wetland ecosystems in Southeast Asia. These revealed that KBDI is not applicable to the study of wildfire in Tohoku region of Japan. For PDSI, -0.5 is an indicator for the beginning of dry spell. The maximum frequency occurred when the PDSI value is at the interval of -1.0 to -1.99, which

stands for mild dryness. The total frequency of PDSI values less than -0.5 was approximately 67% when the burned area was more than 10 hectares, 66% when the burned area was 1-10 hectares, and 56% when the burned area was less than 1 hectare. Regardless of the size of the burned area, more than half of wildfires in 1995-2012 occurred during periods of dryness. The results show that dryness increases the probability of wildfire. When the PDSI is less than -3.0, it indicates that the area is in severe dryness and extreme dryness, and the frequency of wildfires with burned areas greater than 10 hectares is much greater than that of small burned areas. It turned out that the degree of dryness affects the severity of wildfires and severe dryness is likely to cause widespread burning. But PDSI results also show that nearly 40 percent of wildfires, even those burned more than 10 hectares, occurred during periods that are not dry. The PDSI is based on a physical water-balance model, uses more variables as input and takes the precedent condition into account. Nevertheless, snowfall, snow cover, and frozen ground are not included in the index. All precipitation is treated as rain, so that the PDSI values may be inaccurate in the winter and spring months in regions where snow occurs. Statistics displayed that most wildfires in Tohoku region occurred between March and May, therefore, PDSI has limited applicability in the Tohoku region of Japan, which is covered by snow in winter and spring.

4 Conclusions

In this study, KBDI and PDSI were used to analyze the effects of dryness on Tohoku region of Japan. The application of KBDI in other climates may still be problematic without any adjustment to the model structure, as the drying rate of the index depends on the mean annual precipitation in Florida state [2]. It was shown that KBDI is not suitable dryness index for wildfire research in the Tohoku region of Japan. On the other hand, more than half of wildfires in 1995-2012 occurred during periods of dryness (PDSI<-0.5), which indicates that dryness increases the probability of wildfire. In addition, the degree of dryness affects the severity of wildfires and severe dryness is likely to cause widespread burning. Although KBDI and PDSI have been widely used for dryness monitoring and wildfire risk monitoring, but they still have some limitations. In Tohoku region of Japan, the area is covered with snow for a long time in winter, and the melting of snow in spring causes more dryness in the area. These two dryness indexes all cannot take into account the impact of snowmelt on dryness. Therefore, we need to use other dryness index to consider the effect of snowmelt on dryness in the future.

Acknowledgements

This research was supported by the Ministry of Education, Science, Sports and Culture, Grant-in Aid for Scientific Research(B), 2020-2023(20H02248, Yoshiya Touge).

Reference

- [1] Keetch, J.J., Byram, O.M., 1968. A dryness index for forest fire control. USDA Forest Service Research Southeastern Forest Experiment Station, Asheville (2004). pp. SE-38.
- [2] Taufik et al., 2015 M. Taufik, B.I. Setiawan, H.A.J. van Lanen Modification of a fire dryness index for tropical wetland ecosystems by including water table depth Agric. For. Meteorol., 203 (2015), pp. 1-10.

Evaluate the effect of fuel moisture content on the heat required for ignition in the Tohoku Region of Japan

○ Qin HUANG^{1*}, Yoshiya TOUGE¹

¹Department of Environmental Engineering, Environmental University, Miyagi 980-8579, Japan.

*E-mail: huang.qin.p5@dc.tohoku.ac.jp.

Abstract

The research of litter layers in forests is of great significance to the control and prevention of wildfires. The duff moisture content is an important characteristic of the fuel. In this study, through on-site sampling experiments, the changes in the water content of deciduous leaves of four tree species in Tohoku Region of Japan were observed and analyzed. And taking into account the general combustion process of forest combustibles, uses formulas to calculate the heat required for combustibles to be heated to ignition temperature. Evaluate and demonstrate the effect of moisture content in the sample on heat required for ignition and fire process. The results show that the vast majority of the heat required for ignition is used for the evaporation of water in combustibles, almost 80% to 90% of the total.

Keywords: heat required; duff moisture; ignition; combustibility; evaporation.

1 Introduction

Ignition is the initial stage of combustion and is one of the most important processes of fire disaster. As the main fuel source for surface fires, to a certain extent, the in-depth study of the duff layers is the key to the simulation of the subsequent fire development and spreading process, also for the subsequent reduction of the fire risk. And the control of fire danger provides a certain theoretical basis.

The duff litter on the woodland is the main kindling. When the fire source falls on the ground, it first comes into contact with these potential combustibles, causing combustion. If the combustibles are continuous, the combustion moves from the primary reaction to the secondary reaction, and the combustion process alternates. The so-called primary reaction means that after the combustibles are heated, they evaporate the moisture content and undergo thermal decomposition to produce combustible gas and start spontaneous combustion. According to the combustion process, Rothermel proposed the equation of the heat energy required for pre-ignition [1]. Based on this equation, Zhang after further analysis and modification, and a special discussion on the energy required for the escape of water [2]. A heat energy balance equation including four factors of ignition point, calorific value, moisture content, and water evaporation rate in combustibles was proposed to reveal the combustion characteristics of different plant species.

The fuel moisture affects the combustibility of combustibles and is a major factor of the occurrence and development of wildfires, which in turn affects the fire probability, spread speed, and fire behavior [3].

In this research, considering the general process of forest combustible combustion, calculate the amount of heat energy required when the combustible is heated to the ignition point so that the heat required for ignition of different combustibles can be distinguished more accurately, to determine the combustibility of combustibles. Evaluate and demonstrate the influence of sample moisture content on the ignition heat and ignition process.

2 Materials and methods

2.1 Field sites and sampling

Aoba Mori, located in Sendai City, Miyagi Prefecture, was selected as the observation field. The observation period is from March 18 to April 4 and August 20 to August 28 in 2020.

Selected four fuel species. Respectively cedar, broadleaf, cypress and pine zone. Three collection points were selected at each site, and the surrounding terrain was taken into consideration. Samples from litter layers were collected daily on no-rain days, and randomly collect the duff sample at each point. In March, mixed sampling of the upper and lower layers of the garbage layer was carried out, and in August, only the upper layer of the garbage layer was collected. Measure soil moisture at the same place. Dry in the laboratory and weigh wet and dry mass.

2.2 Heat required for ignition

Rothermel put forward in the mathematical model of forest fire spread, the calculation equation of heat required for ignition of unit mass combustibles is;

$$Q_{ig} = C_{pd} \cdot \Delta T_g + M_f (C_{pw} \cdot \Delta T_b + V_b) \quad (1)$$

Where: C_{pd} is the specific heat of wood ($\text{kJ} \cdot \text{kg}^{-1} \cdot \text{°C}^{-1}$); ΔT_g is the temperature range to ignition (°C); M_f is the fuel moisture content (%); C_{pw} is the specific heat of water ($\text{kJ} \cdot \text{kg}^{-1} \cdot \text{°C}^{-1}$); ΔT_b is the temperature range to boiling (°C); V_b is the latent heat of vaporization ($\text{kJ} \cdot \text{kg}^{-1}$).

Rothermel takes the ignition temperature to be 320°C and the boiling temperature of water to be 100°C , then the heat required for ignition can be expressed by an equation containing only M_f :

$$Q_{ig} = 250 + 1116M_f \quad (2)$$

However, at the same moisture content level, due to the different physical and chemical properties and size of the combustibles, especially the difference in specific surface area, the moisture escape speed is different, and the difference in the amount of heat required for ignition is caused. For this reason, Zhang proposed the following equations of heat energy requirement for pre-ignition considering moisture content, ignition point, and moisture evaporation rate:

$$Q_{ig} = C_{pd} \cdot \Delta T_g (1 - M_f) + M_f (C_{pw} \cdot \Delta T_b + k \cdot V_b) \quad (3)$$

Where k is the vaporization coefficient of water vaporization in wood combustible equivalent to pure water, dimensionless. Through the water evaporation measurement experiment on

pure water and water in combustibles, the k value can be calculated. Due to the different calculation methods of water content, the dry matter content turns to $(1 - M_f)$.

3 Results and discussion

For northeastern Japan, the traditional peak wildfires period is during the dry season, which is generally throughout March and April, it makes sense to sample and experiment with forest combustibles during this period. The end of August is the hottest time of the year, but fires are rare during this period, experiments with forest combustibles during this period show how the duff moisture content of litter layers is different from that of spring at the highest temperatures. The observation results are shown in Fig.1.

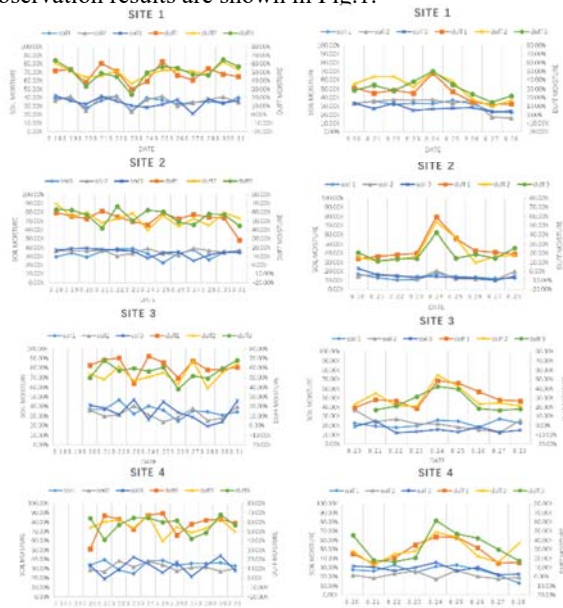


Fig. 1. The duff moisture contents and soil moisture contents of four sites in March and August

As can be seen from the figure, soil moisture at sites 1, 3 and 4 at the end of August changes between 20% and 40%, while site 2 content changes between 10% and 30%. The duff moisture basically maintained between 20% and 40%. As a result of the rain on the morning of August 24th, we can see the 24th day of the moisture content increased significantly, in the absence of rain days to maintain a decline. In general, there were similar trends in duff moisture content changes in the four sites. Compared with August, the trend of duff moisture change in March is wide and not obvious, generally between 30% and 60%, but the situation larger than 60% is also very common, because 22nd and 29th had rainfall, moisture content had a small increase. Soil moisture in site 3 changes in 30% to 50%, while changes in other sites range from about 20% to 40%. Although the comparison between the two periods is somewhat different from what was expected, I think it may be due to a change in sampling methods and will continue to be observed in the next spring.

According to equation (3), we can divide the required heat into three parts, the first of which is the heat to increase the amount of dry matter contained in a unit of combustible from room temperature to the point of ignition; The second item is the heat to increase the moisture in a unit of f combustible from room temperature to 100°C; The third item is the heat required for the complete vaporization of water under 100°C.

By analyzing Zhang's experimental results, the results are shown in the fig. 2.

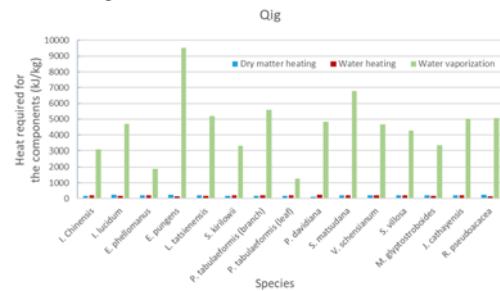


Fig. 2. The values of the three components of heat required for 15 species of samples.

It can be seen from the above figure that the third item of the heat required equation requires several dozens of times the energy required by the first and second items, almost 80-90% of the total. So that the most of the heat required for the ignition of forest combustibles is used for the evaporation of water. Combustibles with high moisture content consume a large amount of heat energy for water evaporation before being ignited. Although the moisture of all samples is not uniform, the range is between 45-60%, but due to the large difference in the k , which is 7-45%, it has a greater impact on the required heat. It can be explained that the water vaporization coefficient has a greater impact on heat required. Among them, *P. tabulaeformis*, its branches and leaves were tested separately, and the energy required by the branches was 3.6 times that of the leaves. This conclusion reasonably explains why fine combustibles can burn earlier than thick combustibles under the same moisture content.

4 Conclusions

By calculating the heat required for ignition, analyzing the combustibility of fuels, and judging the difficulty of combustion. As a result, among the components of the heat required, the part used to evaporate the water in the accounts for most of the total. This shows that the moisture content affects the required heat, i.e. the effect on the combustibility of the fuel. Meanwhile, the moisture escape intensity is also a significant factor. We plan to observe the moisture content of the litter layers at the four selected observation sites, and use it to calculate the heat required for ignition in this place, then evaluate the combustibility. Due to results from the obtained, sampling experiments will continue in the next spring.

5 Acknowledgements

This research was supported by the Ministry of Education, Science, Sports and Culture, Grant-in Aid for Scientific Research(B), 2020-2023 (20H02248, Yoshiya Touge).

Reference

- [1] Rothermel, Richard C. A mathematical model for predicting fire spread in wildland fuels. Vol. 115. Intermountain Forest & Range Experiment Station, Forest Service, US Department of Agriculture, 1972.
- [2] Zhang, J. Q., et al. Heat Balance Analysis on Burning Process of Woody Plants, Journal of Northeast Forestry University (1998), 26 (5). 34-38.
- [3] Fang, M. X., et al. Kinetic study on pyrolysis and combustion of wood under different oxygen concentrations by using TG-FTIR analysis, Journal of analytical and applied pyrolysis 77.1 (2006): 22-27.

High loading capacity of EGSB reactor with anammox-HAP sludge at extremely low temperature of 7°C

○ Ying SONG^{1*}, Lan LIN¹ & Yu-You LI²

¹Department of Environmental Engineering, Environmental University, Miyagi 980-8579, Japan.

²Department of Water Environment, Engineering University, Miyagi 980-8579, Japan.

*E-mail: song.ying.q2@dc.tohoku.ac.jp

Abstract

Anammox process as an autotrophic nitrogen removal appears to be a cost-effective and high-efficient technology in wastewater treatment field. The main challenges to overcome of this new frontier have been widely thought as lower temperature, together with a requirement of high and stable nitrogen removal efficiency. In this study, an EGSB reactor with anammox-HAP granules was operated more than 200 days at constant 7°C to explore the nitrogen capacity and activity of the anammox bacteria. The nitrogen concentration of influent was kept at 250mg-N L⁻¹ and the nitrogen loading rate was improved from 1.0 g-N L⁻¹ d⁻¹ to 3.5 g-N L⁻¹ d⁻¹ by shortening the hydraulic retention time from 6 h to 1.7 h. The high settling velocity of anammox-HAP granules guaranteed no sludge washout under lower HRT conditions. The yield of biomass and microbial community were also investigated. Anammox-HAP granular sludge adapted to 7°C was used for batch experiments at different temperatures, representing the recoverability of anammox activity when turning to higher temperature.

Keywords: Anammox; Hydroxyapatite(HAP); Low temperature

1 Introduction

Anaerobic ammonium oxidation(anammox), as one of the most attractive and promising nitrogen removal processes, has been gradually advanced to engineering applications in recent years. No demand of oxygen and organic carbon addition are the advantages of anammox process in which nitrite and ammonium could be converted to nitrogen gas by autotrophic deep-branching Planctomycetes.

High temperature dependency(20 to 30°C), notoriously long doubling time(10 to 25 days) and stability of operation have been hindering the implementation of mainstream anammox. To further broaden its applications for the regions with low temperature, several attempts have been made to explore the impact of lower temperature on the anammox activity and biomass growth (e.g. long-term, short-term cold shock and ambient temperature operation). Both in the long-term exposure and batch tests of low temperature, sludge activity was considerably inhibited with heterotrophic denitrification bacteria proliferation. For the one-stage anammox process, the response of anammox bacteria to low temperature was more intense than ammonia-oxidizing bacteria(AOB), resulting in imbalance the nitrification and anammox process, further disturbing and deteriorating the performance of the reactor. As reported, anammox activity was dramatically decreased with a sharp drop of temperature from 15°C to 11°C and was barely undetectable after operated at 11°C for a month(Laureni et al., 2016b). However, sufficient biomass retention time could compensate for the lose in anammox activity caused by low temperature, which indicated lower temperatures was not necessarily a problem for anammox process(Hendrickx et al., 2012).

A new concept combining anammox and phosphorus recovery by forming hydroxyapatite(HAP) was proposed(Ma et al., 2020). The distinct double-layer granules of the anammox biofilm attached to the HAP-core were observed. It is proven that the settling velocity and retention performance were remarkably improved by anammox-HAP

granules. The feasibility of anammox-HAP granules has yet to be proven, as granule disintegration may occur due to lower temperature, as was previously observed for anaerobic granules.

This study was conducted to a explore the nitrogen removal capacity, activity and metabolism of the anammox bacteria using an Expanded Granular Sludge Bed(EGSB) reactor with anammox-HAP granules under extremely low temperature of 7°C which is by far the lowest reported in the literature.

2 Materials and methods

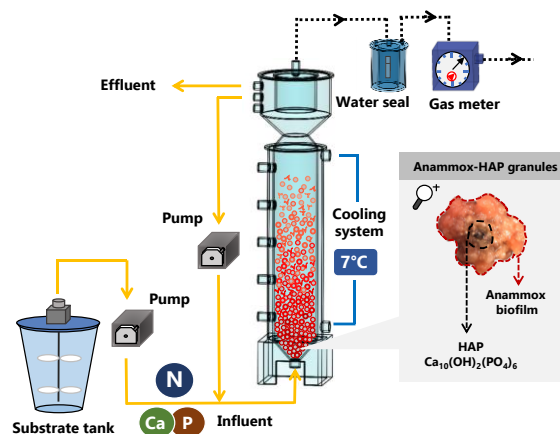


Fig.1 Schematic diagram of the EGSB reactor with anammox-HAP sludge

The schematic diagram of the expanded reactor set-up was shown in the Fig.1. The nitrogen species of liquid samples were tested by Agilent 7100 capillary electrophoresis (CE) system. Specific anammox activity and stoichiometry was calculated according to previous research(Zhang et al., 2018). VSS (volatile suspended solid) was measured based on the

APHA methods. The temperature in the reactor was controlled at around 7°C by a water jacket.

3 Results and discussion

3.1 Nitrogen removal performance

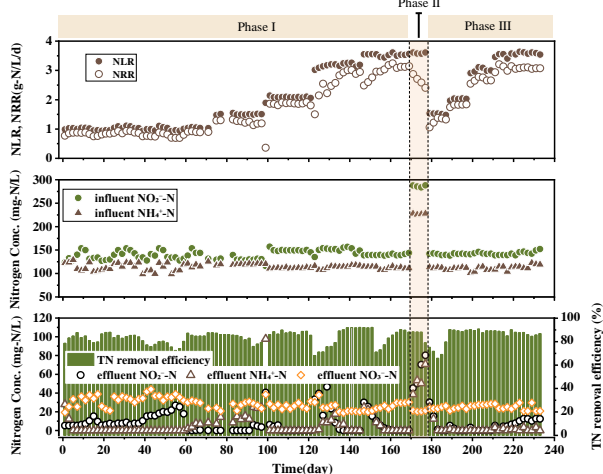


Fig.2 Nitrogen Loading Rate (NLR), Nitrogen Removal Rate (NRR), influent $\text{NH}_4^+\text{-N}$, $\text{NO}_2^-\text{-N}$ concentration, effluent $\text{NH}_4^+\text{-N}$, $\text{NO}_2^-\text{-N}$, $\text{NO}_3^-\text{-N}$ concentration and Total Nitrogen(TN) removal efficiency during the continuous experiment.

The long-term performance of the EGSB reactor is shown in Fig. 2. The reactor was operated in three phases over an operational period of 230 days. In phase I, the total nitrogen(TN) concentration was kept at 250mg/L and the nitrogen loading rate(NLR) was increased from 1.0 g-N/L/d to 3.5 g-N/L/d by shortening hydraulic retention time from 6 h to 1.7 h. The nitrogen removal efficiency was slightly decreased by residual nitrite of the effluent at the beginning of increased NLR, then stable nitrogen removal efficiency of 83.9%-91.9 was obtained. The concentration of TN was doubled and HRT was prolonged to 3.5 h to maintain the same NLR in the reactor. However, the performance of the reactor was steadily worsening in a week. Therefore, the operation condition in the following phase was reverted to the same as phase I and the performance was recovered soon.

3.2 Specific anammox activity(SAA)

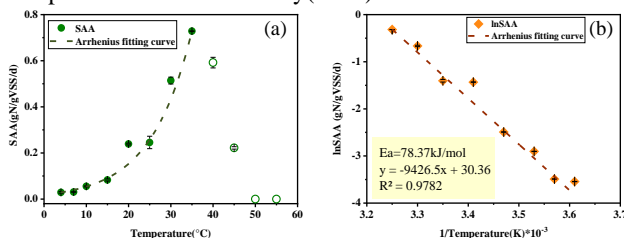


Fig.3 (a): SAA measured at different temperatures and Arrhenius fitting curve; (b): Arrhenius fitting curve and activation energy (E_a) calculation.

SAA tests were performed at different temperatures after 230th of the operation day. The results were simulated by the modified Gompertz equation and E_a was calculated by Arrhenius equation. The optimal temperature for Anammox bacteria(*Ca. Kuenenia*) is 35 °C and only 10% and 5% activity remains when the temperature is reduced to 10 °C 7 °C. The activation energy was calculated to be 78.37kJ/mol which is consistent as reported 63–70 kJ/mol determined for anammox biomass enriched at temperatures 20 °C previously,

indicating anammox species was a little sensitive to the temperature change.

3.3 Yield of biomass and stoichiometry under 7°C

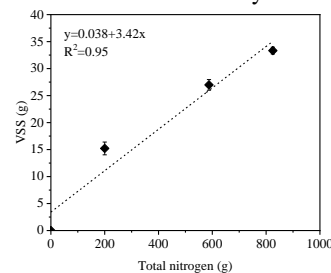


Fig.4 Yield of biomass under 7°C

At the NLR of 2.5 g-N/L/d, the biomass was drew from the top of the reactor periodically. The yield of biomass was 0.038VSS/g-total nitrogen, assuming the increase of the VSS was caused by anammox growth. The value of 0.038VSS/g-total nitrogen was quite lower than 0.046 and 0.050 VSS/g-total nitrogen reported by (Hendrickx et al., 2012) and (Strous et al., 1999). Since nitrite is partly oxidized to nitrate to provide electrons for carbon fixation, produced nitrate is resulted from the growth of anammox bacteria. In this study, the ratio of produced nitrate and consumed ammonium was only 0.212, which was also lower than the universally acknowledged 0.26 at mesophilic temperatures, indicating the less biomass yield under low temperature. As reported, the yield of biomass production on NH_4^+ uptake was calculated to be 0.071 C-mol/ NH_4^+ -mol(C-mol=22.1 gVS/C-mol), in correspondence with 0.051 mgVSS/mgN. This difference might be contributed to sludge washout or microbial population since the yield of biomass of 0.051 mgVSS/mgN was obtained using membrane bioreactor (MBR) and the dominant species was *Brocadia*. Besides, most bacteria cannot adapt to 7 °C. Another possible reason was considered as the cavitation formation and floatation behavior of anammox-HAP granular.

4 Conclusions

Nitrogen loading rate of 3.5 gN/L/d was achieved at 7°C in long-term operation indicating anammox could be stably processed even in cold weather. Biomass yield at 7 °C was 0.035 g VSS/g-total nitrogen, lower to that at higher temperatures. Average biomass specific activity was 30.5 mg N/g VSS /d at 7 °C.

Reference

- [1] Hendrickx et.al, Autotrophic nitrogen removal from low strength waste water at low temperature. *Water Res.*(2012) Vol.46, 2187–2193.
- [2] Marc Strous et.al, Key Physiology of Anaerobic Ammonium Oxidation, *Appl Environ Microbiol.* 1999 Jul; 65(7): 3248–3250.
- [3] Haiyuan Ma et.al, Simultaneous nitrogen removal and phosphorus recovery using an anammox expanded reactor operated at 25 °C, *Water Res.*(2020)Vol.172, 115510
- [4] Yanlong Zhang et.al, Stoichiometric variation and loading capacity of a high-loading anammox attached film expanded bed (AAEEB) reactor, *Bioresour. Technol.* 253 (2018) 130–140
- [5] Lauren, M. et.al, Mainstream partial nitritation and anammox: Long-term process stability and effluent quality at low temperatures. *Water Res.*(2016) 101, 628–639.

Development of an energy saving type municipal wastewater treatment system by combining AnMBR and Anammox processes: pilot-scale plant study and system evaluation

○ Chao RONG^{1*}, Tianjie WANG², Zhe KONG² & Yu-You LI^{1,2}

¹Department of Frontier Science for Advanced Environment, Graduate School of Environmental Studies, Tohoku University, 6-6-20 Aoba, Aramaki-Aza, Sendai, Miyagi 980-8579, Japan.

²Department of Civil and Environmental Engineering, Graduate School of Engineering, Tohoku University, 6-6-06 Aoba, Aramaki-Aza, Sendai, Miyagi 980-8579, Japan.

*E-mail: rong.chao.p7@dc.tohoku.ac.jp.

Abstract

An innovative municipal wastewater treatment process which combined AnMBR and Anammox was investigated by a pilot-scale plant under 25 °C for the first time. The working volume of submerged AnMBR and one-stage Anammox reactor were 5 m³ and 1.67 m³, respectively, with a maximum treatment capacity 20 m³/d. During the long-term operation period, excellent performance has been achieved both in the pollutants removal and bioenergy recovery. In AnMBR unit, more than 90% COD and 95% BOD₅ in the raw wastewater were removed, and accompanied by 0.27 L/gCOD_{removal} biogas recovery with a methane content at a high 75-81%. In the Anammox part, almost all of the NH₄⁺-N was removed, resulting in a TN removal efficiency >80% and remained TN in effluent less than 10 mg/L. Serious membrane fouling was encountered after one year's operation, both on-line chemical enhanced backwash and off-line manual cleaning are showed limited effectiveness in membrane permeability recovery. The SEM result suggested that the membrane aging should be blamed to the membrane performance degradation.

Keywords: Municipal wastewater treatment; AnMBR; Anammox; membrane fouling; pilot-scale plant.

1 Introduction

The conventional activated sludge (CAS) process has been applied in municipal wastewater treatment for almost 100 years, which have made great contribution to the environmental protection. However, due to the high energy consumption for aeration and tremendous amount excessive sludge production, which make the CAS no longer meet the higher wastewater treatment standard in the future, in where the wastewater should be accepted as a potential nexus resource (e.g. nutrients, energy and water reuse) rather than waste.

As one of the most potential alternatives to CAS, AnMBR-Anammox was considered to have promising future in wastewater treatment and has attracted increasing attention over the world. In the AnMBR part, due to the combination of conventional anaerobic technology with modern membrane system, the sludge retention time (SRT) and hydraulic retention time (HRT) can be totally separated, which have compensated the disadvantage of the slow growth speed of anaerobic microorganism and obtain the high concentration of biomass in the reactor to achieve excellent waste removal efficiency and bioenergy production. After most of organics in the raw wastewater were removed and different forms of nitrogen were converted into ammonia nitrogen (NH₄⁺-N), the effluent of AnMBR which characterized by low carbon ratio (C:N ≈ 1:1) is most suitable to be further treated by Anammox. In the Anammox part, the major functional microorganisms, ammonia-oxidizing bacteria (AOB) and anammox bacteria, can achieve high nitrogen removal efficiency by partial nitrification/anammox (PNA), and the aeration demand is only 30% of the traditional denitrification process.

Currently, there are plenty of researches on individual unit application, AnMBR or Anammox, but few focus on the application of the entire system. And this happens to be the most important for the future application of this process in large-scale.

In this study, a pilot-scale AnMBR-Anammox plant was constructed and applied in real municipal wastewater treatment. The process performance including pollutants removal, bioenergy recovery and membrane permeability were systematically studied during the long-term operation. It is expected that the results from this research can provide useful reference to promote the AnMBR-Anammox process widely application in the future.

2 Materials and methods

The flow chart and real photograph of the entire AnMBR-Anammox system are illustrated in Fig. 1.

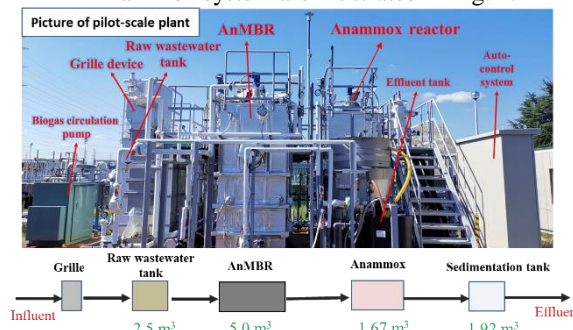


Fig. 1. The flow chart and real photograph of pilot-scale AnMBR-Anammox plant

Due to the auto-control system and thermostatic system, this plant can realize automatic operation at 25 °C. A total area of 72 m² hollow fiber membrane module was installed

in the submerged AnMBR, and a novel carrier was added to the Anammox reactor to increase the contact area between microorganism and water.

Biogas, temperature, pH and TMP were daily recorded in-site, while other parameters and indicators like COD, BOD et al. were measured in the laboratory three times a week. The detailed procedures were reported in our previous research (Kong et al., 2020).

3 Results and discussion

About 100 days' operation data was provided in Fig. 2, which include three different HRTs and two membrane module, the old one and the new one.

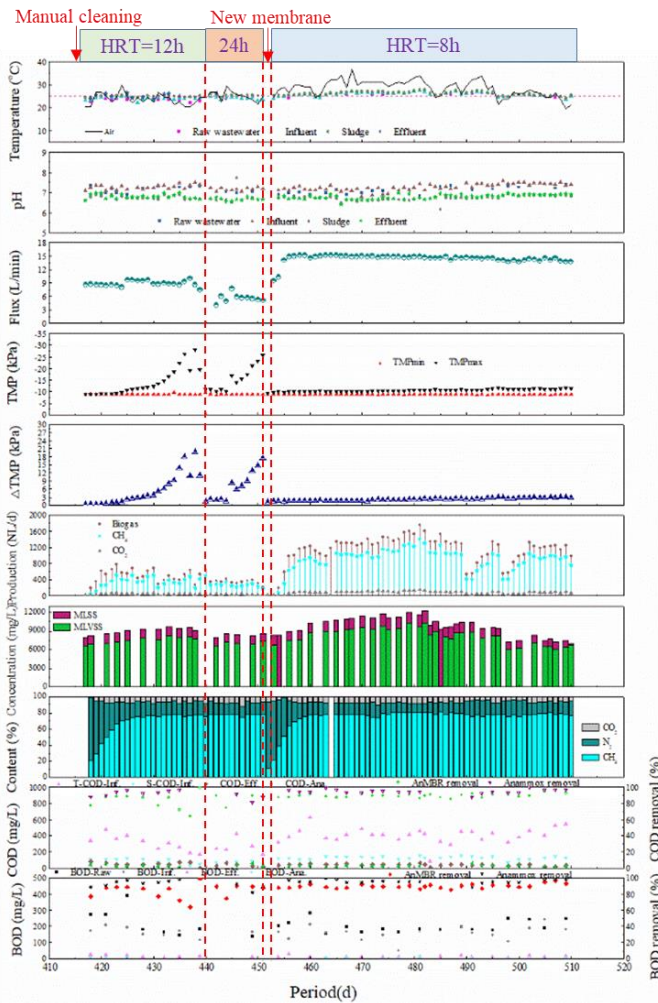


Fig. 2. The long-term performance of entire process.

A good organics removal efficiency has been achieved during the entire stable operation period. The total COD removal efficiency for different HRTs is over 90% and BOD₅ removal efficiency is over 95%. It should be noted that, Anammox reactor also contributes to the removal of organics, which lead to a great effluent with residual COD and BOD₅ less than 40 mg/L and 10 mg/L, respectively.

The biogas is smoothly produced in the AnMBR with a consistently methane content over 75% and reaching a high of 81% under stable operation period. By the calculation, the biogas production was 0.25-0.27 L/g removed COD and 0.09-0.10 L/L raw wastewater, in which the methane production rate was around 0.18-0.23 L/g COD removed and 0.07-0.08 L/L raw wastewater.

For the nitrogen removal in the whole system (shown in Table 1), the NH₄⁺-N in the raw wastewater represents the majority of TN_{inf}, accounting for nearly 65%. After AnMBR, the organic-N (soluble protein) and particle-N (influent SS) were all transformed into NH₄⁺-N, and about 7% nitrogen was transferred to the sludge in AMBR. Anammox showed an excellent performance in nitrogen removal, about 80% TN was removed and the remained TN in the effluent < 10 mg/L.

Table 1 Nitrogen removal in the entire process

	Raw wastewater	AnMBR influent	AnMBR effluent	Anammox effluent
NH ₄ ⁺ -N	23.1±3.3	23.7±3.3	33.6±2.4	1.2±1.3
NO ₂ ⁻ -N	0	0	0	1.6±0.7
NO ₃ ⁻ -N	0	0	0	2.5±1.7
TN	35.9±2.8	37±2.2	33±2.5	24.1±2.2

The membrane was run at a mode of 4 min for filtration and 1 min for relaxation (F:R=4:1). Fixed biogas sparging at rate of 0.9 m³/min and online chemical enhanced backwash with 500 ppm NaClO were employed to maintain the membrane permeability. After achieve a good performance (ΔTMP was relatively stable and remaining lower than 5 kPa) for more than 300 days, serious membrane fouling was occurred and cannot be mitigated by the CEB. The offline manual cleaning with 3000 ppm NaClO and 2% citric acid was also conducted to try recover the membrane performance, but the effect seems temporary and limited (serious membrane fouling reappeared within 15 days). So a new membrane module was installed to replace the old one on day 450.

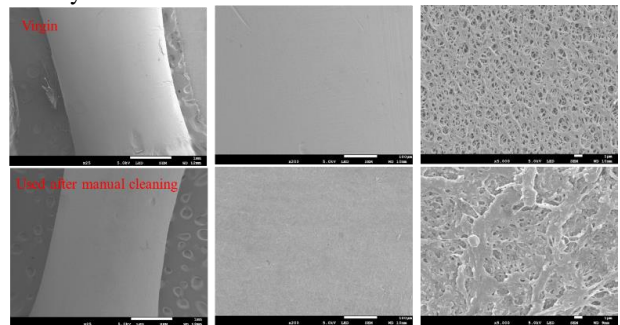


Fig. 3. SEM picture of virgin membrane and used membrane after manual cleaning.

According to the SEM picture of virgin membrane and the used membrane after cleaning in fig. 3, the relative rough surface and pore caused by the membrane aging tend to be one of the main reasons for the poor performance of the old membrane.

4 Conclusions

A pilot-scale AnMBR-Anammox plant has performed successfully in real municipal wastewater treatment. The COD and BOD₅ removal efficiency for the entire process were >90% and >95%, respectively. The nitrogen removal efficiency in Anammox reactor is about 80%. The membrane ageing maybe one of the major reasons lead to the membrane performance degradation.

Reference

[1] Kong Z, et al., 2020. Large pilot-scale submerged anaerobic membrane bioreactor for the treatment of municipal wastewater and biogas production at 25 °C. *Bioresour Technol.* DOI: 10.1016/j.biortech.2020.124123.

Treatment of Municipal Wastewater by Anaerobic Membrane Bio-reactor: Process Performance and Mass Balance

○ Runda Du^{1*}, Yisong Hu^{1,2}, Jiayuan Ji¹, Yu-You Li¹

¹Department of Civil Engineering and Architecture, Tohoku University, 6-6-06 Aoba, Aramaki, Aoba-ku, Miyagi 980-8579, Japan.

²Key Lab of Environmental Engineering, Shanxi Province, Xi'an University of Architecture and Technology, No. 13 Yanta Road, Xi'an 710055, P. R. China

*E-mail: du.runda.t3@dc.tohoku.ac.jp.

Abstract

The performance of real municipal wastewater treatment by an anaerobic membrane bioreactor (AnMBR) was studied through a lab-scale bioreactor. In detail, membrane performance was evaluated by flux, TMP and membrane fouling substances. Mass balance was also conducted to analysis the material flow in this process.

Keywords: AnMBR; municipal wastewater; membrane fouling; mass balance

1 Introduction

The activated sludge process has evolved into a mature method for wastewater treatment for over 100 years. However, there are still some issues such as high energy consumption and high sludge yield to be solved. Recent decades, anaerobic membrane bioreactor (AnMBR) process has been attached to great attention because of its high COD removal, low energy demand, low sludge generation and bioenergy recovery (Rong Chen et al., 2017). Although this technology has been successfully applied in the field of industrial wastewater treatment, it has not yet been applied to the treatment of municipal wastewater, which has complex compositions, and low organic concentrations (Zhen Lei et al., 2018). In this study, a lab-scale AnMBR was used for real municipal sewage treatment to achieve stable operation and to investigate the treatment performance and various material flows.

2 Materials and methods

A 20 L lab-scale AnMBR was installed at a local wastewater treatment plant (WWTP) to treat municipal wastewater. The membrane was submerged in the AnMBR filled with anaerobic sludge as seed sludge from a pilot-scale AnMBR at the same WWTP. During the start-up phase, HRT was adjusted from 12 h to 8 h and 6 h finally (about 30 days after beginning). Then the AnMBR was operated at HRT 6 h.

3 Results and discussion

(1) Removal of organic matters & biogas production

Fig. 1 (b) shows that COD of the municipal sewage basically varies between 200-400 mg/L, lower than that of the pilot AnMBR in the same plant. It was deduced that the fine influent pipe could filter out some sand and large fibers in sewage, resulting in a low SS concentration (120-180 mg/L, Fig. 1 (a)). In addition, frequent rain also reduced influent COD. Through the retention of membrane and anaerobic digestion, COD removal rate maintained at 85%, and effluent COD was less than 50 mg/L.

For the undecomposed SS accumulated in the seed sludge, MLSS showed a negative growth trend during the start-up phase at HRT 12 h in Fig. 1 (c). Then HRT was reduced to 6 h quickly and MLSS was reached 8 g/L by sludge supplement. During the operation at HRT 6 h, except for the sludge required for sampling, the reactor produced almost no excess sludge and the sludge yield was 0.081 gVSS/gCOD_{rem}, keeping MLSS at about 10 g/L, which was

contributed to the low influent SS concentration and high VSS proportion, most of the which were decomposed into biogas by microbes.

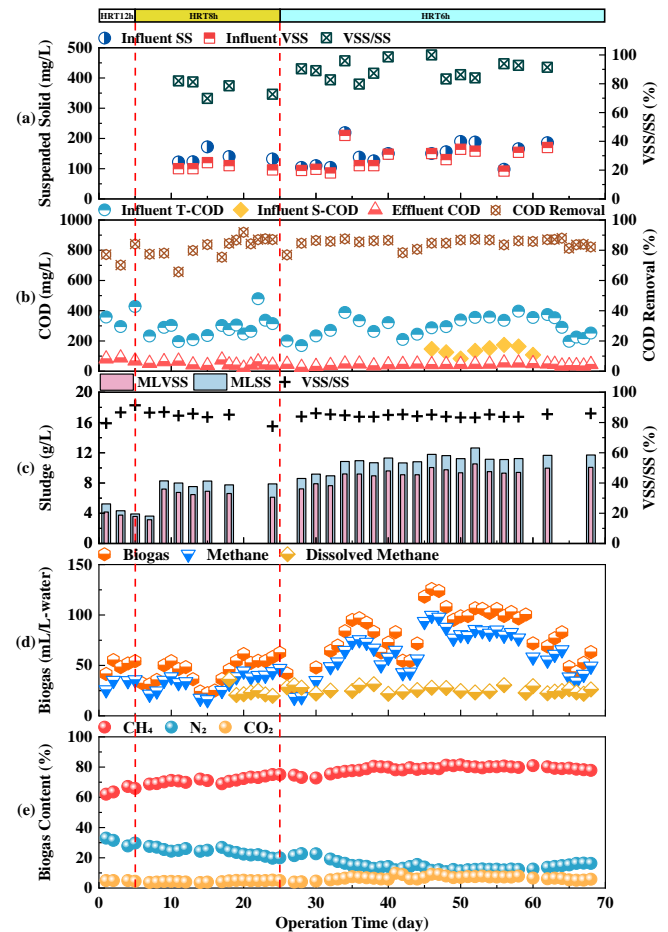


Fig. 1. Performance of sewage treatment.

As shown in Fig. 1 (d) and (e), during the start-up process, as the microbes were in the adaptation stage, the methane production was always below 50 mL/L-water. In the stable operation at HRT 6 h, the methane production gradually increased to more than 75 mL/L-water. Meanwhile, the biogas production showed a good correlation with the influent COD. The methane content in biogas gradually increased and then stabilized at about 80%.

(2) Membrane performance

Fig. 2 shows that the membrane flux is 6, 9, 12 LMH at HRT 12 h, 8 h and 6 h, respectively. Due to the short operation time for just 70 days, Δ TMP (membrane pressure between filtration and relaxation) did not change significantly and remained around 1 kPa. The membrane permeability (flux per unit pressure) was also basically maintained at a constant level.

(3) Mass balance

a. COD balance. As shown in Fig. 3 (a), COD balance was calculated by measuring the equivalent COD counterparts both in the influent and the effluent. About 77% of the influent COD was converted to methane, including 20% of the dissolved methane. In addition to the 13% COD in the effluent, about 4%~5% of COD was consumed by sulfate reduction, and about 6% of COD was converted into MLVSS by microbial growth. It can be seen that AnMBR was characterized by low excess sludge production.

b. Nitrogen balance. From Fig. 3 (b), $\text{NH}_3\text{-N}$ accounts for 60~70% of TN_{inf} , leaving 60~70% in the SS and soluble organic-N (such as protein). $\text{NH}_3\text{-N}$ in effluent was about 80~90%, and the concentration was higher than that of influent, which indicated that part of SS-N and organic-N were decomposed into $\text{NH}_3\text{-N}$ in AnMBR. In addition, 4~5% of TN_{inf} entered sludge by microbial proliferation and nitrogen was not removed in other forms.

c. Sulfur balance. In Fig. 3 (c), sulfate and sulfide accounted for about 80% of TS_{inf} , leaving 20% in SS and soluble organic-S. The sulfate in the influent was reduced to sulfide by sulfate-reducing bacteria in AnMBR, some of which was hydrolyzed to form hydrogen sulfide into biogas. Most of organic-S in the influent was also decomposed into inorganic-S, and about 4% of TS_{inf} was assimilated by microbes.

d. Phosphorus balance. Similar to nitrogen, phosphorus in influent existed in the form of phosphate and organic phosphorus, each of which accounted for about 50%. The ratio of phosphate in effluent was 70~80%, which was higher than that in influent, indicating that organic phosphorus in influent was partly decomposed into phosphate, and about 16% of TP_{inf} was used for sludge proliferation. In addition, phosphorus was also not removed in the AnMBR.

4 Conclusions

The AnMBR showed excellent COD removal and biogas production for municipal wastewater treatment with low excess sludge generation. The transformation paths of C, N, S, P in the system are investigated, which will be helpful for the research of element removal and resource recovery.

Reference

[1] Rong Chen, Yulun Nie, Jiayuan Ji, Tetsuya Utashiro, Qian Li, Daisuke Komori and Yu-You Li, (2017), Submerged anaerobic membrane bioreactor (SAnMBR) performance on sewage treatment: removal efficiencies, biogas production and membrane fouling, *Wat. Sci. and Technol.*, 76(6): 1308-1317.
 [2] Zhen Lei, Shuming Yang, Yu-you Li, Wen Wen, Xiaochang C. Wang and Rong Chen, (2018), Application of anaerobic membrane bioreactors to municipal wastewater treatment at ambient temperature: A review of achievements, challenges, and perspectives. *Bioresour. Technol.*, 267: 756-768.

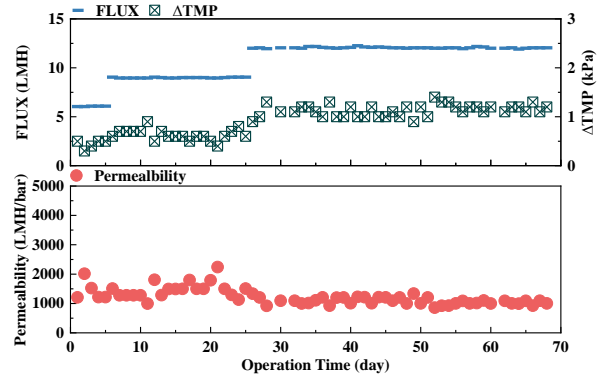


Fig. 2. Performance of membrane filtration.

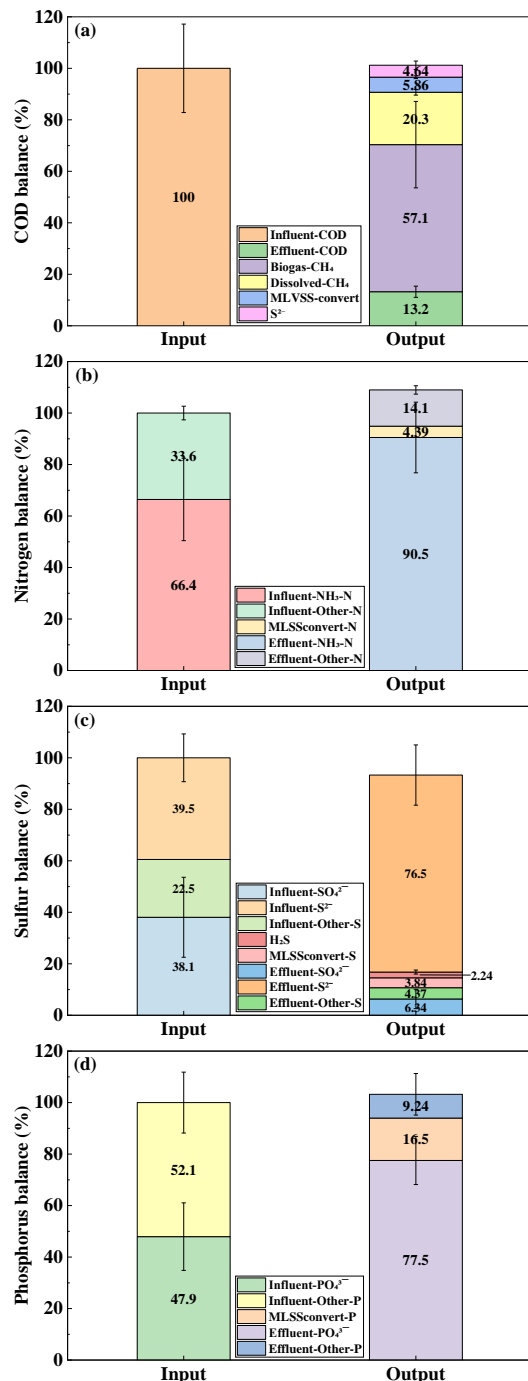


Fig. 3. Mass balance.

Virus removal by membrane bioreactors: mechanisms and modeling efforts

○ Yifan ZHU^{1*}, Rong CHEN², Yu-You LI³ & Daisuke SANO^{1,3}

¹Department of Frontier Sciences for Advanced Environment, Graduate School of Environmental Studies, Tohoku University, Miyagi 980-8579, Japan.

²Key Laboratory of Northwest Water Resource, Ecology and Environment, Ministry of Education, Shaanxi Key Laboratory of Environmental Engineering, Xi'an University of Architecture and Technology, Xi'an 710055, China.

³Department of Civil and Environmental Engineering, Graduate School of Engineering, Tohoku University, Miyagi 980-8579, Japan

*E-mail: zhu.yifan.t1@dc.tohoku.ac.jp & yifanz35@uw.edu

Abstract

The increasing pressure on the global water supply has led to the promptly developing treatment technologies and risk management strategies, and microbial safety is becoming a crucial aspect in the interest of public health. Backed up by the development of membrane technology, membrane bioreactors (MBR) have received substantial attention for their superiority over conventional treatment methods in many ways and are considered promising in the water reclamation realm. This review study provides an overview of the efforts made to manage and control the potential waterborne viral disease risks raised by the use of effluent from MBR treatment processes, including the mechanisms involved in the virus removal process and the attempts to model the dynamics of the removal process. Generalized and integrated virus removal models that provide insight into real-time monitoring are urgently needed for advanced real-time control purposes. Modeling methods that can well handle the inherent uncertainty and nonlinearity of the complex removal process are crucial to the development and promotion of related technologies.

Keywords: Membrane bioreactor, Virus removal modeling, HACCP, Soft-sensor approach, Process-driven modeling, Data-driven modeling.

1 Introduction

Access to sufficient and safe water resources plays a central role in the prosperity and development of human society. Despite the rich history of water reclamation, the latent health risks and the importance of proper sanitation strategy have only become a serious concern in the eyes of the public and authorities in recent decades. In particular, waterborne enteric viruses present in reclaimed wastewater with fecal-oral transmission routes are considered a primary health concern globally since they can cause several acute illnesses including gastroenteritis and hepatitis. Several factors, including the high shedding rate from infected individuals, resistance to environmental factors, and the low infectious dose, have made these viruses a particular threat to public health.

Powered by the rapid development of materials science and engineering, the use of membrane in the realm of water treatment has become increasingly popular with one successful example being the membrane bioreactors (MBR). With the utilization of a membrane, MBR can serve as an effective barrier against waterborne pathogens. This study, therefore, focuses on the efforts dedicated to establishing a mathematical model for the virus removal process in MBR systems. Firstly, the virus removal performance of MBR systems and involved mechanisms are briefly discussed. Secondly, we reviewed the historical and recent attempts to connect easy-to-measure variables with virus removal efficiency via either conventional process-driven approach based on the physicochemical and biological relationship and equations or novel data-driven modeling techniques.

2 Performance and contributing mechanisms

2.1 MBR virus removal performance

Previous studies have reported that depending on the membrane installed, virus strain, and operating conditions, the log reduction value (LRV) can vary from less than 1 to larger than 7, but overall showing a decent and stable performance. Although only a limited number of studies have focused on AnMBR while the virus removal property of AeMBR has been investigated under various settings, as the capability of AnMBR systems is gaining recognition, we expect to see more thorough studies in the near future.

2.2 Mechanisms involved

2.2.1 The role of membrane

When the pore size of membrane is comparable to the size of virus particles (e.g. 0.04 μm), direct membrane rejection is enough to provide decent removal performance, but to maintain throughput and keep operating cost low, many plants prefer membrane with larger pores, when that is the case, mechanical sieving, virus aggregation, membrane adsorption, and electrostatic repulsion come in as the main factors, which form a complex matrix under the influence of membrane material, virus surface characteristics, and environmental conditions such as pH.

2.2.2 Effect of biomass adsorption

As the biomass in the reactor grows, both the suspended solids and the gel/cake layer attached to the membrane surface contribute to virus retention. Generally speaking, higher biomass content provides more adsorption spots and blocks membrane pores, hence resulting in better virus

retention capacity, but a balance must be found between virus removal performance and throughput.

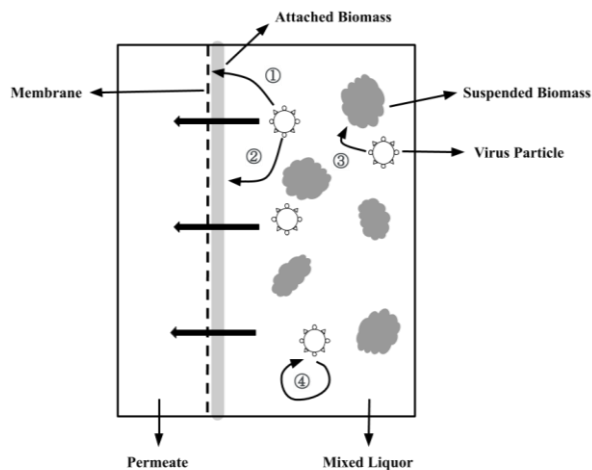


Fig. 1. A demonstration of the mechanisms involved in the virus removal process in MBR. ①, size exclusion, electrostatic repulsion, and sorption onto the membrane; ②, pore blocking and adsorption onto the biomass layer attached on membrane surface; ③, adsorption and predation of suspended biomass; ④, spontaneous decay and inactivation.

2.2.3 Decay and inactivation

Virus particles present in the reactor are subject to natural degradation and the predation of microorganisms. Due to the high bacteria concentration inside the reactor, the recorded decay rate is higher than the expected washout rate, however, considering the relatively short hydraulic retention time, the overall contribution is likely not to be as pronounced as other mechanisms.

3 Modelling efforts

3.1 Process-driven models

Process-driven models are generally based on the physical interpretation of the underlying mechanisms, although sometimes statistical methods also help select and calibrate the coefficients. Considering the involvement of membrane, many studies have focused on the membrane filtration process, more specifically, how the membrane rejection and fouling translate to the virus particle retention. Commonly used physical models include Darcy's law and mechanical sieving equation, but the growth of biomass has yet to be mathematically connected to membrane fouling and the increase in virus removal performance, which may sacrifice the model's responsiveness to the reactor dynamics. Also, as previously mentioned, the adsorption onto suspended biomass plays a critical role in the virus adsorption, which is often described by first-order kinetic model. However, from the perspective of preventive water safety management, existing physical models may find trouble being applied as a real-time control measure as they tend to be overwhelmingly complex with tens of parameters and coefficients.

3.2 Data-driven models

Since the complexity of the virus removal process happened in MBR is still a huge hindrance, some studies advocate using data-driven models to bypass the actual process and build the

connection between input and output variables purely using existing dataset and algorithms, albeit at the sacrifice of the understanding of the underlying mechanisms. So far, data-driven modeling methods have found successful applications in the water-related research realm, most commonly serving as a tool of water quality or plant status prediction. Especially, artificial neural network (ANN), adaptive neuro-fuzzy inference system (ANFIS), principal component analysis (PCA), and partial least squares (PLS) are more frequently employed among others. The former two can be categorized as machine learning methods that specialize in establishing nonlinear input-output relationships without prior knowledge, and the latter two belong to the family of multivariate statistics which comes in handy when trying to find the variables that are most correlated with the desired output.

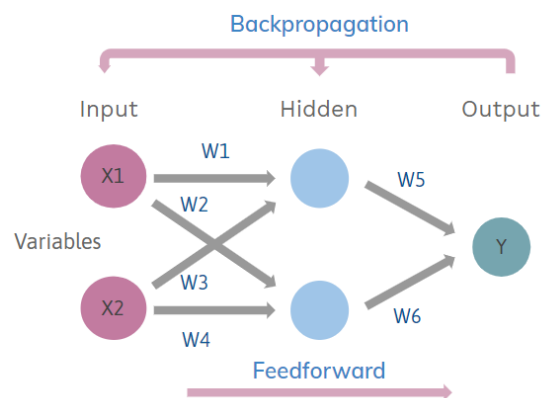


Fig. 2. The structure of a 2-input, 1 output artificial neural network with one hidden layer and two nodes.

3.3 Hybrid model

Driven by the intention of overcoming the respective inherent shortcomings of both types of models, the discussion about combining them to develop a hybrid model has also been raised. Conceptually, the overwhelming superiority of data-driven approaches in perceiving non-linear patterns can greatly reduce the workload, while physical model would give better interpretation and elasticity to the model. As promising as it sounds, despite some attempts related to water quality and membrane permeability have been reported, the true potential of hybrid models, especially in predicting virus removal performance, is yet to be fully explored and verified.

4 Conclusions

With the employment of membrane that efficiently retains large particles, MBR systems have the potential to deliver decent and stable virus removal performance that can be put under real-time monitoring, paving its way for its acceptance in a field where advanced risk management is gaining importance. Although the intricate nature of the process makes the modeling an arduous task, as related research carries on, new methods and models will continue to thrive.

Reference

[1] Zhu Y. et al, Virus removal by membrane bioreactors: A review of mechanism investigation and modeling efforts, *Water Res.*, 188 (2021), 116522.

Mechanisms of MS2 bacteriophage removal in an anaerobic membrane bioreactor

○ Jinfan Zhang¹, Zhendong Liu¹ & Rong Chen^{1,2*}

¹ Key Lab of Environment Engineering, Shanxi Province, Xi'an University of Architecture and Technology, No. 13 Yanta Road, Xi'an 710055, PR China

² International S&T Cooperation Center for Urban Alternative Water Resources Development, Key Laboratory of Northwest Water Resource, Environment and Ecology, MOE, Xi'an University of Architecture and Technology, No. 13 Yanta Road, Xi'an 710055, PR China

*E-mail: chenrong@xauat.edu.cn

Abstract

To investigate MS2 removal performance for municipal wastewater using an anaerobic membrane bioreactor (AnMBR) and attachment and inactivation of MS2 in the mixed liquor. The results revealed that the removal of MS2 by AnMBR mainly depends on the attachment and inactivation of MS2 in mixed liquor before the formation of serious membrane fouling. In addition, the anaerobic intermediated acetic acid (CH₃COOH) in mixed liquor inactivated MS2 mainly by destroying the proteins involved in MS2 replication.

Keywords: Anaerobic membrane bioreactor; Mixed liquor; Attachment; Inactivation; Acetic acid

1 Introduction

Viral from wastewater have a potential harm to the environment and human health. Therefore, control of virus has been a major concern in wastewater treatment and water reclamation and reuse. AnMBR combine the benefits of anaerobic treatment: bioenergy recovery, low sludge production, with the benefits of MBR: solid-liquid separation, safe and clean, reduce pathogens. AnMBR technology has the ability to meet the increasingly stringent regulations for recycled water, including virus removal. Bacteriophage MS2 was used as a conservative virus surrogate in this study because of its smaller size compared with human enteric virus. The objectives of this study to better understand AnMBR behavior in virus removal for municipal wastewater and the roles of mixed liquor in removal.

2 Materials and methods

2.1 AnMBR and operation condition

Fig.1 shows a diagram of the AnMBR. AnMBR was operated with a working liquid volume of 2.0 L, hydraulic retention time of 8 h. The SS of seed sludge inoculated into the reactor was 8.0 g/L. The membrane module, with a surface area of 0.036 m² and nominal pore size of 0.2 μm, was immersed in AnMBR.

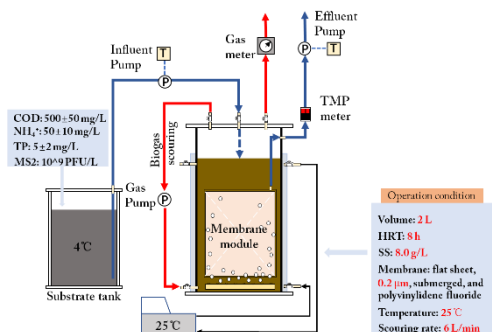


Fig.1. Schematic of anaerobic membrane bioreactor

2.2 Samples

The influent and effluent of AnMBR were determined by double agar layer (DAL) according to EPA Method 1602.

Solid and liquid fractions of mixed liquor samples were quantified separately to determine the quantity of MS2 in mixed liquor.

2.3 Virus functionality assay

RNase protection assay. Inactivation-treated MS2 samples and untreated MS2 controls were incubated with RNase, followed by heat-inactivation of enzyme. RNA of MS2 was extracted and quantified with qRT-PCR.

Binding Assay. MS2 samples were incubated with *E.coli* for 90 min at 4°C which allowed the MS2 to attach to the bacterial host without injecting or replication the genomes, and the RNA of MS2 was extracted and enumerated by RT-qPCR [1].

Injection Assay. MS2 samples were bound to host cells at 4°C for 30 min. 0.2 mM chloramphenicol was then added to the bacterial-viral suspensions and the samples were incubated at 4°C for 60 min. the RNA of MS2 was extracted and enumerated by RT-qPCR [1].

Replication Assay. Replication was calculated based on the rate constants for infectivity, binding, injection loss: $K_{replication} = K_{infectivity} - K_{binding} - K_{injection} - K_{RNA\ damage}$

2.4 MS2 attachment to different size particles

The mixed liquor was filtered step by step through membranes of 10 μm, 5 μm, 1 μm and 0.45 μm to determine the quantity MS2 attachment by biomass flocs, micro-particles, sub-micro particles, insoluble colloids, respectively. Mg²⁺ was added into the filtrate after 0.45 μm, and then filtered with 0.22 μm membrane to obtain the MS2 in the liquid phase. MS2 was determined by RT-qPCR.

2.5 MS2 inactivation in mixed liquor

Regular sampling from mixed liquor to study MS2 inactivation in mixed liquor. 2 mL of mixed liquor samples was separated into solid and liquid components by centrifugation at 10 000g for 1 h. The supernatants were harvested for infectivity assay. The solid fraction was suspended in 2 mL of 10% tris-glycine beef extract buffer. Elution and then centrifugation at 10 000g for 30 min. The supernatants were harvested for infectivity assay. MS2 in solids was calculated based on MS2 recovery rate. MS2 in mixed liquor is the sum of MS2 in the liquid and solid.

3 Results and discussion

3.1 MS2 removal by AnMBR

Fig. 2 is the log removal value (LRV) in the short-term AnMBR treatment of municipal wastewater. During the AnMBR operation, the LRV was between 0.2~1.2 log₁₀. With the slow increase of transmembrane pressure (TMP), the efficiency of MS2 removal in the AnMBR increased gradually. This is because the nominal pore size of membrane is larger than the diameter of MS2. Before serious membrane fouling, the interception of MS2 by membrane is weak.

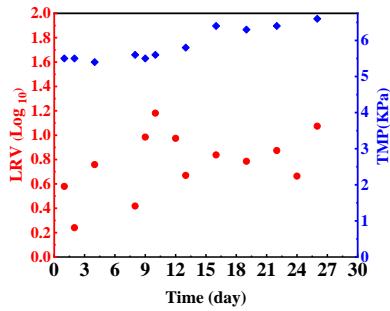


Fig.2. MS2 removal by AnMBR

3.2 Attachment/inactivation of MS2 in mixed liquor

Fig. 3 (A) shows that attachment of MS2 by biomass flocs, micro-particles, sub-micro particles, insoluble colloids, respectively. The results showed that attachment of MS2 mainly depended on the biomass flocs. However, sub-micro particles had higher attachment capacity. Fig. 4 shows that kinetics of MS2 inactivation in liquid, sludge and mixed liquor, respectively. The first-order inactivation rate constants of MS2 in liquid, sludge and mixed liquor were 1.38 day⁻¹, 0.99 day⁻¹, 0.90 day⁻¹, respectively. The inactivated rate of MS2 in sludge is lower than that of MS2 in liquid.

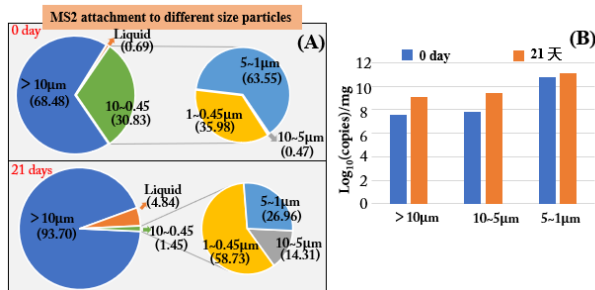


Fig.3. Contribution of different sizes to MS2 attachment (A), MS2 adsorption capacity of different size particles (B)

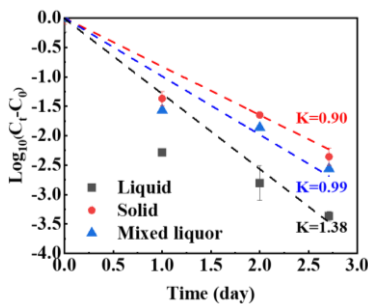


Fig. 4. Kinetics of MS2 inactivation in liquid, sludge and mixed liquor, respectively

3.3 Mechanisms of CH₃COOH inactivation regarding virus function

Figure 5 (A) shows that the concentration of CH₃COOH was 0, 500, 1500, 3000 and 5000 mg/L, the first-order inactivation rate constants were 1.68, 2.27, 1.14, 2.47, 2.09, respectively. The results showed that CH₃COOH has an effect on the inactivation of virus. There was no significant difference in the RNA signal (Fig. 5(B)). Therefore, structural protein and RNA damage was negligible following CH₃COOH treatment. Fig. 5(C) and (D) shows that CH₃COOH concentration of 500 mg/L causes to the injection protein and the replicated protein of MS2, while the CH₃COOH of 1500 mg/L only affects the replicated protein.

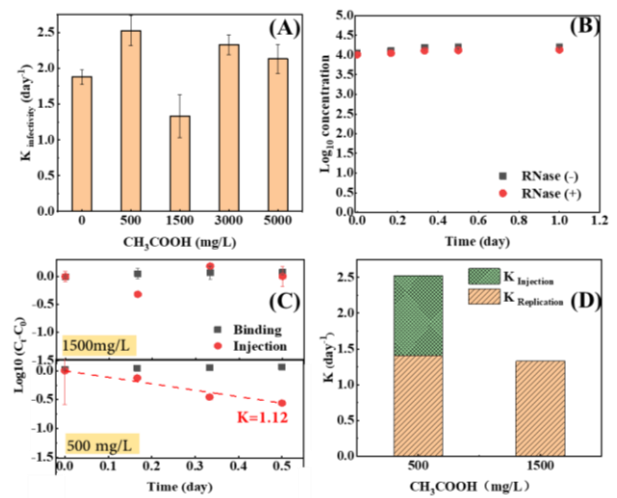


Fig.5. Pseudo-first-order rate inactivation constant (K) of MS2 inactivation in different CH₃COOH concentration (A), RNase protection assay (B), The first-order rate constant of binding loss and injection loss (C), Relative contribution of RNA damage, binding, injection and replication loss to CH₃COOH (D)

4 Conclusions

Removal of MS2 by AnMBR mainly depends on the attachment and inactivation in mixed liquor before the formation of serious membrane fouling. Anaerobic intermediated acetic acid in mixed liquor inactivated MS2 mainly by destroying the proteins involved in MS2 injection and replication.

Reference

[1] Krista R. W., Brian M. P., Therese S., Franziska B., Tamar K., Virus inactivation mechanisms: Impact of disinfectants on virus function and structural integrity, Environmental Science & Technology, (2012) 69-78

High rate anaerobic digestion of food wastewater in an anaerobic membrane bioreactor

○ Mengmeng JIANG¹, Renjie DONG¹, Yu-You LI², Wei QIAO^{1*}

¹College of Engineering, China Agricultural University, Beijing 100083, China

²Department of Civil and Environmental Engineering, Graduate School of Engineering, Tohoku University, Japan

*E-mail: qiaowei@cau.edu.cn

Abstract

Food wastewater was treated by two anaerobic membrane bioreactor systems (AnMBR) consist of a completely stirred tank reactor (CSTR) and a separated membrane chamber under thermophilic condition (50±1) °C for 75 days. Both of the two systems were started with a hydraulic retention time (HRT) of 20 days, and operated at HRT 15 days. About 3 L biofilm carriers were immersed at the bottom of CSTR unit in one AnMBR as biofilm membrane bioreactor (Bf-AMBR) at HRT 15 days. The results showed that both the AnMBR and Bf-AMBR showed stable methane production of 0.32 L/kgCOD_{in} and a comparable COD removal efficiency of 86%. The maximum TMP of AnMBR risen significantly from 4.2 to 25 kPa after 55 days, the flux dropped from 8.2 to 6.5 LMH. In comparison, the maximum TMP of Bf-AMBR rises slowly from 4.2 to 19.6 kPa after 75 days, and the flux can be maintained at a high state around 8 LMH at HRT 20 days and 7.7 LMH at HRT 15 days. After biofilm carrier introduced into the system, the TS and VS concentration was 22% and 14% lower in Bf-AMBR than AnMBR, showed an adsorption of biofilm carriers on microorganisms. The biofilm carriers were effective in alleviating membrane pollution.

Keywords: Bf-AMBR; AnMBR; biofilm carrier; membrane fouling.

1 Introduction

In China, food waste was produced at 100 million tons in 2018. Food waste treatment consists of sorting, crushing and high temperature degreasing, etc. Commonly used anaerobic reactors such as UASB and IC were not suitable for those wastewater due to the high suspended solids concentration. The anaerobic membrane bioreactor (AnMBR) has advantages of enhanced biogas production and improved effluent quality over conventional reactors and was developed to treat a variety of high strength wastewater. However, the membrane fouling was a long-term challenge to the application of AnMBR. Measures must be taken to prevent membrane fouling and thus reduce operational cost. It was found that adding inorganic particulates in AnMBR can effectively alleviate membrane fouling (Akram & Stuckey, 2008). From this point, particulates which can provide bacterial attach growth would be a promising solution considering the reduced membrane fouling factors such as suspended biomass concentration, liquid viscosity and soluble organics.

In this study, polyurethane biofilm carriers were immersed in the AnMBR system to establish a biofilm enhanced AnMBR (Bf-AMBR). The fermentation and membrane performance were investigated through long-term continuously operated experiment.

2 Materials and methods

Food wastewater was taken from a full-scale industrial plant located in Jiangsu province. The wastewater was produced after sorting, crushing, pulping and high temperature degreasing treatment. Trace elements were added with a concentration of Fe: 100 mg/L, Co: 1 mg/L and Ni: 1 mg/L before feeding. The inoculum was taken from a mesophilic sewage sludge digester. As an acclimation process, the temperature was increased in steps of 5 °C everyday until it reached to 50 °C, and then maintained in 50 °C for 3 days activation before starting experiment.

Table1 Characteristics of food wastewater and inoculum

Parameters	unit	Food wastewater(n=15)	Inoculum (n=2)
TS	g/L	83.1±3.4	62.7±0.0
VS	g/L	71.1±3.5	43.1±0.0
SS	g/L	39.4±7.1	56.5±0.4
VSS	g/L	37.1±6.9	22.9±0.1
TCOD	g/L	114.3±9.3	49.4±1.3
SCOD	g/L	57.3±6.3	10.4±1.3
NH ₄ ⁺ -N	mg/L	557±67	1034±11

The hollow fiber membranes used in this study were made of polytetrafluoroethylene (PTFE) with a mean pore size of 0.1~0.2 μm and an effective filtration area of 0.1m² (Sumitomo Electric, Japan). The filtration mode (off/on cycle) of the two AnMBR were 4 min on and 1 min off. The polyurethane biofilm carrier cube has a side length of 1 cm and porosity of 98%. The filling volume of the biofilm carrier in the reactor was around 3 L.

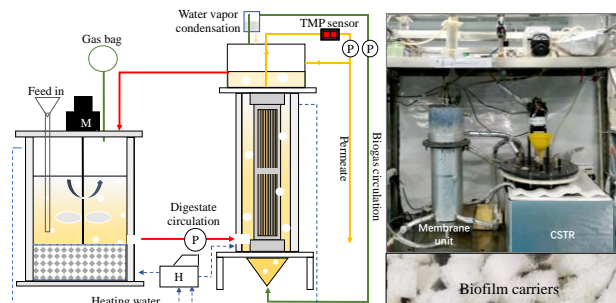


Fig. 1 Flow chart of the Bf-AMBR

The AnMBR system consists of a CSTR and a separated membrane chamber. The biogas recirculation was implemented with a diaphragm pump and a sparging rate of 7 L/min. Two systems were operated during this study: parallel operated during the startup period which was HRT

20 days (SRT 100 days); biofilm carrier was added in one CSTR bottom unit as the HRT was shortened to 15 days (SRT 50 days). The setup of Bf-AMBR was given in Fig. 1. The calculation of permeability was given below:

$$Y = \frac{J}{P} \quad (1)$$

Where Y is the permeability of the membrane, LMH/kPa; J is the flux of membrane, LMH; P is the TMP, kPa.

3 Results and discussion

AnMBR and Bf-AMBR performance: The long-term operation performance was given in Fig. 2 and was organized in Table 3. The OLR was increased from 4.2 to 5.4 kgCOD/(m³·d) at HRT 20 days, and improved to 7.1 at HRT 15 d (Fig. 2(1)). The methane production performance of the two reactors was similar while VFA and sludge concentration were much different after biofilm carriers introduced into Bf-AMBR showed in Fig. 2(2, 3). The specific methane yield at HRT 20 days was around 0.27 m³/kgCOD in both AnMBR and Bf-AMBR, while 0.32 m³/kgCOD in AnMBR at HRT 15 days. A low VFA concentration were found in both reactors. But the relative lower VFA was observed in Bf-AMBR. The acetate in Bf-AMBR was 18% and 32% lower than AnMBR at HRT 20 days and 15 days, respectively. At HRT 20 days stage, the TS and VS concentration of the bulk sludge were similar in AnMBR and Bf-AMBR which has a value of 38.3g/L and 21.3 g/L at HRT 20 days showed in Fig. 2(4), while differ parentally at HRT 15 days which was 30.5 g/L of TS and 26.3 g/L of VS in Bf-AMBR, almost 22% and 14% higher than the TS and VS concentration in AnMBR, respectively. This may due to the attached growth of microorganism on biofilm carrier which also causing a decrease of bulk sludge concentration.

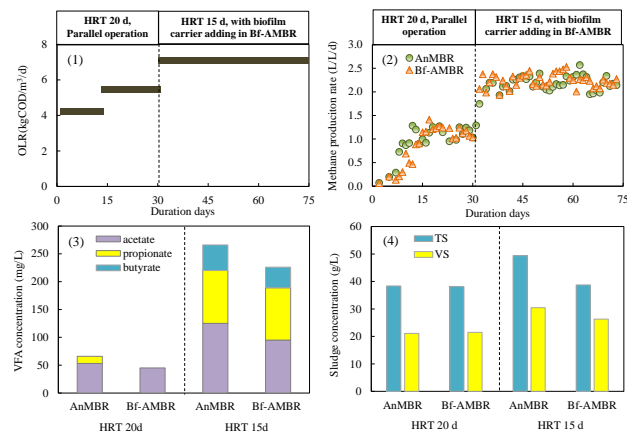


Fig. 2 The reactor operation performance

Table 3 Performance summary of the two systems

Parameters	HRT20d (AnMBR/AnMBR)		HRT15d (AnMBR/Bf-AMBR)	
	1~30	31~75	1~30	31~75
Duration (d)	1~30	31~75	1~30	31~75
CH ₄ (%)	60.7±2.7	59.6±37.6	60.2±0.7	59.7±0.9
Methane production rate (L/L/d)	1.18±0.08	1.18±1.11	2.23±0.18	2.26±0.13
Methane yield (m ³ /kgCOD _{in})	0.27±0.03	0.27±0.02	0.32±0.03	0.33±0.02
pH in reactor	7.7±0.2	7.7±0.2	7.7±0.1	7.7±0.1
NH ₄ ⁺ -N(mg/L)	1366±158	1326±188	1618±140	1636±173
Permeate SCOD	1.08±0.36	1.09±0.27	3.58±1.85	3.77±2.11

Membrane filtration performance: The membranes filtration operation was start-up with a flux of around 8.1±1.0 LMH and initial negative TMP was around 4.2~4.3 kPa of both the two systems showed in Fig. 3A. While the AnMBR and Bf-AMBR behaved difference as the experiment progresses. The maximum TMP of both the two membranes risen significantly with a decrease of permeability (Fig. 3A). The maximum TMP of AnMBR reached to 25 kPa after 55 days while raised slowly and reached to 19.6 kPa in day 72 in Bf-AMBR (Fig. 3(A1)). The flux of AnMBR dropped to 6.45 LMH and needs to be adjusted frequently but had difficulty adjusting to initial value, while in Bf-AMBR, the flux can be maintained at around 7.7 LMH (Fig. 3(A2)). In addition, periodic TMP comparison within 1 off/on cycle was analysis showed in Fig. 3(B). At HRT 20 days, the two reactors showed similar TMP variation curve (Fig. 3B1). At HRT 15 days, the TMP of both membranes began to increase, but the increase of AnMBR was relatively obvious (Fig. 3(B2)); after 20 days operation, the max TMP of AnMBR jumped to 19 kPa, while the Bf-AMBR was below 10 kPa (Fig. 3B3). After 68 days running, there was a high TMP for about 200s in one on/off cycle in AnMBR which was around 25kPa (Fig. 3(B3)). The periodic TMP comparison showed an outstanding release of membrane fouling of Bf-AMBR.

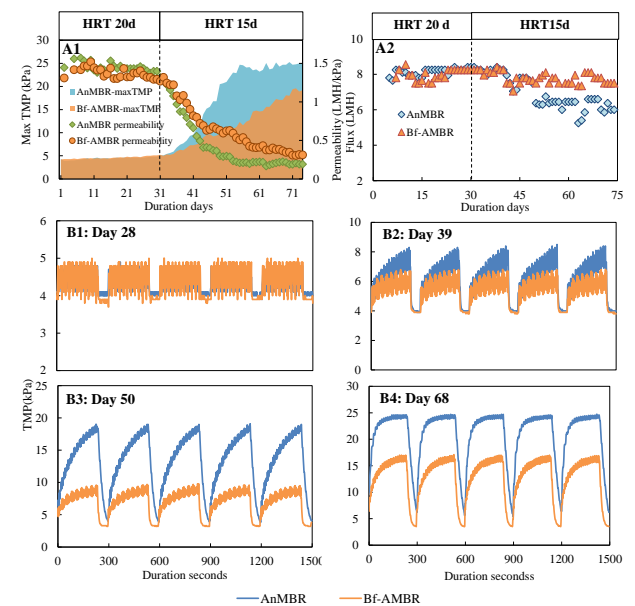


Fig. 3 Membrane filtration performance

4 Conclusions

Thermophilic AnMBR achieved a high degree digestion of food wastewater with low VFA and stable biogas production. Embedded biofilm carriers significantly reduced membrane fouling and thus prolong membrane service time.

5 Acknowledgement

This work was partially supported by National Science Foundation of China (51778616) and International Training and Promotion Project of China Agricultural University (00119521).

Reference

[1] Akram A, Stuckey D C. Flux and performance improvement in a submerged anaerobic membrane bioreactor (SMBR) using powdered activated carbon (PAC). Process Biochemistry, 2008, 43(1):93-102.

Using an expanded granular sludge bed reactor for advanced anaerobic digestion of food waste pretreated with enzyme

Jinghuan LUO*, Sitong ZHANG & Jianyong LIU

School of Environmental and Chemical Engineering, Shanghai University, 333 Nanchen Road, Shanghai 200444, China.

*E-mail: jhuanluo@shu.edu.cn.

Abstract

The high content of solid organics in food waste (FW) results in a low and unstable anaerobic digestion (AD) efficiency. Improving methane production rate and process stability is attracting much attention towards advanced AD of FW. The feasibility of advanced AD of FW pretreated with enzyme was investigated by batch experiments and 164 days running of an expanded granular sludge bed (EGSB) reactor. Simulation study based on the results of batch experiments indicates it is possible to treat enzymatically pretreated FW using an EGSB reactor. During the running of an EGSB reactor, the organic loading rate went up to 20 g chemical oxygen demand (COD)/L.d, and the total COD removal rate reached 88%. The significance of this study is to achieve an advanced AD of enzymatically pretreated FW with a stable and efficient methane production with biogas residue being reduced greatly.

Keywords: Food waste; Advanced anaerobic digestion; Suspended solid; Expanded granular sludge bed; Enzymatic pretreatment.

1 Introduction

Food waste (FW) contains a large amount of organic matters and has a good potential for methane production via anaerobic digestion (AD). However, the poor system stability and the low methane production efficiency are the two main problems [1]. In order to get an advanced AD (AAD) to improve the efficiency of methane production from FW, many pretreatment methods were performed to improve the hydrolysis rate. Among them, enzymatic pretreatment performs well with the best hydrolysis effect [2]. It can convert a mass of suspended solids (SS) to soluble chemical oxygen demand (SCOD) [3], and also results in an obvious reduction of solid content of FW to improve methane production with a higher organic loading rate (OLR) of the AD reactor.

Because of the high SS concentration of FW as a feedstock, continuous stirred tank reactor (CSTR) is the only used reactor to treat FW in practice, with a low OLR of 2~4.5 g VS/L.d and a long hydraulic retention time (HRT) of 15~30 d [2]. With the solid organic matters in FW hydrolyzed enough by enzymatic pretreatment, it could be expected to treat FW by using an efficient anaerobic digestion reactor (such as an expanded granular sludge bed (EGSB) reactor). Furthermore, a higher biodegradation of FW pretreated with enzyme will result in a higher ammoniacal nitrogen and alkalinity production in the AAD system, which can help much to address the acidification problem [4, 5].

The objectives of this study were: 1) to investigate the hydrolysis and degradation performance of enzymatically pretreated FW via batch AD experiments; 2) to predict the SS accumulation rule in an EGSB reactor by mathematical simulation, and to study the feasibility of AAD of FW using an EGSB reactor; and 3) to investigate the methane production and reactor performance of an EGSB reactor treating FW pretreated with enzyme.

2 Materials and methods

2.1. Batch anaerobic digestion of FW

To enzymatically pretreat FW, fungal α -amylase and glucoamylase were added with the dosage of 32 U/g FW, acid protease was added with the dosage of 50 U/g FW. Then, pretreatment was performed in a water bath at 55 °C for 8 h. The batch AD experiments were set up in serum bottles, including three groups: only sludge, control with unpretreated FW, and enzymatically pretreated FW. The F/M ratio was set at 0.6, and the pH was adjusted to an initial value of 7.5. An air bath oscillator was used to maintain the temperature at 35 ± 1 °C for 34 days.

2.2. EGSB reactor operation

Methane conversion of enzymatically pretreated FW was carried out using an EGSB reactor (with an effective volume of 6 L) as shown in Fig. 1. The experiment was divided into two phases. During phase I (day 0 to day 27), the OLR was increased from 1 to 20 g chemical oxygen demand (COD)/L.d by increasing the COD concentration of the influent using the supernatant of the enzymatically pretreated FW. While during phase II (day 28 to day 164), the enzymatically pretreated FW was fed directly. The temperature of the reactor was maintained at 35 ± 1 °C.

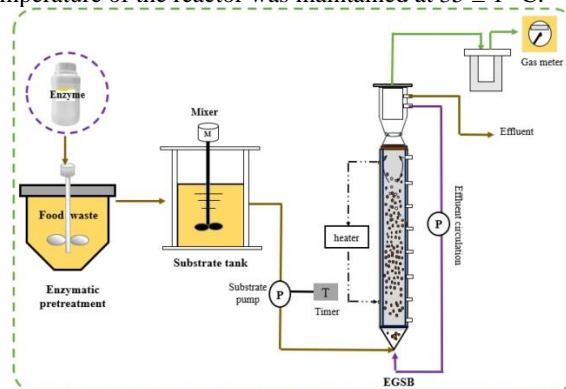


Fig. 1. The flow chart of the EGSB reactor.

3 Results and discussion

3.1. Batch anaerobic digestion of enzymatically pretreated FW to predict the feasibility of FW AAD using an EGSB reactor

The characteristics of the control and pretreated FW for batch experiments are shown in Table 1.

Table 1 Characteristics of the control and enzymatically pretreated FW.

Parameters	Pretreated	Control
pH	4.3 ± 0.1	4.6 ± 0.1
TCOD (g/L)	124.1 ± 2.3	122.3 ± 0.4
SCOD (g/L)	103.2 ± 0.3	71.6 ± 0.5
TSS (g/L)	21.2 ± 0.5	40.6 ± 0.2
VSS (g/L)	20.8 ± 0.4	40.0 ± 0.2
TS (g/L)	92.0 ± 1.1	93.3 ± 1.0
VS (g/L)	82.2 ± 1.0	89.1 ± 1.5
NH ₄ ⁺ -N (mg/L)	1168.9 ± 49.7	70.1 ± 3.6

Enzymatic pretreatment is an efficient way to increase the methane production. On day 34, the methane production of the control and the enzymatically pretreated FW were 4065 mL and 5212 mL, respectively. The methane production of the enzymatically pretreated FW was 28.2% higher than that of the control.

Due to the high hydrolysis of enzymatic pretreatment, the SS of the enzymatically pretreated FW on day 0 was ~49% of the control. The key point of using an EGSB reactor for FW AAD is to ensure its stable operation with a suitable SS accumulation. According to a mathematical simulation based on the SS reduction results of the batch AD experiments, the total accumulated SS were 25.1 g/L and 13.2 g/L, respectively for the control and the pretreated group. In addition, there would be a balance between the daily discharge and the daily growth of microorganisms for the enzymatically pretreated FW, i.e., both 1.6 g VSS/L.d. This indicates that the enzymatically pretreated FW might be beneficial to an EGSB reactor.

3.2. The performance of an EGSB reactor treating FW pretreated by enzyme

The OLR of the reactor was achieved to be 20 g COD/L.d (~15.4 g VS/L.d) with a COD removal rate around 90%. The biogas production rate and the methane yield was 7.8 ± 0.1 L/L.d and 0.27 m³ CH₄/kg COD_{re}, respectively. In addition, the proportion of methane was mostly in the range of 60–64%. The VFA maintained at 380.6 mg/L at 20 g COD/L.d of OLR. The balance between VFA and NH₄⁺-N kept the pH in the range of 7.6–7.8. The EGSB reactor can thus achieve a well buffering performance and a long-term stable operation for AD of enzymatically pretreated FW.

The concentrations of MLSS and MLVSS increased from 36.6 and 32.5 g/L to 59.6 and 53.6 g/L, respectively. Therefore, the daily SS growth rate was less than 0.3 g/L.d.

Based on COD balance calculation, 81.1% of the total COD was converted into methane, meaning that an AAD of FW was obtained. The biomass COD was 1.8%, indicating most of the solid organics were degraded with a very low SS accumulation. About 6.8% of the total COD cannot be accounted due to sampling and test errors.

4 Conclusions

The feasibility and performance of AAD of enzymatically pretreated FW in an EGSB reactor was investigated using batch experiments and long-term reactor operation. Simulation study based on results of batch experiments indicated that the enzymatically pretreated FW could be treated using an EGSB reactor. The performance of the bioreactor was demonstrated with different OLRs. At the OLR of 20 g COD/L.d, the methane yield and COD removal rate was 0.27 m³ CH₄/kg COD_{re} and 88%, respectively. The significance of this study is to make it possible to achieve AAD of enzymatically pretreated FW in an EGSB reactor.

Reference

- [1] M. Ye, J. Liu, C. Ma, Y.-Y. Li, L. Zou, G. Qian and Z.P. Xu, Improving the stability and efficiency of anaerobic digestion of food waste using additives: A critical review, *J. Cleaner Prod.*, 192 (2018), pp. 316-326.
- [2] C.M. Braguglia, A. Gallipoli, A. Gianico and P. Pagliaccia, Anaerobic bioconversion of food waste into energy: A critical review, *Bioresour. Technol.*, 248 (2018), pp. 37-56.
- [3] E.U. Kiran, A.P. Trzcinski and Y. Liu, Enhancing the hydrolysis and methane production potential of mixed food waste by an effective enzymatic pretreatment, *Bioresour. Technol.*, 183 (2015), pp. 47-52.
- [4] N. Gu, J. Liu, J. Ye, N. Chang and Y.Y. Li, Bioenergy, ammonia and humic substances recovery from municipal solid waste leachate: A review and process integration, *Bioresour. Technol.*, 293 (2019), pp. 122159.
- [5] L. Zhao, C. Su, S. Chen, Z. Ye, X. Wei, T. Yao, G. Li and P. Wang, Expanded granular sludge blanket reactor treatment of food waste at ambient temperature: Analysis of nitrogen compositions and microbial community structure, *Bioresour. Technol.*, 294 (2019), pp. 122134.

Biochar sustained high-efficient anaerobic co-digestion by enhancing direct interspecies electron transfer and alleviating thermodynamic restriction

Yaqian Liu¹, Qian Li^{1,2*}, Rong Chen^{1,2}

¹Key Lab of Environmental Engineering, Shaanxi Province, Xi'an University of Architecture and Technology, No.13 Yanta Road, Xi'an 710055, PR China.

²International S&T Cooperation Center for Urban Alternative Water Resources Development, Key Laboratory of Northwest Water Resource, Environment and Ecology, MOE, Xi'an University of Architecture and Technology, No.13 Yanta Road, Xi'an 710055, PR China.

*E-mail: Qian.LI@xauat.edu.cn (Qian Li)

Abstract

To investigate the kinetic and thermodynamic effects on the stimulating effect of biochar in thermophilic co-digestion process of food waste (FW) and waste activated sludge (WAS), a series of batch experiments were carried out. This study confirms that compared with control group, the sustained and high-efficiency promotion of biochar is mainly due to the effect on syntrophic methane production. Further, biochar alleviated the restriction of high concentration hydrogen to the main pathway of interspecies hydrogen transfer (IHT), significantly expanded the thermodynamic reaction window of the syntrophic oxidation process. And in terms of electron transfer efficiency, based on the redox capacity of biochar, the equivalent current of the maximum direct electron transfer (DIET) flux obtained is $1.1 \times 10^{-4} \text{A}$, which is 10^8 and 10^4 times than that of IHT and conductive electron transfer process respectively. In addition, for the suspended sludge system, the hydrogenotrophic methanogens were enriched as the main microorganism, while on the surface of biochar, main functional microorganism *Methanosarcina* is likely to be a participant of DIET, which indicates the synergistic effect of biochar surface through DIET alleviated the direct adverse impact of on the IHT path, thereby improving the stability and efficiency of the system.

Keywords: Anaerobic co-digestion, Organic wastes, Thermodynamics, Biochar, Direct interspecies electron transfer.

1 Introduction

Thermophilic anaerobic digestion (AD) process (55-60 °C) to be considered a highly-efficiency strategy, but for high-loading easily degradable organic matter, the high temperature aggravated the rate imbalance between the hydrolysis and syntrophic oxidation methanogenesis stage, resulting in the large accumulation of volatile fatty acids (VFAs) accompanied by the high concentration of hydrogen, which inhibits the interspecies hydrogen transfer (IHT) process, it is further to result in the system collapse.

Biochar (BC) added into AD systems for energy recovery enhancement has been widely confirmed, in recent years, researchers revealed that the redox-active organic functional groups to make BC act as electron transfer mediators, and BC can selectively enrich functional microbes located on the surface and protected them from high-loaded substrate.

However, researchers more often than not paid more attention to the impact of BC on the degradation process of different substances, but ignored the promotion of the mitigation of thermodynamic. In fact, studies have shown that the maximum reaction rate of the syntrophic oxidation bacteria of acetate is much faster than that of acetoclastic methanogen, thus, the syntrophic oxidation process will show a faster reaction rate when the thermodynamic constraints are alleviated.

Therefore, in the long-term experiment, whether the microorganisms enriched on the surface of BC can influence the thermodynamic window is a valuable problem

for revealing the action mechanism of biochar, and on this basis, the coupling effect of different paths on electron transfer efficiency and microbial community is also worthy of further investigation.

2 Materials and methods

All series of batch experiments were conducted using 120mL serum bottles on the thermophilic condition. The organic wastes used in the co-digestion test were a mixture of food waste (FW) and dewatered activated sludge (DAS) with the ratio of 1.5:1. BC was made of sawdust, which pyrolyzed in a 500°C muffle furnace. The concentration of individual VFA (acetate, propionate) was 2500mg-COD/L. Related parameters and electrochemical characteristics of BC were measured, and by high-throughput DNA sequencing techniques to analyze the microbiology community structure.

3 Results and discussion

Compared with the control group, the addition of BC obviously promoted the degradation of the three-period co-digestion process. What's more important is the pure effect of BC has different promoting effects in multi-period after removing the effects of microbial domestication (Fig.1). This means it can relief the rate imbalance of hydrolysis and syntrophic oxidation and become the main reason for the long-term application of BC in complex co-digestion systems.

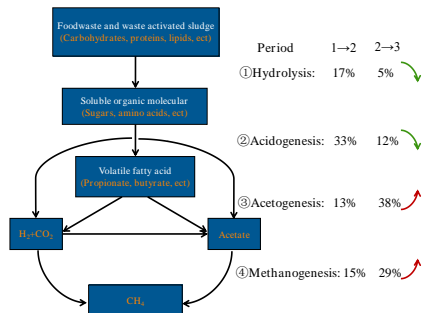


Fig. 1. Promotion effect of biochar on conversion rate of the four stages in three periods.

Fig. 2 shows the degradation process of acetate and propionate. In the first period, when BC was added, the degradation rate of acetate and propionate was observed to increase significantly. In the second period, the environment was under a condition of high hydrogen concentration, so that IHT was restrained completely. Methane production in the control group was almost fully suppressed, but when BC was present, VFAs completed the conversion to methane, with the degradation rate of acetate and propionate decreased to 10.4 and 7.9 mg COD/L/d. Thus, it was likely that the addition of BC enhanced the flow of energy and material between syntrophic oxidizers and methanogens via other pathway like DIET.

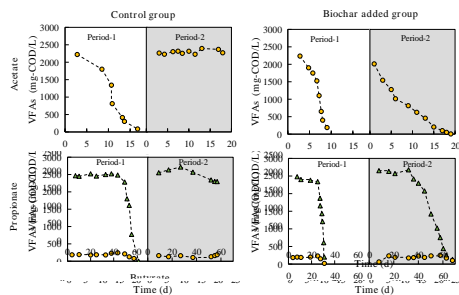


Fig. 2. Variation of individual VFA when biochar was present or absent.

From Fig.3, the addition of BC significantly expands the thermodynamic windows both for acetate and propionate. Specifically, whether or not to add BC is very different for the changes of H₂ and the actual Gibbs free energy in the syntrophic oxidation process. For propionate, BC may perform as a buffer to make the hydrogen content was 0.08% lower than control group, which made the overall actual Gibbs free energy was favorable (-51~84KJ/mol to -64~-87KJ/mol) and the reaction rate faster. In addition, with some assumptions, we got that the maximum carrier flux transferred through the redox reaction was 10⁸ and 10⁴ times than that of IHT and the conductivity mechanism respectively. Therefore, in the case that high hydrogen partial pressure inhibits IHT, BC as an efficient electron carrier through redox ability, expand the thermodynamic window and promote the degradation of VFAs.

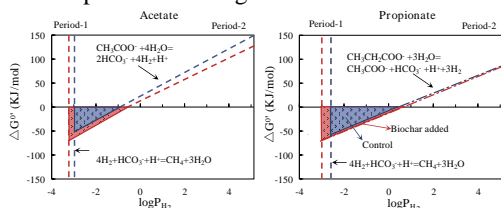


Fig. 3. Changes of thermodynamic windows when biochar was present or absent.

More notably, in the archaeal community of the biofilm on BC, the microbial population distribution was unique, especially for *Methanosarcina*, it became the most abundant genus (49.6%), which was 6.9 times than that in the suspended sludge.

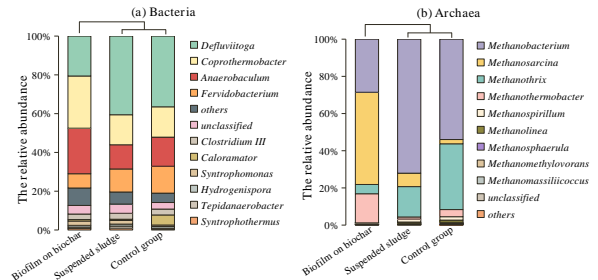


Fig. 4. Comparison of bacteria (a) and archaea (b) relative abundance differences with control group, suspended sludge, and biofilm on biochar.

The abundances of functional enzymes involved in the propionate metabolism, carbon reduction and acetate decarboxylation pathways of three systems were analyzed (Fig.5). It should be noted that acetate kinase (EC: 2.7.2.1) and phosphotrans acetylase (EC: 2.3.1.8) showed higher relative abundance in the sample of biofilm on biochar whereas acetyl-CoA synthase (EC: 6.2.1.1) was main enzymes in control group. Also, informylmethanofuran dehydrogenase (EC: 1.2.7.12) and coenzyme F₄₂₀ hydrogenase (EC: 1.12.98.2) were enriched on the surface of BC, of which coenzyme F₄₂₀ hydrogenase is involved in the last step of the conversion of CO₂ to CH₄.

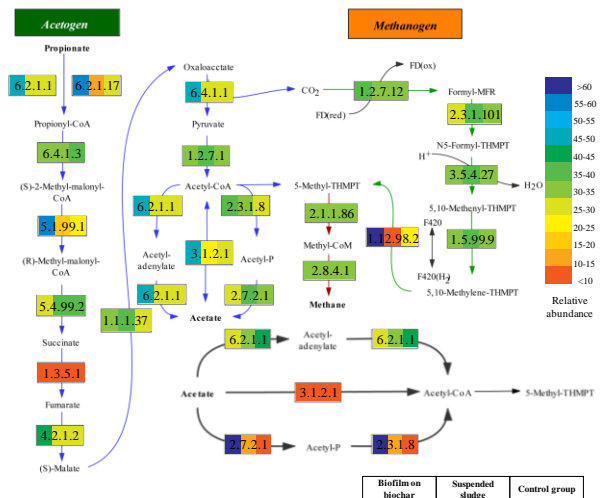


Fig. 5. Comparison of functional enzymes involved in the propionate metabolism, carbon reduction and acetate decarboxylation pathways.

4 Conclusions

The sustained and effective stimulation of BC is mainly manifested in the process of syntrophic methane production, while the reason for this may be due to that the surface of BC triggers a electron transfer pathway like DIET, which accelerates electron transfer, and more importantly, the enriched *Methanosarcina* may through synergistic action alleviate the inhibition effect of high hydrogen partial pressure on IHT and hydrogenotrophic pathway, to make the thermodynamic window expanded and promote the AD process more efficiently.

Effect of Thermal Pretreatment on Digestion of Sewage Sludge in An Anaerobic Membrane Bioreactor

○ Guangze GUO^{1*}, Yemei LI², Hui CHENG² & Yu-You LI^{1,2}

¹Graduate School of Environmental Studies, Tohoku University, Miyagi 980-8579, Japan.

²Department of Civil and Environmental Engineering, Tohoku University, Miyagi 980-8579, Japan.

*E-mail: guo.guangze.t1@dc.tohoku.ac.jp

Abstract

The treatment of sewage sludge has become an important environmental issue all over the world. Anaerobic digestion is a simple method that converts chemical energy from sewage sludge into biogas like methane as a substitute for fossil fuels in contemporary society while eliminating pathogens and eliminating odors. According to the previous study, hydrolysis becomes a rate-limiting step in the anaerobic digestion process due to the complex floc structure of the sewage sludge (eg, extracellular polymer) and hard cell walls. In order to accelerate the hydrolysis process and increase the efficiency of anaerobic digestion, a thermal pretreatment method is applied to carry out the solubilization reaction to decompose the organic matter in the sludge. This study explored the effects of thermal treatment on sludge properties, methane production efficiency, and membrane reactor performance. Current results showed that thermal pretreatment had a more obvious influence on the property of excess sludge than on that of primary sludge.

Keywords: Thermal pretreatment; Sewage sludge digestion; AnMBR.

1 Introduction

With the increase in sewerage penetration rate, the amount of sludge generated is increasing to a large extent (about 75 million tons per year). There is scientific evidence that the application of converting sewage sludge to fuels provides a series of agronomic benefits, in particular the reducing of greenhouse gas emissions such as carbon dioxide, and construction of a resource recycling society.

The conventional sewage sludge treatment method has high energy consumption and treatment cost with a large amount of excess sludge production. Therefore, it is necessary to develop and disseminate technologies which are able to reduce greenhouse gases and produce energy from sewage sludge. In recent years, the AnMBR technology (Anaerobic Membrane Bio-reactor) combines anaerobic digestion and membrane separation method to utilize biomass as a substrate, which can reduce organic pollutants and recover energy at the same time.

AnMBR technology provides improved effluent quality, reliability, high loading rate and removal rate of organic substances. In order to contribute to the long-term environmental profitability for society by utilizing AnMBR, strategies for promoting decomposition of sewage sludge and membrane mitigation fouling are expected for research and development. Moreover, since the excess sludge is composed of microbial flocs and bacterial cells, hydrolysis step is considered to the rate-determining step.

In this study, in order to clarify the characteristics of high-concentration (TS=5%) anaerobic digestion through AnMBR and the effect of thermal pretreatment, batch experiment and long term continuous experiment at mesophilic temperature (35°C) were conducted.

2 Materials and methods

2.1 Biochemical methane potential (BMP) assay

Biochemical methane potential (BMP) assay was carried out at mesophilic temperature conditions to measure the methane yield of the thermal pretreated sludge samples. 55

mL of seed sludge and 15 mL of substrate sludge were transferred into serum bottles with total volume of 120 mL according to the VS ratio of seed sludge and substrate sludge. A blank assay, only filled with 70 mL of inoculum, was conducted in order to determine the biogas production from endogenous inspiration of the inoculum. Once the reactors were loaded the headspace was purged with high-purity nitrogen gas at the flow rate of 0.5 L/min for 1–2 min to remove oxygen. After sealed with rubber stoppers secured by aluminum crimp, the bottles were placed in a water bath (35 ± 1 °C) (BT100, Yamato, Japan) under continuous shaking (110 ± 1 rpm). Seed sludge was taken from AnMBR reactor which continuous operating for long period. Analysis of the composition of biogas was performed through a TCD gas chromatograph. The amount of biogas production of various heat-treated samples was measured everyday. The digestion period was 30 days by which stage the methane production nearly ceased.

2.2 Configuration and long-term operation of AnMBR

Figure 1. shows a schematic diagram of the hollow fiber anaerobic membrane bioreactor and equipment used in this study. The AnMBR consists of a substrate tank, CSTR and a membrane unit. The total effective capacity is 15 L. The membrane material is a tetrafluorinated ethylene resin (PTFE) hollow membrane. The pore size is 0.1 μm and the effective filtration area is 0.1m².

In this study, in order to clarify the effect of thermal pretreatment, operating stages of the reactor were divided into Stag1 and Stag2. The substrate sewage sludge used in Stag1 was a mixture of primary sludge and excess sludge (primary sludge: excess sludge = 45%:55%). In Stag2, Excess sludge was thermal pretreated in a water bath at 70°C and then mixed with the primary sludge (primary sludge: excess sludge=45%:55%). The substrate was stored at 4°C in a mechanically stirred tank and charged into the CSTR reaction tank 10 times everyday (100 ml each time) by a timer-controlled peristaltic pump. TS concentration of the substrate was adjusted to 5%, HRT was fixed on 15 days,

and a long-term continuous operation experiment was conducted at a temperature of 35°C. The effects of reactor operation stability, biogas production status, organic matter decomposition and mass balance due to the introduction of thermal pretreatment were evaluated. The continuous operation management factors of AnMBR are summarized in figure 3.

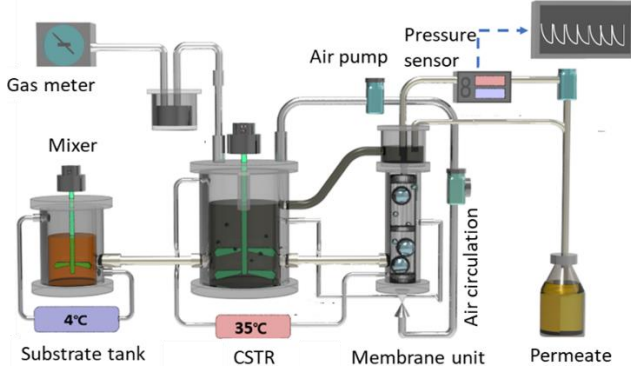


Fig. 1. Configuration of AnMBR

3 Results and discussion

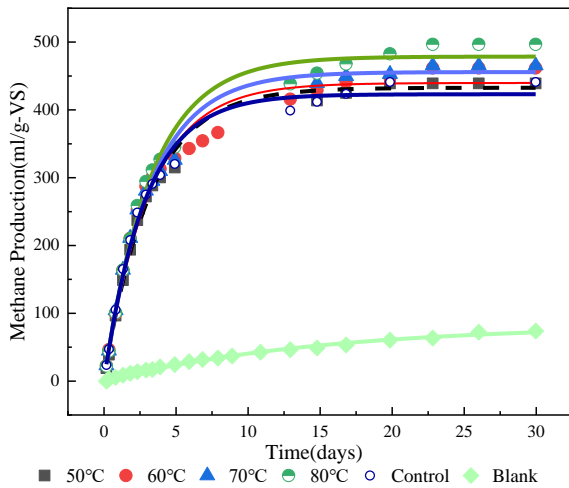


Fig. 2. Net cumulative methane production for different pretreated sludge samples.

The results of the excess sludge gas generation potential of the thermal pretreatment sludge at 50°C, 60°C, 70°C, 80°C were 432.62, 439.75, 455.85 and 478.65 mL/g-VS, respectively. Gas production potential improved 2.4%, 4.1%, 8.0% and 13.35% comparing with the untreated sample. It was clarified that the thermal treatment promoted anaerobic digestion of excess sludge and increased the amount of methane gas generation. The best thermal pretreatment condition is 80 °C and the biogas production potential was 478 mL/g-VS, which was an increase of about 13% compared to the untreated sample. The effect of thermal treatment on excess sludge is more remarkable as the temperature higher.

Fig. 3 shows changes in pH, biogas production rate, methane content, TAN concentration, alkalinity and COD removal rate in the AnMBR reactor during the Stag1 and Stag2. The COD concentration of membrane filtration permeate were 767.5 mg/L and 719.0 mg/L, and the COD removal rates were 99.14% and 98.35%, respectively. With the introduction of thermal pretreatment sludge, the gas generation rate increased significantly to 1.36 L/L/d.

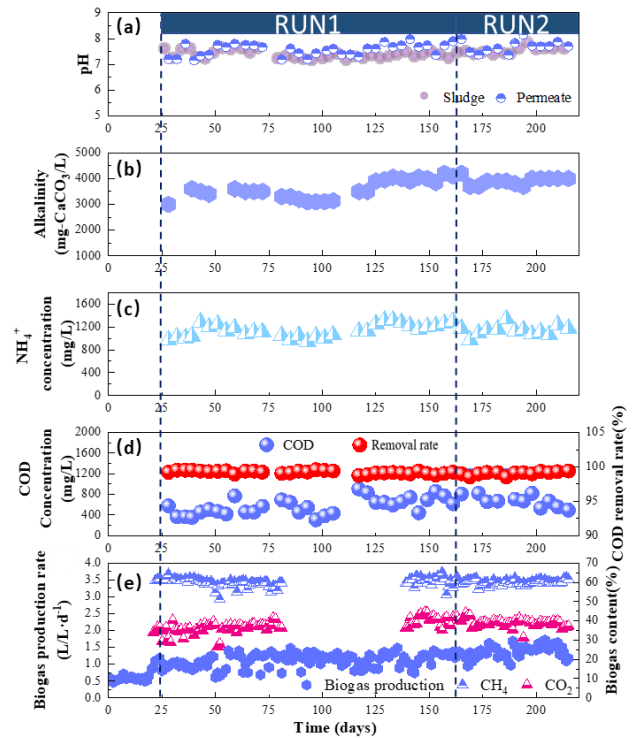


Fig. 3. Variations in pH (a), Alkalinity(b), NH₄⁺-N (c), COD (d) and biogas production (e) during the whole operation.

It was 7.9% higher than the untreated sewage sludge operation stage. At each stage of AnMBR long-term continuous operation, the pH is in the weak alkaline range of 7.0-8.0, and there is no VFA accumulation. The alkalinity of 4.8 is about 3088 and 3850 mg-CaCO₃/L, respectively. TAN was 1128 and 1145 mg/L. The methane content of the biogas was stable at about 60%, and it can be said that good operation was performed.

4 Conclusions

(1) Excess sludge showed a remarkable solubilizing effect and methane production potential by thermal pretreatment. The best thermal pretreatment condition is 80°C which soluble COD concentration and the soluble protein improved 29.98%, 252.0% and biogas production improved 13.4% comparing with untreated excess sludge.

(2) After transferring the thermal pretreated excess sludge into the AnMBR, methane production rate increased 7.9%. The COD removal rate in the two operation stages is 98%.

(3) During the stage2, the membrane fouling rate increased to a large extent. The main substance which lead to membrane contamination is inorganic substances.

Reference

- [1] Zhen G, Lu X, Kobayashi T, et al. Mesophilic anaerobic co-digestion of waste activated sludge and *Egeria densa*: performance assessment and kinetic analysis[J]. Applied energy, 2015, 148: 78-86.
- [2] Chen R, Nie Y, Ji J, et al. Submerged anaerobic membrane bioreactor (SAnMBR) performance on sewage treatment: removal efficiencies, biogas production and membrane fouling[J]. Water Science and Technology, 2017, 76(6): 1308-1317.

Assessment of the secondary salinization impact to the water resources in the Uzbekistan

○ Temur KHUJANAZAROV^{1*}, Kristina TODERICH², Yoshiya TOUGE³, Kenji TANAKA¹

¹Disaster Prevention Research Institute, Water Resources Research Center, Kyoto University, Kyoto 611-0011, Japan

²Department of Civil and Environmental Engineering, Tohoku University, Tohoku, 980-8579, Japan

³International Platform for Dryland Research and Education, Tottori University, Tottori, 680-0001, Japan

*E-mail: khujanazarov.temur.7n@kyoto-u.ac.jp

Abstract

Demand for water resources has been increasing over last decades, growing population, anthropogenic and climate change impacts have increased pressure on natural resources. However, current practises that are generally applied in Uzbekistan induce mineralization of both water and soils. Agricultural water availability and its quality has direct impact to the crop yield and are especially important here. Water mismanagement and overuse exaggerates secondary salinization, the condition when irrigation waters salinize soils and increases mineralization of itself. This activity further increases pollution of all surface flows and deficit of the drinking waters to local communities. Defining such regions and reducing these areas impacts to the whole basin is a subject of this paper discussion. In this research field measurement of both soil conditions and water quality during irrigation season is presented. Water quality sampling to understand extend of the mineralization and its distribution in the basin are compared with soil salinity during irrigation of the agricultural fields, especially in the downstream flow of the Amu Darya and Zeravshan Rivers.

Keywords: salinization; Uzbekistan; water quality;

1 Introduction

Water resources mismanagement has long being one of the main issues for Central Asian agriculture production. Historically, this region has developed a comprehensive irrigation system at the same time increasing pressure to water and land resources. Converting river flow of the Amu Darya River and the Syr Darya River to create wide distributed irrigation canals has resulted in significantly reduced flows to the Aral Sea [1], which had reduced surface area of the Aral Sea significantly [2]. Dried seabed created desert with sands of concentrated salt remained after water evaporation that is currently spread with winds over the whole region, increasing soil salinization.

Nevertheless, main impact to salinization of soils and lands comes from irrigation and the secondary salinization. Although, facing severe consequences of decisions made in the past, current irrigation practices and water management have not changed significantly. In Central Asia there are mainly three irrigation practices: furrow (more than 60%), strip and basin irrigation. Furrow irrigation is dominant here and most of the channels are unlined. Unlined canals greatly reduce amount of flow water that ultimately reaches agricultural fields, as some of it is lost to the groundwater. Furrow irrigation applied over most of the irrigation areas combined with high temperatures and evaporation rates, creates favorable conditions of soil salinization, waterlogging and water quality deterioration. Accumulated salts and minerals are then washed to the river flow, increasing water salinity in the river, and consequentially downstream flow. The drainage channels are also logged and abandoned for long period of time.



Fig. 1. Study area, research sites are shown in frames

The predominant reasons for these developments are poor irrigation water management, inadequate drainage, rising groundwater tables and associated mobilization of primary salts within the soil profile. As a result, huge amount of productive irrigated lands are turning into degraded marginal lands, which are then abandoned by farmers. According to the ADB Final Report, 2008 estimation approximately 600,000 ha of irrigated lands in Central Asia has been stressed over the last decade due to water logging and salinization. Farmers' awareness on soil/water conservation and management of marginal lands is also very low. Measurement of water amount applied to crops and an irrigation scheduling for reclamation of salt prone marginal lands are still based on conventional approaches. Touge, [2] had showed that application of the adequate water saving techniques, could had had decreased impact to the Aral Sea, while reducing waterlogging and salinization due to application of different irrigation technique. It is further

aggravated by the fact that there is no available data on basic requirements of water management for crops, soil moisture extraction pattern, water requirements of different crops, impacts of water deficits at different crop growth periods and others.

Several development projects have been realized to reconstruct irrigation canals and drainage in the recent decade. While demand for the water resources has been increasing over last decades here, distribution of the water usage had varied.

Agriculture water withdrawal has been slowly decreasing, while municipal water withdrawal has increased at the same time fertilizer application has been increasing (fig. 2), which impacts for the further soil salinization [3]. Growing population, anthropogenic and climate change impacts can increase pressure on the water and land resources. In case of Central Asian countries, this has not only food availability complications but also huge economic impact, as it threatens security of water resources availability and agriculture itself.

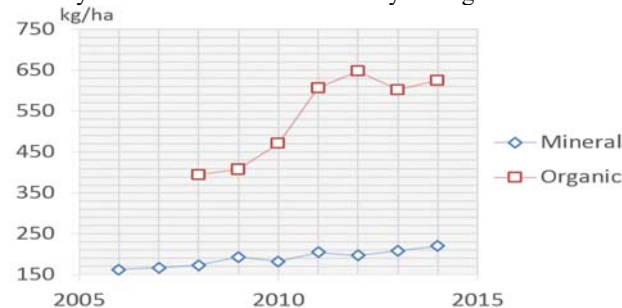


Fig. 2. Distribution of the fertilizers application in Uzbekistan (Source: modified from FAO, 2020).

A current water resources salinization issues in Central Asia has been analyzed. Overall assessment includes analysis of changes happen in last decade, characteristics of different soil and water salinization issues facing Central Asia is summarized and assessed.

2 Materials and methods

To assess water resources mismanagement and rate impacts of the water salinization to the downstream of the river flow a series of the field sampling of the water quality and measurements of the soil salinity during irrigation were conducted. Two locations were selected: the Zeravshan River basin, including one location in the downstream for the soil electro-conductivity measurements, and the Amu Darya downstream area in Karakalpakstan.

Observation sites were on the agricultural farm to confirm irrigation practices and their impact to the salinization process. Water quality sampling was held for the three years along the Zeravshan river flow to analyze how salinization distributes from the upstream to the downstream. Samples were collected on main channels and along the main flow, including drainage and secondary irrigation network canals. Soil electro-conductivity were measured continuously for three location using stationary installed monitoring station.

3 Results and discussion

Results show that salinity concentration increases over the distance from the upstream and reaches the highest values in the downstream (fig. 3). Mineralization concentration increases with drainage water return flows back to the main

river channel. Mainly this are chlorine, calcium concentrated waters that are applied to the irrigation field, thus increasing salinity in the downstream.

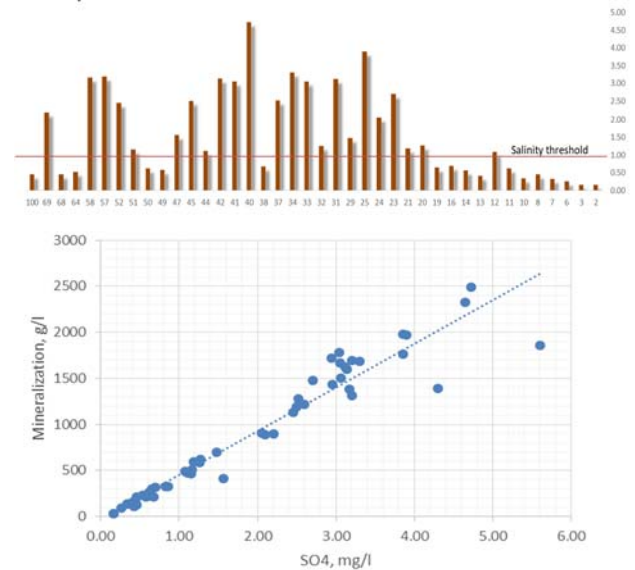


Fig. 3. Water quality analysis of the collected samples (up), mineralization correlation (bellow) in the Zeravshan River Basin

Soil electro-conductivity measurements have confirmed that application of the water for irrigation instantly increases salinization, which then gradually reduces over time. These salts later accumulate on the surface of the soils and therefore required to be removed at the end of irrigation season. Both sites have shown higher salt concentration in the water; however, results in Karakalpakstan are much worth. It is due to a bigger accumulation basin, and high groundwater levels that induces salinization in the upper layers of the soil.

4 Conclusions

Increase in fertilizer application as well as overflow of the irrigation water application is continuously reducing productivity of the soils. This research conducted in two locations in Uzbekistan widens previous research to address water quality deterioration and focuses on understanding of the pollution sources and their distribution during irrigation practices.

Reference

- [1] Micklin, P., 2007. The Aral Sea Disaster. Annual Rev. Earth Planet. Science, 35, pp.47-72.
- [2] TOUGE, Yoshiya. (2018). Development of terrestrial water circulation model in the Aral Sea Basin considering human impacts and climate change. Samarkand, October 2018.
- [3] Kulmatov R., Opp C., Groll M., Kulmatova D., (2013): Assessment of Water Quality of the Trans-Boundary Zarafshan River in the Territory of Uzbekistan. Journal of Water Resource and Protection, 2013, 5, 17-26 doi:10.4236/jwarp.2013.51003

Simulating soil water recession coefficients using satellite-based data for antecedent precipitation index

○ Thapthai Chaithong^{1*} & Daisuke Komori²

¹Department of Geography, Faculty of Social Sciences, Kasetsart University, Bangkok 10900, Thailand.

²Department of Civil and Environmental Engineering, Tohoku University, Miyagi 980-8579, Japan.

*E-mail: thapthai.c@gmail.com

Abstract

The aim of the study is to simulate the soil water recession coefficients (k value) for antecedent precipitation index (API) using the satellite-based data. The soil water recession coefficients (k value) are the main parameter to calculate the API. The k value depends on the maximum soil moisture available and evapotranspiration. Generally, the evapotranspiration is calculated by using the equation such as Penman-Monteith equation, or Priestley-Taylor equation. However, the evapotranspiration value is complicated to calculate by the evapotranspiration equations because they require the many hydro-meteorological parameters to input the equations. Moreover, the hydro-meteorological parameters are measured at meteorological stations which they can represent only small area around the stations. Hence, the study uses the GLEAM (Global Land surface Evaporation) which is the global actual evapotranspiration dataset. Regarding to the calculation, the satellite-based data can apply to estimate the k value for API, but the resolution of GLEAM is coarse for region scale. Therefore, the downscaling method is significant importance.

Keywords: antecedent precipitation index; soil water recession; evapotranspiration; GLEAM.

1 Introduction

Antecedent precipitation index (API) is the indicator to represent the moisture condition in soil [1]. The API is based on rainfall that has fallen over the previous day. The API is applied to a regional landslide and flashflood early warning systems. The API can be expressed as follows [2]:

$$API_t = (k \cdot API_{t-1} + P_t) \cdot I_t \quad (1)$$

where API_t is the API on the “t” the day (mm), P_t is the amount of rain on the “t” the day (mm), API_{t-1} is the API on the previous day (i-1) and k is the soil water recession coefficient.

The soil water recession coefficients (k value) can be calculated using the equation which can be expressed as follows [3]:

$$k = \frac{E_t}{W_m} \quad (2)$$

where E_t is the evapotranspiration (mm), and W_m is the maximum soil moisture available. Considering to the k value equation, there are two main parameters to control the k value which are the evapotranspiration and soil properties. The maximum soil moisture available is amount of moisture in soil for evaporation process. It depends on the volumetric water content at field capacity and permanent wilting point of soil and bulk density of soil. The satellite-based evapotranspiration can be applied to estimate the k value. The Global Land Evaporation Amsterdam Model (GLEAM) is the global evaporation model which is driven by remote sensing observations [4]. The GLEAM considers only three sources of evaporation: (1) bare soil, (2) Short vegetable, and (3) vegetable with a tall canopy [4]. Based on the fundamental concept of the GLEAM, four modules were departed in the GLEAM. First module focuses on the evaporation of intercepted rainfall from the forest canopies. Second module describes the soil-water budgets. Third module is the stress module. Last module is the evaporation form each of three surface components which is computed

based on the Priestley-Taylor equation. Figure 1 presents the four modules for the GLEAM.

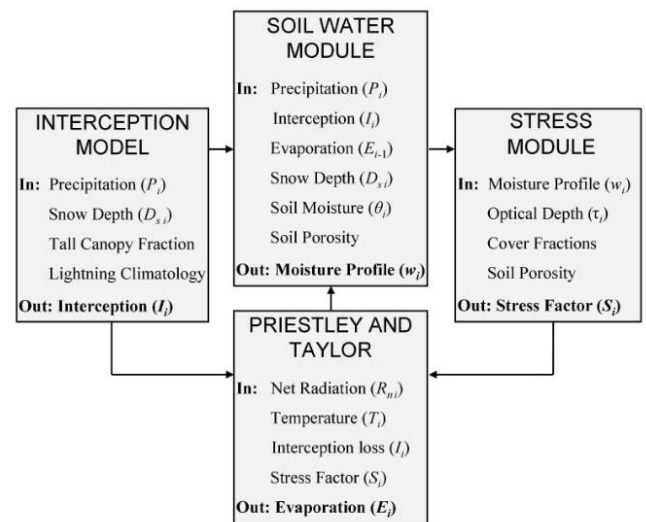


Fig. 1. Four modules for GLEAM.

2 Materials and methods

The study area of the research is the South of Thailand where is a part of Malay Peninsula because there are many landslides occurred in this region such as Krabi landslide on 2011 or Nakhon Si Thammarat landslide on 1988 and 2011. In the study, there are two required parameters. First, the study used the 21 years of GLEAM data from 1989 to 2009 for the evapotranspiration dataset. Second, the bulk density of soil is provided by the ISRIC world soil information. The ISRIC world soil information provided the open-access dataset about the texture and chemistry of soils.

3 Results and discussion

Figure 2 presents the soil water recession coefficients (k value) for 12 month for the South of Thailand. According to calculation, we found that the k value is in range between 0.84 and 0.96. Considering to the spatial detail, the k value vary depending on the evapotranspiration and soil texture.

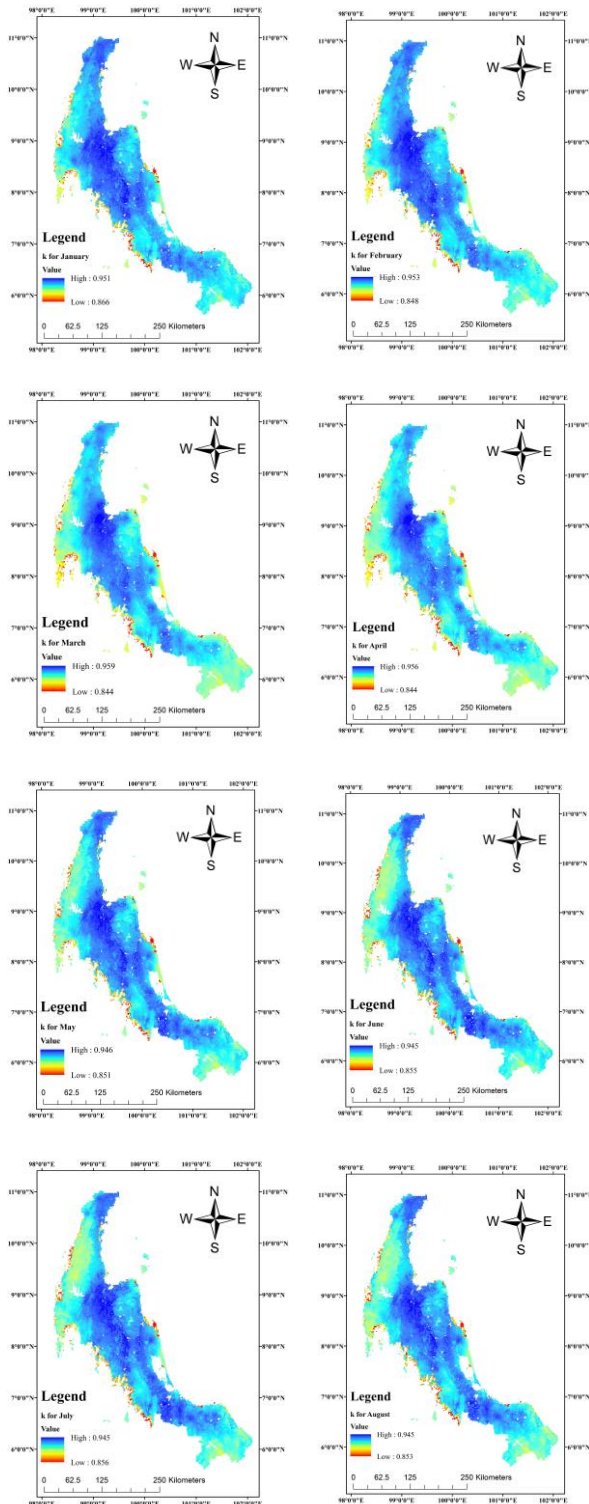


Fig. 2. Soil water recession coefficients.

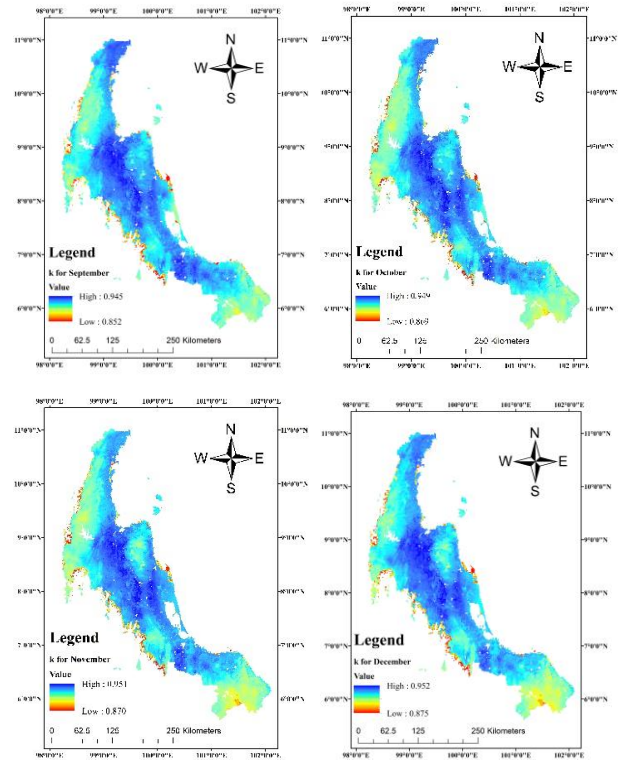


Fig. 2. Soil water recession coefficients (continues).

4 Conclusions

The satellite-based evapotranspiration dataset can be applied to simulate the soil water recession coefficient. The key advantage of satellite-based dataset is the spatial detail of evapotranspiration which can cover the entire region. However, the horizontal resolution is the important limitation of satellite-based evapotranspiration. The original resolution of GLEAM is 0.25 degree, hence the downscaling method is significantly important for regional scale.

Reference

- [1] Zhao B, Dai Q, Han D, Mao J, Zhuo L, and Rong G, Estimation of soil moisture using modified antecedent precipitation index with application in landslide predictions, *Landslides*, 16(2019), 2381-2393.
- [2] Choudhury B J, and Blanchard B J, Simulating soil water recession coefficients for agricultural watershed, *WATER RESOURCES BULLETIN*, 19:2(1983), 241-247.
- [3] Teng W L, Wang J R, and Doraiswamy P C, Relationship between satellite microwave radiometric data, antecedent precipitation index, and regional soil moisture, *INT. J. REMOTE SENSING*, 14:13(1993), 2483-2500.
- [4] Miralles D G, Holmes T R H, De Jeu R A M, Gash J H, Meesters A G C A, and Dolman A J, Global land-surface evaporation estimated from satellite-based observations, *Hydrol. Earth Syst. Sci.*, 15(2011), 453-469.

Understanding Seasonality and Evapotranspiration of Soil Water under Tree and Grass Cover Using Natural Isotopes

○ Danila PODOBED^{1*}, Daisuke KOMORI², Kei YOSHIMURA³, Masahiro TANOUE⁴

¹Graduate School of Environmental Studies, Tohoku University, Miyagi 980-0845, Japan.

²School of Engineering, Tohoku University, Miyagi 980-0845, Japan.

³Institute of Industrial Science, University of Tokyo, Chiba 277-0882, Japan.

⁴Satellite Observation Center, National Institute for Environmental Studies, Ibaraki 305-8506, Japan.

*E-mail: ilmarinen87@yandex.ru.

Abstract

This study employed naturally-occurring isotopes ¹⁸O and ²H as tracers of water origin and evapotranspiration dynamics to understand the soil water environment in the unsaturated zone under tree and grass cover in northeastern Japan. Over the course of one year, ¹⁸O and ²H concentrations were observed in soil water profiles under tree and grass cover. The observed soil water isotope concentrations were then compared with precipitation isotope data simulated by the IsoRSM model. ¹⁸O was used as the primary indicator of evaporative processes and d-excess was used to assess seasonality. The changes in relative and absolute concentrations of ¹⁸O and ²H with depth were analyzed to understand water transport mechanisms. The results indicated that summer rainfall was excluded from the soil profile below ~2m, and likely played no role in groundwater recharge. Additionally, the results suggested preferential transport of heavy, isotopically-depleted precipitation under tree cover, as well as differences in the way snowmelt and summer precipitation are affected by different land cover regimes. Additional work is needed to verify the interpretation of observed data by numerical simulation.

Keywords: water isotopes; unsaturated zone; land cover; seasonality; preferential flow; snowmelt

1 Introduction

One of the main issues involved in land use changes are the effects of such transformations on local water resources. While there is a general consensus among researchers that afforestation in arid and semi-arid regions produce an overall net reduction in water availability and groundwater levels in particular relative to bare soil or grasslands, such differences are small or negligible in wetter regions or during periods of heavy rainfall. The primary aim of the current study was to achieve an understanding of the snowmelt infiltration and seasonal contributions to deep drainage are affected by different land cover regimes (forest and grass) in a temperate, water-abundant region like Japan. The method selected for investigation in the current study was the so-called “natural isotope tracer” method, whereby soil water concentrations of ¹⁸O and ²H are compared to those in local precipitation. This method has been widely used to study soil moisture seasonality and permeation, as well as to understand the prevalence of preferential vs. piston flow under different ground cover regimes (ex., Allison and Hughes, 1983). The current study attempted to fill a gap in the use of natural isotope tracers by analyzing the relationship between ¹⁸O/²H concentrations found at various depths of the soil profile.

2 Materials and methods

2.1 Field sites and sampling

Sample collection was conducted on the undeveloped section of the Aobayama Campus of Tohoku University, Sendai, Japan. Survey sites under forest and grass cover were selected at 8 locations. Soil moisture sampling was carried out in two stages; in the first stage, boreholes were excavated between April-October of 2017, spaced several months apart. A second, intensive period of sampling at 6 of the original 8

locations took place in April 2018, to better represent the infiltration of the same isotopic input. Excavation of soil samples was conducted by means of a hand auger and a motorized percussion sampler to a depth of 5 meters. The soil moisture content was measured by evaporating sub-samples in an industrial oven and comparing the mass of dried and wet soil. Additional sub-samples were then centrifuged to extract soil water for isotope analysis; this water was filtered and isotope concentrations measured using a Picarro L2120-i CRDS water isotope analyzer.

2.2 Analysis Methods

In order to identify to seasonal patterns in soil moisture isotope profiles, the study considered simulated precipitation isotope data for the years 2016-2017 produced by a regional climate model (IsoRSM). Simulation of 2018 precipitation isotopes was not possible due to lack of model input data for 2018 at the time the model was run; subsequent work will be carried out to correct this omission. Observed precipitation isotope data for Sendai, collected by the Isotope Mapping Working Group of the Japanese Association of Hydrological Sciences in 2013, was used for model calibration (per Tanoue et al., 2016). Additionally, monthly precipitation data for Sendai, acquired from the Japan Meteorological Agency, was used to achieve an understanding of the relationship between isotope concentrations and precipitation volume. Due to the high correlation of $\delta^{18}\text{O}$ and $\delta^2\text{H}$, $\delta^{18}\text{O}$ was used as the primary tracer in this study; $\delta^2\text{H}$ was used in a supplementary fashion to evaluate evaporative processes based on the $\delta^{18}\text{O} / \delta^2\text{H}$ relationship and also to employ d-excess as a second-order tracer. D-excess is defined by the following equation:

$$\text{d-excess} = \delta^2\text{H} - 8 \times \delta^{18}\text{O}$$

As discussed in Waseda and Nakai (1983), d-excess can be used to identify the seasonal origin of precipitation.

3 Results and discussion

The $\delta^{18}\text{O}/\delta^2\text{H}$ relationship of the soil moisture samples and simulated 2016-2017 precipitation was considered. The shallower slope of the $\delta^2\text{H} = 5.25 * \delta^{18}\text{O} - 9.38$ trend for grass cover boreholes, as compared to the $\delta^2\text{H} = 6.67 * \delta^{18}\text{O} + 2.41$ for tree cover, suggested an elevated impact of evaporation on the surface of grass cover plots. An analysis of the $\delta^{18}\text{O}/\delta^2\text{H}$ relationship dynamics by depth also attested to the increased impact of evaporation on grass-cover profiles, as the slope of the grass-cover $\delta^{18}\text{O}/\delta^2\text{H}$ trend line became progressively shallower with depth, while that for the tree-cover profiles remained relatively steady (Fig. 1). Additionally, observed isotopic delta-values under tree cover became progressively more depleted with depth, but were evenly distributed regardless of depth for grass-cover (Fig. 1). This observation indirectly suggested the presence of flow mechanisms under tree cover that preferentially distributed depleted (heavier) rainfall to deeper soil layers.

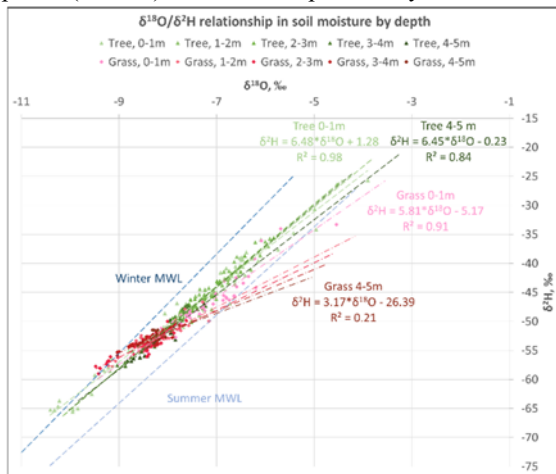


Fig. 1. Depth distribution of $\delta^{18}\text{O}/\delta^2\text{H}$ values and trend lines in the 2017-2018 soil moisture profiles.

Two sets of soil moisture profiles taken at the same time at adjacent tree-cover and grass cover plots - two excavated on September 2017 (E-F17, Fig. 2), and two in April 2018 - were compared directly (E-F18, Fig. 2). The April 2018 tree-cover profile exhibited a depletion bulge at 40-50 cm depth, with a $\delta^{18}\text{O}$ of -11‰ corresponding to simulated winter/spring precipitation; this bulge was entirely absent in 2018 grass-cover profiles. During Sept. 2017, such disparity between grass and tree cover profiles was not observed. This suggested that while ground-level evaporation on grass-cover plots and evaporation of moisture intercepted by the tree canopy on tree-cover plots was nearly equal during summer months, evaporation of snowmelt was more limited under tree cover. The author's hypothesis is that evaporation of snowmelt was delayed until after the snow had already passed through the tree canopy, and was thus reduced, and no significant canopy-level evaporation of snowmelt occurred.

The d-excess values across all boreholes were similar, averaging around ~12‰ below 1.5-2.0 m depth. Following Waseda and Nakai (1983), averages for the months of Dec. - Feb. (winter) and Jun. - Aug. (summer) were used to represent the seasonal extremes in d-excess, with values of 14.06‰ and 7.97‰, respectively. D-excess of soil moisture cannot be higher than the precipitation from which this soil moisture originated; it can only decrease by evaporation. It was therefore considered probable that summer rainfall, with

a simulated d-excess of 5-10‰, was not present in the soil moisture below 2 m. This was likely the result of exceptionally high evapotranspiration during the summer months consuming most of the recent precipitation, as described in a number of studies (for example, Allison and Hughes, 1983).

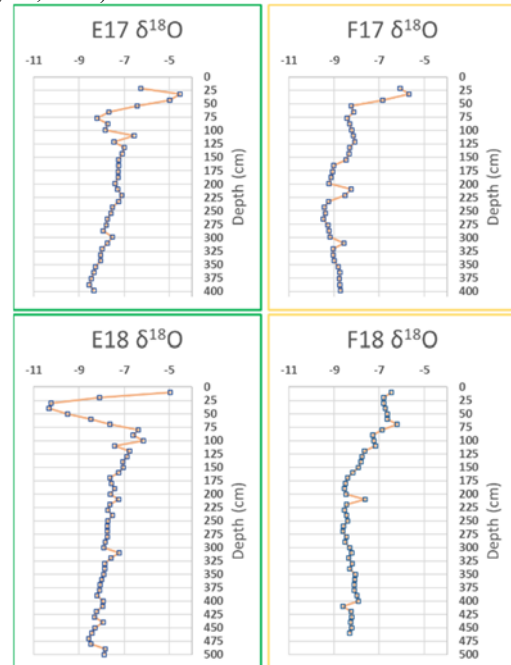


Fig. 2. Selected $\delta^{18}\text{O}$ profiles during the 2017-2018 sampling period (green indicates tree cover, yellow indicates grass cover).

4 Conclusions

The most significant finding of the current study was the apparent exclusion of summer precipitation from deeper soil layers. The exact mechanism causing this phenomenon is uncertain but is suspected to involve very high evapotranspiration during the summer months. This would suggest groundwater recharge by summer precipitation is negligible. Additionally, preferential transport of heavy rainfall is likely the cause of depleted isotopic concentrations below tree cover. Finally, the study provides evidence of differential evaporative effects on snow deposited in the winter and spring months, suggesting it is less affected by canopy-level evaporation than precipitation during other seasons.

Upcoming work will include simulation of soil water transport and evaporation by a land-surface model (TBD) to verify the mechanisms responsible for the observed results.

Reference

- [1] Allison, G. B., & Hughes, M. W. 1983. The use of natural tracers as indicators of soil-water movement in a temperate semi-arid region. *Journal of Hydrology*, 60(1-4), 157-173.
- [2] Tanoue, M., Ichianagi, K., & Yoshimura, K. 2016. Verification of the isotopic composition of precipitation simulated by a regional isotope circulation model over Japan*. *Isotopes in Environmental and Health Studies*, 52(4-5), 329-342.
- [3] Waseda, A., & Nakai, N. 1983. Isotopic compositions of meteoric and surface waters in Central and Northeast Japan (in Japanese). *Chikyukagaku*, 17, 83-91.

Spatiotemporal analysis of drought indicated by scPDSI over Japan

○ Ke SHI^{1*}, Yoshiya TOUGE¹

¹ Department of Civil and Environmental Engineering, Tohoku University, Miyagi 980-8579, Japan.

*E-mail: shi.ke.s5@dc.tohoku.ac.jp

Abstract

Drought disasters, such as water scarcity and wildfires, are severe natural disasters in Japan that are also affected by climate change. However, as drought generally has widespread impacts and the duration of drought can vary considerably, it is difficult to assess the spatiotemporal characteristics of drought comprehensively. Therefore, to identify the drought homogeneous regions and further understand regional drought over Japan, this study provides a spatiotemporal analysis for historical droughts patterns over Japan. The drought characterised by the Self-calibrating Palmer Drought Severity Index (scPDSI) was investigated for the period 1960~2018. Subsequently, patterns of drought were identified through distinct empirical orthogonal function (DEOF). Results indicate that two major subregions of drought variability—the western Japan (W region) and most of the northernmost Japan near the Pacific (N region) were identified. Further, whether in W region or N region, wildfires with large burned area were more likely to occur when the scPDSI was less than -1, which meant that excess dried-out vegetation provided ample fuel for the wildfires. This study is the first to identify homogeneous regions with distinct drought characteristics over Japan. Also, the results are beneficial for regional drought management over Japan.

Keywords: Drought; scPDSI; DEOF; Wildfire.

1 Introduction

Under climate change conditions, especially direct and clear global warming, drought has shown increasing trends in some regions of the world. Considering the duration, intensity, geographical extent, and broad effects of droughts, it is challenging to determine drought occurrences and their effects [1]. Additionally, drought is considered to be the most complex and impenetrable extreme climate event, affecting more people than any other natural hazard. In particular, the deficit in precipitation combined with high evapotranspiration losses during a drought would increase the risk of other disasters such as wildfires. The risk of water scarcity would be exacerbated by long-term drought.

The research on droughts over Japan has been receiving increasing attention. More than 70% of Japan is mountainous, causing rain to flow quickly to the ocean after falling. Historically, most areas of Japan have experienced droughts with varying duration, frequency, severity, and intensity. Particularly, in 1994, almost the whole of Japan experienced a long-lasting drought and the drought caused an economic loss of approximately 1.3 billion dollars as a result of the decline in agricultural production [2]. The number of areas affected by drought in Japan is decreasing but still exists every year.

Overall, to further improve the capacity of early warning and risk assessment of drought at the regional level, it is necessary to identify the homogeneous regions with distinct drought characteristics over Japan. However, there is still a lack of understanding of the specific consequences of droughts in Japan. For this purpose, this study attempts to provide an analysis of historical droughts over Japan to fill these gaps. The drought events were characterised by Self-calibrating Palmer Drought Severity Index (scPDSI) using the most up-to-date data. Major patterns of long-term trends in drought and periodicity were then identified using the distinct empirical orthogonal function (DEOF) and continuous wavelet transform, respectively. Additionally,

the relationship between drought index and wildfire was analysed to identify the effects of the drought.

2 Materials and methods

2.1 Data

The 0.5° high-resolution gridded datasets of precipitation, near-surface temperature, potential evapotranspiration, and scPDSI were obtained from the Climatic Research Unit at the University of East Anglia. In this paper, the selected period ranges from 1960 to 2018. The scPDSI class is shown in Table 1. This scPDSI was presented by Wells et al [3], which was a variant of the original PDSI [4] used to make the results from different climatic regimes more comparable.

2.2 Distinct Empirical Orthogonal Function

The empirical orthogonal function (EOF), which deals with temporal and spatial functions, is used to extract the spatiotemporal modes based on the data variance representations. The EOF analysis method can decompose the time-varying variable fields into the space function part (EOFs) that does not change with time and the time function part (principal components, PCs) that depends only on time. The distinct EOF (DEOF) analysis was subsequently introduced to overcome problems in the EOF analysis [5]. In the DEOF, a continuous spectrum of spatial patterns resulting from a stochastic process can be represented by EOF modes, where some spatial structures will be more dominant than others. Based on the isotropic diffusion null hypothesis, the EOF modes (DEOFs) can be found by rotating the leading EOF modes, corresponding to the distinguished principal components (DPCs). These DPCs take up a large part of the total variance in all the variables in the original field, which is equivalent to the main information of the original field concentrated on a few main components. The higher the eigenvalues, the more typical the corresponding modes, and the more significant the contribution to the total variance.

3 Results and discussion

The DEOF calculation used the scPDSI time series of each grid point on the monthly scale. Fig. 1 (a) and (b) displays the spatial partitioning results of the first two DEOFs. The explained variances in the first two DEOFs were 46.85% and 20.55% respectively, which meant that the DEOFs could explain approximately 67.40% of the total spatial wet/dry characteristics of Japan from 1960 to 2018. The first two had sufficiently explained variances to represent most of the wet/dry conditions in Japan.

The spatial distribution of DEOF1 illustrated that a high positive loading occurred in the western region at approximately 35°N (W region). This finding meant that the W region had similar drought characteristics from 1960 to 2018. Similarly, the spatial distribution of DEOF2 illustrated the common positive spatial behaviour of drought in most of the northernmost region near the Pacific (N region). However, the central region, western region, and most parts of the northwestern region showed common negative spatial behaviour, indicating that these regions showed the opposite drought characteristics as the N region. Notably, the two DEOFs were unable to represent all drought characteristics across the whole of Japan. For the corresponding drought temporal characteristics, the DPC scores are displayed in Fig. 1 (c) and (d). The DPC1 scores showed a decreasing trend, which meant that the W region became drier. However, the N region was getting wetter.

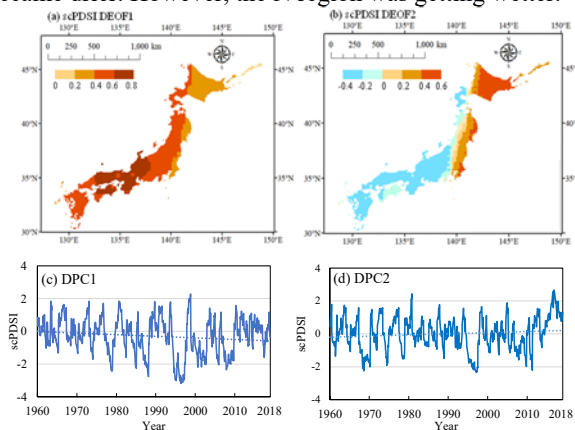


Fig. 1. First two DEOFs and DPCs for scPDSI. (a) DEOF1. (b) DEOF2 (c) DPC1 (d) DPC2.

Considering the ability of scPDSI to represent the water balance adequately, the analysis of combining drought with wildfires would further enhance the understanding of drought-induced natural disasters. Soil drought occurred most commonly in spring, which was also the season when wildfires frequently happen in Japan. Therefore, the comparison between the annual burned forest area in spring (March to May) with DPCs was extracted, as shown in Fig. 2. The burned area data come from fire reports provided by the Fire and Disaster Management Agency, Government of Japan. The burned area data of the W region included the Ishikawa prefecture, Fukui prefecture, Gifu prefecture, Aichi prefecture, Shiga prefecture, Kyoto prefecture, Osaka prefecture, Hyogo prefecture, Nara prefecture, Wakayama prefecture, Tottori prefecture, Okayama prefecture, and Mie prefecture. The burned area data of the N region included the Hokkaido prefecture.

In a wet spring, when the scPDSI was positive, the burned area of western Japan was less than 100 ha. The three springs with severe wildfires, when the burned area was larger than 300 ha, were accompanied by drought events in which the scPDSI was less than -1. Although there were fewer wildfire occurrences in the N region than in the W region, these two regions followed a similar pattern. A total of six wildfires with burned areas of over 60 ha occurred in the N region. The scPDSI values corresponding to these six wildfires were all negative, and four of them experienced drought (scPDSI ≤ -1). When the scPDSI was more than 1, there were only six wildfire occurrences in the N region, and the burned area was less than 60 ha.

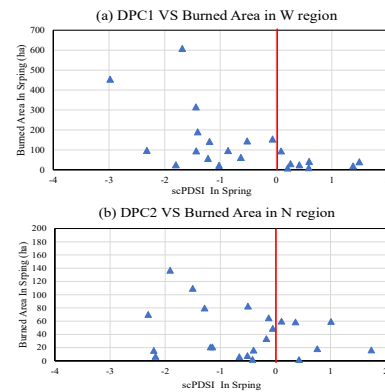


Fig. 2. Comparison of DPCs for annual burned forest area in spring (a) DPC1. (b) DPC2.

4 Conclusions

The main conclusions obtained from this paper are summarised as follows: (1) DEOF was used to identify two major subregions of drought variability—the western region (W region) and most of the northernmost region near the Pacific (N region). The corresponding scores of DPC1 and DPC2 showed a trend of decreasing (increasing in drought) and increasing (decreasing in drought), respectively. (2) When scPDSI was less than -1, wildfires with larger burned areas were more likely to occur.

Reference

- [1] ASONG, Z. E., et al. Historical drought patterns over Canada and their teleconnections with large-scale climate signals. *Hydrology & Earth System Sciences* 22.6 (2018).
- [2] LEE, S., et al. Spatiotemporal characteristics of drought occurrences over Japan. *Journal of applied meteorology and climatology* 51.6 (2012): 1087-1098.
- [3] WELLS, N., et al. A self-calibrating Palmer drought severity index. *Journal of Climate* 17.12 (2004): 2335-2351.
- [4] PALMER, W.C., *Meteorological Drought*, Office of Climatology U.S. Weather Bureau, Washington, D.C. (1965).
- [6] DOMMENGET, D. Evaluating EOF modes against a stochastic null hypothesis. *Climate dynamics* 28.5 (2007): 517-531.

Acknowledgements

The authors declare no conflict of interest. This study was jointly supported by the Ministry of Education, Science, Sports and Culture, Grant-in-Aid for Exploratory Research, 2019-2021 (19K21982, So Kazama) and Grant-in Aid for Scientific Research (B), 2020-2023 (20H02248, Yoshiya Touge).

The Effect of Wealth Level and Community-Based Environmental Activities Participation on Environmental Awareness

○ Erwan Wahyu WIBOWO^{1*}, & Daisuke KOMORI²

¹Pati Regency Government, Central Java Province, Indonesia.

²Department of Civil Engineering, Tohoku University, Sendai, Miyagi, 980-8579 Japan.

*E-mail: r_one7@icloud.com.

Abstract

Pollution degrades the environment and threatens life. In this study, a system dynamics model was proposed for environmental awareness based on Environmental Kuznets Curve (EKC) coupled with the community-based recycling activities. The system dynamics model describes how environmental performance (pollution level), wealth level, community-based recycling participation, population density, and environmental awareness are interrelated and evolve gradually. Moreover, pollution levels decrease dynamically due to increasing environmental awareness. Using quantitative analysis to understand the interrelation of EKC and community-based recycling activity by validating the model. By using the model's quantitative analysis, the community-based recycling activity has potential as a trigger to increase environmental awareness against EKC in Phase 1 to accelerate the achievement of turning points. In addition, it was also confirmed that the community-based recycling activity has no role within increasing environmental awareness in the rural area.

Keywords: *Environmental awareness, Environmental Kuznets Curve (EKC), Engel coefficient (ECF), Community-based waste recycling activities, System dynamics model*

1 Introduction

Pollution having an irreversible impact on the environment, empirical evidence shows that pollution in some countries already has dangerous consequences. Based on Jambeck et al. (2015), there are 275 million tons of plastic waste produced worldwide. Around 4.8-12.7 million tons are polluting the sea. The Environmental Kuznets Curve (EKC) shows that the level of environmental pollution would increase and would later experience a decline or a turning point, in line with the increase in economic growth (Todaro et al., 2006). The EKC phase is divided into two (Kaika and Zervas, 2016). Phase I of EKC is the economic growth phase of the transition from agriculture to industry or changes in economic structure from rural to urban. Phase II is the transition from the post-industry stage to a service-based economic system. The challenge is to accelerate the achievement of turning points of EKC before environmental degradation results in fatalities.

To address environmental problem and create new turning point Environmental awareness is important (Chen et al., 2019). Most study about environmental awareness only focus on factors that influence and study based on the current situation (Culiberg and Rojšek, 2008; Gadenne et al., 2008). Lack of study discusses environmental awareness shift (increase/decrease) by comparing case in two or more sites/situations and its correlated factors. An approach to increase environmental awareness such as community-based waste recycling empowers the community to manage waste wisely by sorting, and 3R practices.

From background of study mentioned before, the objective of study is using quantitative analysis to understand interrelation of EKC and community-based recycling activities.

2 Methods

2.1. Study Area and Data Source

This study was conducted in communities in two different areas (urban and rural) with differences in socio-economic and environmental characteristics. The data were collected

through field surveys conducted on 21 April - 4 May 2020 in Sukoharjo and Wonosekar Village, Pati Regency, Central Java Province, Indonesia. The primary data represents information from individuals', and individuals' motivation.

2.2. Parameter of Variables

This study using Engel coefficient (ECF) to determine the wealth level. The poorer family is, the larger the budget share it spends on food consumption (Engel, 1857 in Chai and Moneta, 2010). ECF implies that Low ECF means wealthy, high ECF mean Poor.

The questionnaire is used to identify respondents' perceptions of environmental awareness trough their current practices of pro-environmental actions, refer to European Commission (2008), Eurobarometer: Attitudes of European Citizens Towards the Environment such as household waste sorting, reduction of plastic waste, and recycling activities.

Community-based recycling participation is determined by participation in the waste bank program. This study used participants, non-participants, and ex-participants groupings.

2.3. Analysis Method

The quantitative analysis applies to the average sample set arranged by respondents' category (participants, non-participants, and ex-participants) and area distributions (urban and rural) to determine the interrelation between the variables. As for qualitative analysis, the method of data analysis used is an interactive model analysis by data reduction, data testing or data analysis after data collection to draw conclusions and verification.

3 Results and discussion

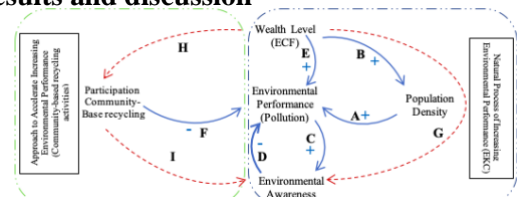


Fig. 1. The system dynamics model combines EKC and community-based recycling activities to describe environmental awareness shifting.

This study designed a system dynamics model for environmental performance based on EKC and the community-based recycling activity.

Based on previous research, population density increases pollution levels (A), with excessive consumption patterns, the environment becomes more polluted as the wastes are produced (Jambeck et al., 2015). The relationship between economic growth and population density (B) depicts that industrialization's massive growth focuses on advancing the economy and absorbing labour. This growth drives urbanization.

An increase in pollution levels causes an increase in environmental awareness among the public (C) (Wang et al., 2016), when consequence of fatalities occur, people get aware and government set a regulation to control pollution. Increasing in environmental awareness has an impact on increasing environmental performance (D) (Chen et al., 2019). Many research of the EKC shows that environmental pollution increases in the early stages of development during an economic growth—as we know as Phase I of EKC (E) (Stern, 2004). Previous studies found that the community-based recycling activities is a form of social engineering at the community level to reduce waste piles (F).

There are three interrelation to be investigate in this study; the interrelation between the wealthy level and environmental awareness (G), the relation between the wealthy level and participation of community-based recycling (H) and the effect of participation of community-based recycling toward environmental awareness (I).

Responses from each groups of respondents in urban and rural areas used to examine the interrelation between variables.

Table 1. Comparison of variables on communities in target areas

Target Area	Group	Wealthy Level (ECF)		Environmental Awareness		Environmental Index*
		Group	Community	Group	Community	
Rural	Participants & Ex-Participants	38%	40%	3.8	4.2	0.8
	Non-Participants	44%		4.6		
Urban	Participants & Ex-Participants	39%	38%	4.3	3.9	0.6
	Non-Participants	42%		2.8		

*(Source: Statistics Agency of Pati Regency, 2019)

On the community scale, it can be seen that an increase in wealth level from 40% to 38% ECF causes the decrease of environmental awareness, from 4.2 to 3.9. The interrelation of wealth level and environmental awareness is negative

The interrelation between ECF and environmental awareness among participants and ex-participants versus non-participants in rural areas shows an increase in environmental awareness (from 2.8 to 4.3) in spite of ECF was slightly decreased or steady. This finding can explain the importance of community-based recycling activity to keep/increase environmental awareness against EKC in urban area. In rural areas is negative (from 3.8 to 4.6). Even environmental awareness, both high but interrelation towards ECF, is negative. This might explain that there is no effect of the community-based recycling activity in the initial Phase I of EKC because those who live in rural areas do not face environmental problems.

In the urban area, people who reluctant to join the waste bank activities are people with a moderate level of wealth (Fig. 2). Based on this distribution of ECF in non-participants group, it cannot conclude the interrelation of wealth level and community-based recycling activities.

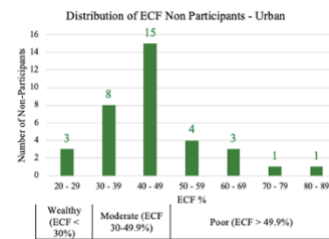


Fig. 2. The wealth level of non-participants in urban area

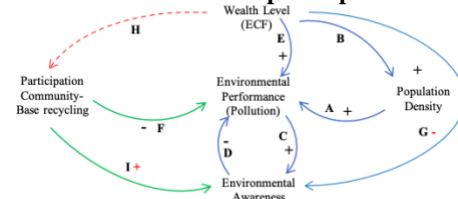


Fig. 3. The system dynamics model of the target area. Red +/- were confirmed in the case of this study. Red dash line still unconfirmed

Quantification of the relationship between the wealth level of individuals – environmental awareness in the target area as pure EKC in Phase 1 (G), is negative, suggests that with increasing wealth levels, environmental awareness decreases, that increasing wealth levels from rural to urban, resulted in a decrease in environmental awareness (Table 1).

The interrelation between the community-based recycling activity (waste bank) and environmental awareness (I) is positive. Moreover, community-based recycling activities has the potency to increase environmental awareness against pure EKC in Phase 1 (G). Community members who participate in the waste bank program have higher environmental awareness comparing with those who not participate, resulting in a comparison of environmental awareness between non-participants and participants group (Table 1). Waste banks help foster collective awareness of the community to start sorting, recycling and utilizing waste.

On the other hands, the interrelation of the wealth level and participation in the target area (H) is still not confirm. Using both cases in urban and rural areas cannot be concluded that wealth level implies participation increase or decreases.

4 Conclusions

Based on quantitative analysis, system dynamics model can explain the interrelationship of variables in target areas. In addition, community-based recycling activity has potential as a trigger to increase environmental awareness against EKC in Phase 1 to accelerate the achievement of turning points.

Reference

- [1] Chai, A., & Moneta A., (2010). Retrospectives: Engel Curves. *Journal of Economic Perspectives*, 24(1), pp. 225-40.
- [2] Chen, X., Huang, B., & Lin, C. T., (2019). Environmental Awareness & Environmental Kuznets Curve. *Economic Modelling*, 77, pp. 2-11
- [3] Culiberg, B., and Rojšek, I., (2008). Understanding Environmental Consciousness: A Multidimensional Perspective. In *Insights for measuring environmental awareness*, Ham M., Mrčela D., Horvat M., (2016). *Ekonomski Vjesnik*, 29, pp. 159-176
- [4] Gadonne, D.L., Kennedy, J., and McKeiver, C., (2008). An Empirical Study of Environmental Awareness and Practices in SMEs. *J Bus Ethics* 84, pp. 45-63
- [5] Jambeck, J. R., Geyer, R., Wilcox, C., Siegler, T. R., Perryman, M., Andrady, A., Narayan R., & Law, K. L., (2015). Plastic Waste Inputs from Land into The Ocean. *Science*, 347(6223), pp. 768-771
- [6] Kaiika, D., and Zervas, E., (2013). The Environmental Kuznets Curve (EKC) theory—Part A: Concept, causes and the CO2 emissions case. *Energy Policy*, 62, pp. 1392-1402
- [7] Kuznets, S., (1955). Economic Growth and Income Inequality. *The American Economic Review* 45(1), pp. 1-28.
- [8] Stern, D. L., (2004). The Rise & Fall of the Environmental Kuznets Curve. *World Development*, 32(8), pp. 1419-1439.
- [9] Todaro, Michael P., and S.C. Smith, (2006). *Economic Development*, 9th edition. Pearson Education Limited. Essex.
- [10] Wang, Y., Sun, M., Yang, X., & Yuan, X., (2016). Public awareness and willingness to pay for tackling smog pollution in China: a case study. *Journal of Cleaner Production*, 112, pp. 1627-1634

Hydrological assessment of precipitation products over high mountain regions: case study of Issyk-Kul Lake.

○ Sanjar SADYROV^{1*}, Kenji TANAKA², Shigenobu TANAKA², Temur KHUJANAZAROV²

¹Graduate School of Engineering, Kyoto University, Kyoto 615-8530, Japan.

²Disaster Prevention Research Institute, Kyoto University, Kyoto 611-0011, Japan.

*E-mail: sadyrov.kalinurovich.82m@st.kyoto-u.ac.jp.

Abstract

The evaluation of reanalysis data is essential in improving the accuracy of forcing data for hydrological and land surface models (LSMs). It is especially important for regions with complex terrain and limited in-situ data, such as high mountainous regions of Central Asia. This study aims to assess the accuracy and limits of the spatial distribution of various precipitation products (JRA55, GSMaPv6, ERA5, GPCC, APHRODITE) over Issyk-Kul Lake Basin located in the Northern Tian-Shan Mountains compared to daily observation data in 5 meteorological stations located around Issyk-Kul Lake. The GPCC includes observed data from some stations and thus outperforms other products in monthly values with RMSE of 15.8 (mm). Additionally, modified APHRODITE precipitation data incorporating in-situ gauge data and altitude gradient for precipitation was included in the evaluation. The Land Surface Simple Biosphere including Urban Canopy Model (SiBUC) and Rainfall-Runoff Inundation Model (RRI) integration was used to estimate lake's water level. Results of Jason-2 Satellite Altimetry Data of Issyk-Kul Lake water level were used to compare outputs between several precipitation products. The spatial pattern of precipitation is crucial for the water balance of the basin. However, results have shown that neither product were able to successfully represent precipitation distribution in the basin, and only combination of several reanalysis data and integration of the observed dataset have given positive outcome.

Keywords: Precipitation; Hydrological modeling; Water balance; reanalysis datasets; Issyk-Kul.

1 Introduction

The water resources system in Central Asia is under stress due to multiple interrelated drivers. The water supply from seasonal snow and glacial melt is already impacted by climate change, and water demands continue to increase with population growth and land-use change.

Issyk-Kul Lake is the tenth largest lake in the world by volume (1783 km³). It is endorheic, with relatively consistent low irrigation rate and water outflow from the catchment is mainly driven by evapotranspiration. Located at 1607 meters above sea level, the catchment represents the typical High Mountainous Watershed of Tian-Shan or so-called Northern Himalaya. Modeling and validation of the lake surface fluctuations provide an understanding of hydrological processes in the catchment, including snow and glacier melt with a minimum of uncertainty; it will further help assess climate change impact on the basin. However, due to the scarcity of available observed data and complex terrain, it is challenging to assess model performance at its best. Evaluation of reanalysis and gauge-based precipitation products is thus essential in improving the accuracy of forcing data for hydrological and land surface models (LSMs), especially important for the regions with complex terrain and limited in-situ data.

Satellite-based reanalysis data, especially in the mountainous areas, need bias correction that requires a continuous long period observed data. Kyrgyzstan, the former part of the Soviet Union, had been conducting local observations since the 1950s, but after collapse of the Soviet Union, only one-third of stations continued to operate, so there is a lack of data since the 1990s. Nowadays, more and more meteorological stations start their operation, but it is not enough for continuous analysis.

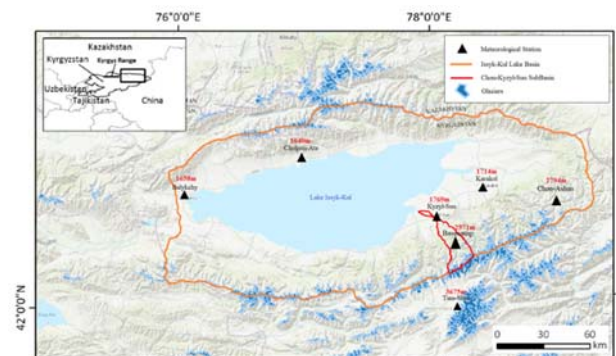


Fig. 1. Location of Issyk-Kul Lake Basin and spatial distribution of glaciers from Randolph Glaciers Inventory (RGI 6.0).

2 Materials and methods

2.1 Statistical analysis and performance

Precipitation data of five meteorological stations located in Balykchy, Cholpon-Ata, Kyzyl-Suu, Karakol, and Chon-Ashuu were compared with global precipitation products: JRA-55, ERA-5, APHRODITE, GSMaP, and GPCC. The performance of the products was evaluated by Pearson correlation factor and value difference using RMSE. No precipitation product ERA showed a significant correlation with observed data. ERA-5 has shown a better value, but only for the single event values. It is possibly due to the limitation of the station equipment's measurements, as precipitations with less than 1mm are not detected but are abundant in reanalysis products. Resolution of precipitation products is important for regional scale modeling.

Table 1. Analysis of Pearson Correlation and root mean squared error (RMSE) among 5 stations:

Dataset	KZLS	KRKL	BLKC	CHAS	CHAT
ERA5	0.53	0.59	0.55	0.63	0.44
(RMSE)	52.8	37.0	46.2	31.7	39.0
JRA55	0.44	0.45	0.41	0.49	0.35
(RMSE)	36.4	34.9	48.6	26.4	37.3
GSMaPv6	0.48	0.49	0.33	0.48	0.37
(RMSE)	19.4	23.2	22.9	31.1	28.9
APHRO	0.43	0.46	0.33	0.54	0.3
(RMSE)	23.3	25.8	15.0	38.3	22.9
GPCC	0.43	0.43	0.43	0.51	0.37
(RMSE)	7.5	17.9	19.4	16.9	18.1

Analysis of the Pearson correlation and RMSE of different reanalysis products is shown in table 1. Some of these products usually include in-situ observation data; that is why GPCC, APHRODITE, and GSMaPv6 can outperform other datasets. GPCC shows the best results but is limited with the resolution of (1°x1°) for daily precipitation. This resolution doesn't provide enough accuracy for the mountainous catchment with complex terrain.

2.2 Modification of precipitation data

Orography impact on precipitation distribution is crucial in this study, though reanalysis products are inaccurate in regional scale precipitation estimation for mountainous regions. The altitude difference in the basin is 1607m and 4772m, with considerable variations in precipitation. For example, the mean annual precipitation at Kyzyl-Suu station (1750m) is 400mm, while at high elevations (>3500m), mean annual precipitation can reach 1000mm.

Precipitation distribution research in the Chon-Kyzyl-Suu River Basin, a part of Issyk-Kul Lake Catchment was conducted during 1956-1967. 30 precipitation gauges were installed at different altitudes and different points for a period of 1956-1967. Results showed that mean annual precipitation increases as altitude increases. Altitude coefficients were developed using same concept of the altitude and precipitation correlation.

APHRODITE precipitation product has shown good applicability in water related studies [1], and its algorithm considers orography in the estimation of precipitation from in-situ stations. This approach can be useful for mountainous regions and particularly for this study. Precipitation distribution based on 6 observation stations with a resolution of 5km was created for Issyk-Kul Lake Basin and compared to other global products.

2.3 Hydrological modeling

State-of-the-art Land Surface Models are used as effective, physically based models to describe land surface processes. In this study SiBUC model is used to evaluate hydrological components of the water cycle. Water level fluctuation of the lake is estimated using Rainfall-Runoff Inundation Model, a kinematic model for runoff and evapotranspiration outputs from SiBUC.

2.3.1 Glacier component

Tian-Shan High Mountain Research Centre's observations data on Karabatkak Glacier since 2007 is also used. The methodology includes measurement of daily ablation stakes during a summer ice melting period. The observation

scheme was further expanded to higher locations in the accumulation zone from 2013.

From these measurements, it is possible to assess runoff from the glacier. We assume that every glacier in the basin is melting the same way as Karabatkak glacier with the area of ~2.5km² while the area of all glaciers is 650.5km². We also assume that area of all glaciers is not changing over time period (2008-2016). It means such approach is not able to consider the dynamical shrinkage of the glaciers in the region.

3 Results and discussion

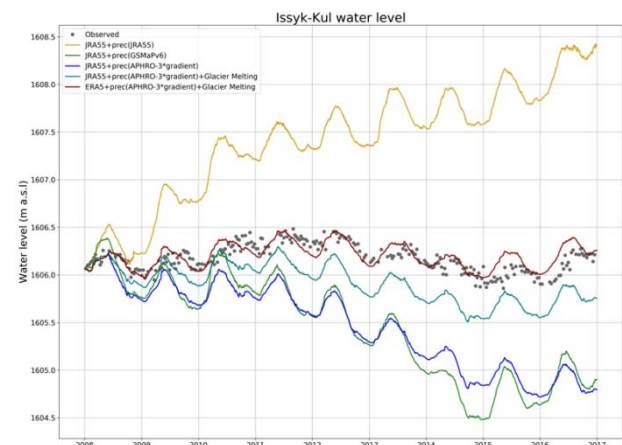


Fig. 2. Issyk-Kul Lake water level variations observed and modeled

Figure 2 shows JRA55 precipitation product overestimates overall precipitation for the whole catchment, and GSMaPv6 underestimates. APHRO-3 precipitation dataset includes in-situ meteorological station data using APHRODITE algorithms for interpolation. *gradient is an altitude coefficient for precipitation in high elevation.

The model run using JRA55 forcing data (temperature, humidity, air pressure, wind speed, downward radiation) shows a slight underestimation in overall water level fluctuation. It can be affected by the output component of the water balance, which is evapotranspiration. Results are improved with the dataset from ERA5 forcing data. The best result is found using an effective combination of various reanalysis products and incorporated simple glacier components.

4 Conclusions

Hydrological modeling of high mountainous areas is very challenging in terms of data availability and consideration of various water balance components. This study show that the efficiency of global products on the regional scale, especially remote ungauged areas, may not give precise results and proper downscale approaches should be implemented in order to improve accuracy of the input data.

Reference

[1] Yatagai, A., K. Kamiguchi, O. Arakawa, A. Hamada, N. Yasutomi, and A. Kitoh, APHRODITE: Constructing a Long-Term Daily Gridded Precipitation Dataset for Asia Based on a Dense Network of Rain Gauges. Bull. Amer. Meteor. Soc., 2012, 93, 1401–1415, doi 10.1175/BAMS-D-11-00122.1.

Application of simple paddy field dam model for typhoon event at basin scale

○ Yikai CHAI^{1*}, Yoshiya TOUGE¹, So KAZAMA¹

¹Department of Civil Engineering, Tohoku University, Miyagi 980-0845, Japan.

*E-mail: chai.yikai.r1@dc.tohoku.ac.jp

Abstract

In recent years, to mitigate the flood disaster caused by the increasing intensity and frequency of torrential rain events, some places have adjusted the retention of the paddy field by installing the runoff control device called paddy field dam. In comparison with other flood control facilities, the installation cost is much lower mainly for drainage control devices at the drain outlet of the paddy field, while the expected effect is significant since paddy fields are widely distributed in Japan. Therefore, this research aims to evaluate the potential flood mitigation effect of the paddy field dam for typhoon 19th in October 2019 in the Naruse River basin using the Rainfall-Runoff-Inundation model. To consider the potential effect of all paddy fields inside the basin, a simple one-dimensional paddy field dam model was developed, which can be applied for the whole basin. Moreover, the scenario analysis was conducted for different heights of free-drain and proportion of application. In conclusion, the paddy field could store about 90 million m³ water in whole paddy fields in the basin using 15 cm height of free-drain, and it significantly mitigated flood in the downstream of the Naruse River basin.

Keywords: paddy field dam, RRI model, Naruse River basin, flood control.

1 Introduction

In 2019 from Oct. 12th to 13th, Typhoon No.19 attacked the Kanto and Tohoku regions of Japan. Naruse River basin was also suffered severe damage, especially in the Yoshida River basin, where the total rainfall during the event was 343.0 mm, 26% of the annual precipitation. Around 5,700 ha of land along the Yoshida River was covered with water, and the maximum inundation depth was about 4.5 m.

Paddy field dam is one of the flood control facilities that is getting more consideration recently in Japan. It takes advantage of the paddy fields' temporary storage capacity by installing drainage control devices at drain outlet. Since the drainage control devices reduce the cross-sectional area of the drain outlet, rainwater is temporarily stored in the paddy field, and the peak discharge downstream from the river will therefore reduce. In 2014, there were approximately 1,580,000 ha of paddy fields in Japan. Consequently, it can be expected that paddy field dams installed in this wide area have a significant capacity to store rainwater. Due to existing models are developed for application in small areas, they are detailed and required many structural data of paddy fields and channels. To consider the paddy field dam for an entire basin water management, evaluation of the paddy field dam's effect on flood control in the whole basin is required.

Therefore, the objective of this research is firstly to develop a simple paddy field dam model that can be applied for the whole basin, and secondly to evaluate the potential flood mitigation effect of the paddy field dam. The target rainfall event and basin is typhoon No.19 in 2019 in the Naruse River basin, where 21% of the area consists of paddy fields. The flood inundation area was analyzed using the Rainfall-Runoff-Inundation (RRI) model and a newly developed simple one-dimension paddy field dam model. Moreover, several scenarios were analyzed for different heights of free-drain, and the proportion of the paddy fields applied for dam operation.

2 Materials and methods

2.1 RRI Model

RRI Model is a two-dimensional model which can simulate rainfall-runoff and inundation simultaneously¹⁾. The model assumes that both river and slope are located at the same grid cell where the river channel is located. This model considers slopes and river channels independently. The flow on the slope grid cell is calculated by the two-dimensional diffusion wave model, and the channel flow is calculated by the one-dimensional diffusion wave model simultaneously.

2.2 Paddy field dam model

The developed paddy field dam model is a simple one-dimensional model to be applied for the whole basin for assessing the potential effect of water outflow through the paddy field dam to confirm the effect of water storage capacity. The structure of the paddy field dam includes two parts: a cone with an orifice (α) and a cylindrical free-drain pipe (β), as shown in Fig.1. According to the water depth of the paddy field, the factor of outflow from the paddy field dam will be changed from the cylindrical weir to the orifice. The outflow rates of the two were calculated sequentially and selected the smaller one as the outflow from the free-drain.

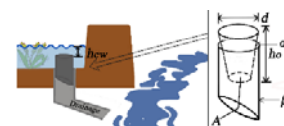


Fig.1 Runoff control device for free-drain system.

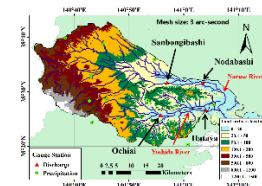


Fig.2 The location of Naruse River basin.

2.3 Study area and model application

The Naruse River, located in the northern part of Miyagi prefecture with a total length of 89 km. The catchment area of the Naruse River basin is approximately 1290 km².

The topographic data used in this study were obtained from Merit DEM with 3 arc-second after adjusted. The flow accumulation data and flow direction data were computed by ArcGIS. The hourly rainfall distribution obtained from twelve rainfall gauge stations were spatially interpolated over the Naruse River basin using the Inverse Distance Weighting. For the river cross-sections, the following equations were used to estimate a simple river cross-section: width (m) = $7S^{0.42}$, depth (m) = $1.5S^{0.18}$ where S (km²) was the flow accumulation area. The other model parameters were determined after calibration, as shown in Table.1.

In addition, the paddy field dam was designed to be arranged in all paddy fields mesh in the entire basin, only one paddy field dam was installed for one mesh with paddy field, and the resolution of mesh was 100 m × 100 m. To estimate the potential of the paddy field in whole basin approximately, two scenarios were formulated. The first scenario was to change the height of free-drain. There were six scenarios: 5 cm, 10 cm, 15 cm, 20 cm, 25 cm, 30 cm height. And the second scenario was to change the proportion of paddy fields applied for paddy field dam in the case of 15 cm height of the free-drain. There were five scenarios: 20%, 40%, 60%, 80%, 100% of paddy field mesh have been installed paddy field dam.

Table 1 Model parameter setting.

Parameter	Mountains	Plains	
n	(m^3/s)	0.3	0.3
d_a	(m)	2	-
k_a	(m/s)	0.4	-
k_v	(m/s)	-	1.67×10^{-7}
ϕ		-	0.475
S_f	(m)	-	0.3163
n_r	(m^3/s)	0.03	

3 Results and discussion

RRI model was applied to the Naruse River basin, and the comparisons of the observed and simulated discharge at gauging stations are showed in Fig.3. These four gauging stations showed high corresponding.

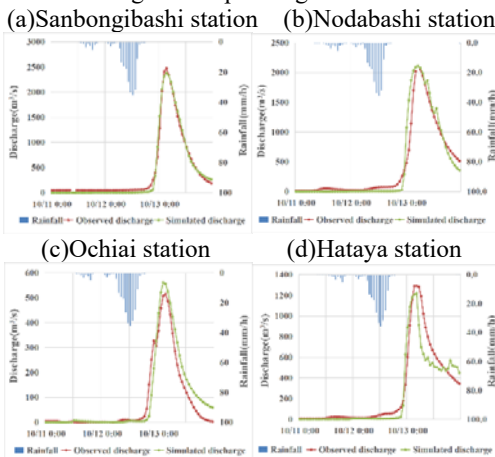


Fig.3 Comparison of simulation and observation discharge at four gauging observation stations.

In the first scenario, as shown in Fig.4, the peak discharge was reduced by increasing the height of free-drain. However,

the difference between the 0 cm and 5 cm scenario was significant. In the second scenario, as shown in Fig.5, the more paddy field dam installed in the paddy field, the effect of flood mitigation was more significant.

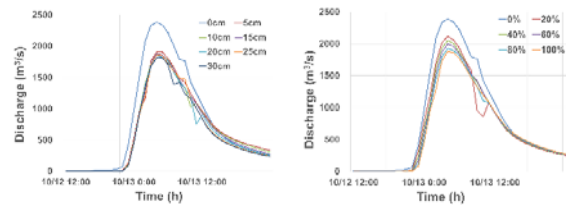


Fig.4 Comparison of discharge using the different height of free-drain with paddy field dam applied in the 100% of paddy field. (Left)

Fig.5 Comparison of discharge using the different proportion of paddy field dam in the paddy field with 15 cm height of free-drain. (Right)

To evaluate the flood mitigation effect of paddy field dam, total stored water in the whole basin and maximum inundated volume was calculated for each scenario.

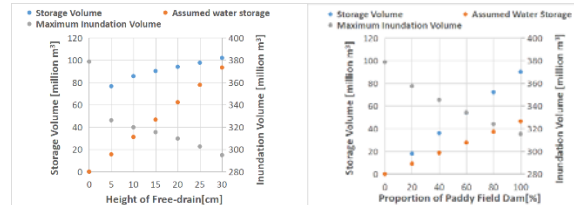


Fig.6 Water storage volume in different height of free-drain. (Left)

Fig.7 Water storage volume in different proportion of paddy field dam. (Right)

In Fig.6, when all of the paddy fields were applied for the paddy field dam, 15 cm of free-drain could store 90 million m³, while assumed water storage under the outlet of free-drain was more than 40 million m³, and it had mitigated about 50% of inundated water. Total stored water increased by higher height of free-drain, but the difference between assumed water storage and storage volume was getting close because outflow from the paddy field was mainly regulated by free-drain. In Fig.7, when the installation rate increased, its effect of flood mitigation was getting higher. Changing trends were linear even for inundation volume.

4 Conclusions

Overall, to evaluate the potential effect of the paddy field dam distributed in the whole basin, a simple one-dimension paddy field dam model has been developed and applied for Typhoon 19th event in 2019 in Naruse River basin using the RRI model. The peak discharge in the river and inundation volume decreased as the height and proportion of paddy field dam increasing. Clearly, the results showed that the paddy field dam had a significant effect on flood control.

Acknowledgment

This research was supported by the Environment Research and Technology Development Fund (S-18) of the Environmental Restoration and Conservation Agency of Japan.

Reference

[1] Sayama, T., Ozawa, G., Kawakami, T., Nabesaka, S. and Fukami, K.: Rainfall–runoff–inundation analysis of the 2010 Pakistan flood in the Kabul River basin. *Hydrological Sciences Journal*, 57 (2), 298–312, 2012.